Scientific Papers of the
Institute of Electrical Power Engineering of the
Wrocław University of Technology

PRESENT PROBLEMS OF POWER SYSTEM CONTROL

No 1

Wrocław 2011

Editor
Mirosław Łukowicz

Cover design
Piotr Pierz

Institute of Electrical Power Engineering
Wroclaw University of Technology
Wybrzeze Wyspianskiego 27
50-370 Wroclaw
Poland
phone: +48 71 320 26 55
fax: +48 71 320 26 56
www: http://www.ie.pwr.wroc.pl/
e-mail: Inst.Energ@pwr.wroc.pl

ISSN xxxxxxxxxxxx

Wydrukowano w Drukarni Oficyny Wydawniczej Politechniki Wrocławskiej z dostarczonych materiałów.

CONTENTS

Keywords:
Thevenin's equivalent, stability margin, local voltage stability

Bartosz BRUSILOWICZ*, Janusz SZAFRAN*

DETERMINATION OF THEVENIN'S EQUIVALENT MODEL AT THE RECEIVING NODE

This paper presents the properties of the equivalent Thévenin's model of a network as seen from a network receiving node. Such a simplified model can be applied in protective and preventive gear installed at the considered receiving node. Thévenin's circuit can be determined either from of the power system configuration diagram or by use of algorithm based on local current and voltage phasor measurements. Local measurements are used to calculate the derivative of apparent power against the voltage d*S*/d*V*. Paper describes the d*S*/d*V* algorithm accuracy tests according to the approximate angle of the series system impedance. An important problem of the Thévenin's model updating due to the changing configuration of power system is discussed in the paper. The advantages and disadvantages of both described methods are also presented

1. INTRODUCTION

Commonly the analysis of power flow in the power system is based on a full system model. The model contains complete information about the current system configuration (state of switches, power lines and transformers). Assuming the symmetry of loads and generators the model is represented as single-phase circuit. Based on such model full analysis of system security may be determined including calculation of the theoretical lines load and margins of global and local stability. In the full model disturbances occurring during the normal operation e.g. a line switch off for service as well as emergency disturbances may also be analyzed. However, the full system models, in spite of obvious advantages, have numerous disadvantages which make it unfeasible in many applications. The main disadvantage is the previously mentioned requirement of knowledge of the full network configuration. Another one is the number of possible incidents that may have the impact on the considered system node and the time required for analysis. Usually, the current configuration of the power system

* Wroclaw University of Technology, Institute of Electrical Power Engineering, Wybrzeze Wyspianskiego 27, 50-370 Wroclaw, Poland.

is known to the transmission system dispatcher only so it is impossible to apply the full model in protective and preventive devices. When there is a need to analyze the condition of node by using local measurements the equivalent Thevenin's model can be very useful. This paper presents the characteristics and the possibilities of such a Thevenin's model as well as its determination and updating.

2. THEVENIN'S MODEL DETERMINATION AND UPDATING

2.1. DETERMINATION OF THE MODEL

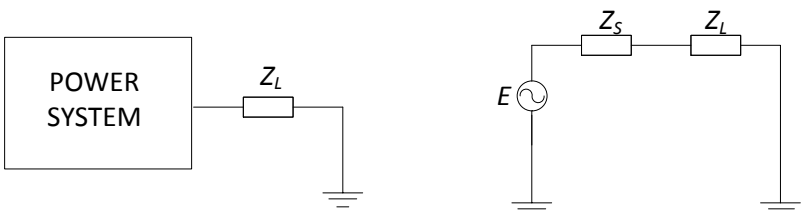

Fig. 1. Power system model and its Thevenin's equivalent

Thevenin's circuit includes: ideal voltage source E, series system impedance Z_S and load impedance Z_L or alternatively load admittance Y_L. Example of a full model and its Thevenin's equivalent is shown in Fig. 1. To calculate the parameters of the Thevenin's model several methods can be used. The paper presents two selected methods. The first well known method is based on a network configuration and parameters of devices installed on power system. The second one, developed by the authors, employs a local measurements of current and voltage phasors.

a) According to the first method the series impedance is calculated using fundamental circuit simplification rules for all voltage sources grounded. The source voltage is the voltage that occurs in the node considered in 'no load' conditions.

b) In the second method the of Thévenin's circuit parameters calculation algorithms are based on local measurements. The algorithm considered in the paper and applied to the Thévenin's circuit from Fig. 1 is defined by the following formulas [1, 2]:

$$V = \frac{E}{\sqrt{1 + 2W\cos\beta + W^2}} \tag{1}$$

$$S = \frac{E^2}{Z_S} \frac{W}{1 + 2W\cos\beta + W^2} \tag{2}$$

where: V – voltage at the node, S – apparent power in the load, E – equivalent source voltage, Z_S – equivalent series system impedance, $W=Y*Z_S$, Y – load admittance, $\beta=\varphi_S-\varphi_L$, φ_S and φ_L –system and load impedance phase angles, respectively.

Differentiating formulas (1) and (2) one gets:

$$\frac{\mathrm{d}V}{\mathrm{d}W} = \frac{-V^3\left[\cos\beta + W\left(1 + \frac{\mathrm{d}(\cos\beta)}{\mathrm{d}W}\right)\right]}{E^2} \tag{3}$$

$$\frac{\mathrm{d}S}{\mathrm{d}W} = \frac{S^2\left[1 - W^2\left(1 + 2\frac{\mathrm{d}(\cos\beta)}{\mathrm{d}W}\right)\right]}{E^2 Y_L W} \tag{4}$$

Dividing the equations (3) by (4) one obtains:

$$\frac{\mathrm{d}S}{\mathrm{d}V} = -\frac{1 - W^2\left(1 + 2\frac{\mathrm{d}(\cos\beta)}{\mathrm{d}W}\right)}{W\left[\cos\beta + W\left(1 + \frac{\mathrm{d}(\cos\beta)}{\mathrm{d}W}\right)\right]} \frac{S}{V} \tag{5}$$

Derivative dS/dV may be used to determine the value of parameters of Thevenin's circuit but also as an indicator of the stability margin. Solving the second order equation, W may be calculated from formula:

$$W = \frac{-\frac{\mathrm{d}S}{\mathrm{d}V}\cos\beta - \sqrt{\left(\frac{\mathrm{d}S}{\mathrm{d}V}\right)^2\cos^2\beta - 4\frac{S}{V}\left[\frac{\mathrm{d}S}{\mathrm{d}V}\left(1 + \frac{\mathrm{d}(\cos\beta)}{\mathrm{d}W}\right) - \frac{S}{V}\left(1 + 2\frac{\mathrm{d}(\cos\beta)}{\mathrm{d}W}\right)\right]}}{2\left[\frac{\mathrm{d}S}{\mathrm{d}V}\left(1 + \frac{\mathrm{d}(\cos\beta)}{\mathrm{d}W}\right) - \frac{S}{V}\left(1 + 2\frac{\mathrm{d}(\cos\beta)}{\mathrm{d}W}\right)\right]} \tag{6}$$

Factor W is equal to Z_S*Y. So from the equation (6) value of series system impedance Z_S can be directly specified. Formula

$$E = V\sqrt{1 + 2W\cos\beta + W^2} \tag{7}$$

defines value of voltage source E by using W factor. It should be noticed that for an idle node $Y=0$ so also $W=Y*Zs=0$. Thus the node voltage value is equal to voltage source in Thevenin's circuit $E=V$. It is also true for equation (7).

Thevenin's model parameters determined by algorithm which employs the derivative dS/dV correspond to the current system configuration. However, to define these parameters the information about states of the power system components is not required. To calculate the series impedance Z_S and voltage source E the following quantities should be measured: S – apparent load power, V – node voltage and load parameters, namely, magnitude and angle of load impedance. All values in equation (6) can be calculated using measurements except φ_S - angle of system impedance. This angle can be determined using the full model. Small fluctuations of system impedance angle with respect to its assumed average value do not cause significant errors.

2.2. REAL TIME UPDATING OF THE MODEL

Configuration of the power system is not fixed. It is continuously changing due to switching or disconnection of the system components. Such operations are taking place during normal operation and also during faults. Operations that impact the elements of Thevenin's model are the connection or disconnection of power lines, transformers as well as significant loads.

Thus the Thevenin's model based on the first method should continuously be updated. According to the Thevenin's rule each fragment of the power system can be replaced by a series system impedance and voltage source. Using this principle base the full model can be slightly simplified by replacing the distant parts of the system by the impedance and source. To approximate parameters of Thevenin's equivalent there is no need to know entire power system configuration but only the state of the elements that have the greatest impact on the series system impedance. An example of such a simplification can be a fragment of power system connected to node with one power line. In case of receiving information about disconnection of a given power line, information about area that has been disconnected is unnecessary. In the future, when the Smart Grid technology will be developed, access to global data will be fully disposable. Then, this method will give very accurate results.

As it has been written earlier, the algorithm that calculates the Thevenin's model parameters using dS/dV derivative does not require system configuration data. Local measurements of current and voltage phasors are sufficient. This is a big advantage when the data about system are not known for the node considered. The major disadvantage of the method is the need of changing the load admittance to make calculation of Thevenin's circuit parameters possible. This disadvantage is patched automatically.

When system impedance changes the node voltage increases or decreases. The voltage change causes transformer tap changer acting. Activation of tap changer changes load admittance. Another disadvantage is the difficulty of determining the angle of series system impedance.

3. SOME PROPERTIES OF THEVENIN'S EQUIVALENT MODEL

To study the properties of Thévenin's equivalent and accuracy of *dS/dV* algorithm the full model and its equivalent shown in Fig. 2 were used.

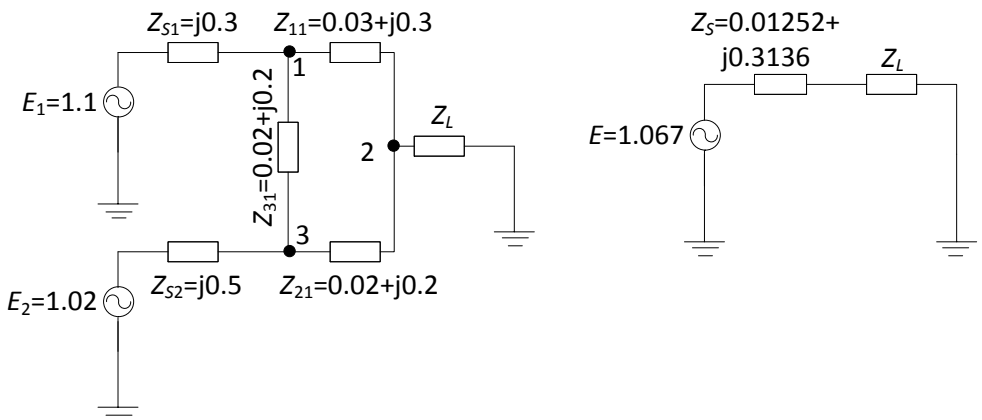

Fig. 2. Test of the full model and its Thévenin's equivalent

Fig. 3 shows the nose curves received by using the full model and simplified Thevenin's circuit. Curves are exactly the same. The differences between them are at level of 10^{-3} and caused by rounded calculations. Thus the safety analysis of the node (e.g. voltage stability margin) can be based on nose curve from Thévenin's equivalent.

The impact of the assumed value of series impedance angle on accuracy of approximation the Thévenin's model parameters was also investigated. The test model consists of three nodes, lines between them and two voltage sources connected to transmission nodes through transformers. Two nodes are transmission nodes (1, 3) and one is receiver node (2). Significant RL loads (resistance in series with inductance) were connected to the nodes (1, 3). The volume of load has been increased until voltage in node reached the level of 0.9 of nominal. Obtained limits of series angle variation for the full model test are shown in Table 1.

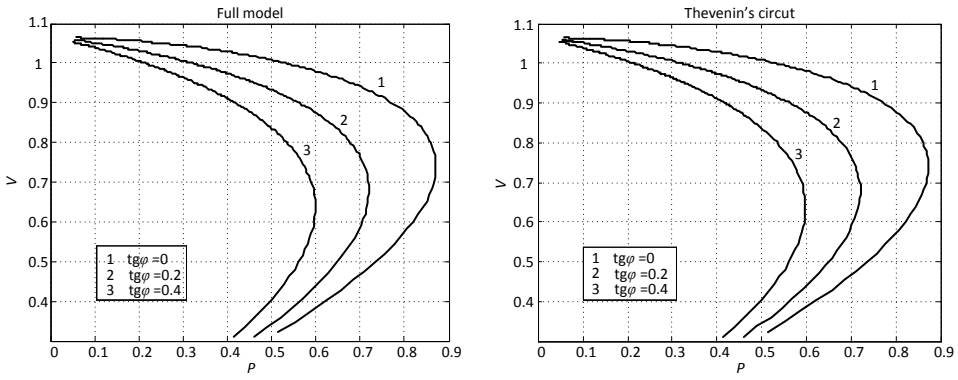

Fig. 3. Nose curves from the full model and Thevenin's circuit

Table 1. Value of system angle at the receiving node

System angle in node 2		
Load angle	Load location	
	Node 1	Node 3
[deg]	[deg]	[deg]
0	75.3	76.5
90	87.3	87.2

Specified values of the angle were applied in d*S*/d*V* algorithm. Then curves obtained from calculation of series system impedance value and voltage source were plotted. The curves are shown in Fig. 4. The correct values of system impedance *Zs* and voltage source *E* are 0.01252 + j0.3136 and 1.067, respectively. Impedance angle calculated from full model series system is 87.7°. When the Z_S/Z_L ratio is low, the errors can be significant. The errors can reach a value up to 28%. However, when load admittance is low, margin of voltage stability is high, so the error can be tolerated. Coming closer to the stability limit errors decrease nearly to zero. So the worse situation implies the more accurate determination of Thevenin's model parameters. Fig.4 also shows that for load impedance angle value higher than the correct one the calculated value of system impedance is greater. Overestimated system impedance means a greater voltage stability margin.

Thus a better solution is revaluation of system impedance angle because this makes the algorithm more sensitive. The curves in Fig. 4 show that applying angle 3 degrees higher or lower than current value cause similar errors.

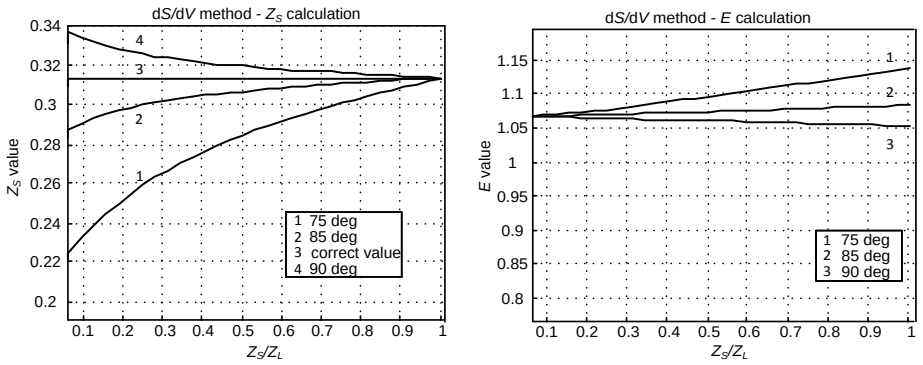

Fig. 4. Calculation of E and Z_s values

The case of Thevenin's model parameters determination for the working point located in the middle of the stability margin (85 degrees entered) is shown in Fig. 5. The curves show that calculation errors do not exceed 10%.

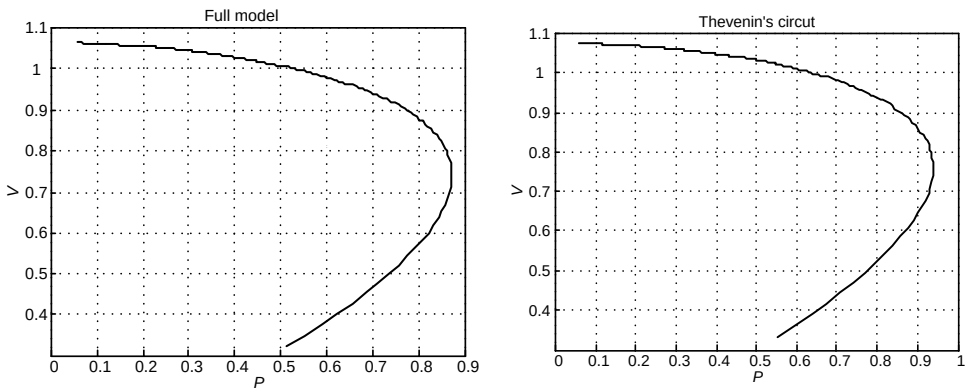

Fig. 5. Nose curves from full model and Thevenin's circuit

4. CONCLUSIONS

Thevenin's equivalent can be a useful tool for determining of local voltage stability margin. Method which uses only local measurement for calculation of model parameters can be applied in protective and preventive devices. Calculation of series system impedance can also be a measure of local voltage stability margin. The limit of stability occurs when $Z_S/Z_L=1$ or $Y^* Z_S =1$ [3]. Value of load admittance Y can be measured and the value of Z_S can be determined by using one of two methods presented.

When wide area measurement will be easily available then the combination of both presented methods will be the best solution to the Thevenin's model parameters determination. This will eliminate the disadvantages of both methods. When power system configuration data will be available the system impedance value and angle will be able to determine by use of the full model method. If these data are not available then the Thevenin's model will be updated by the d*S*/d*V* method.

ACKNOWLEDGMENT

The paper was realized in framework N N511 472439 project sponsored by the Polish Ministry of Science and Higher Education.

REFERENCES

[1] WISZNIEWSKI A., *New criteria of voltage stability margin for the purpose of load shedding*, IEEE Transactions on Power Delivery, Vol. 22, NO. 3, July 2007.
[2] KLIMEK A., REBIZANT W., WISZNIEWSKI A., *Intelligent voltage difference control maintaining the voltage stability limit*, CIGRE 2010 Paris.
[3] BEGOVIC M.M., NOVOSEL D., SAHA M.M., VU K., *Use of local measurements to estimate voltage stability margin*, in Proc. PICA, Columbus, OH, May 1997, pp. 318-323.

OKREŚLANIE MODELU EKWIWALENTU THEVENINA W WĘŹLE ODBIORCZYM

Artykuł przedstawia właściwości modelu Thevenina. Uproszczony model reprezentujący aktualną konfigurację systemu może mieć zastosowanie w automatyce zabezpieczeniowej oraz prewencyjnej montowanej w punkcie odbiorczym. Model Thevenina może być tworzony przy użyciu dwóch metod: korzystając z informacji o pełnej konfiguracji systemu oraz z algorytmu wyliczającego parametry modelu na podstawie pomiarów lokalnych fazorów napięć i prądów. Korzystając z pomiarów lokalnych, wyliczana jest pochodna mocy pozornej po napięciu d*S*/d*V*. Przeprowadzono testy dokładności algorytmu d*S*/d*V* w zależności od założonego kąta impedancji systemowej. Ważnym problemem, jaki jest poruszony w artykule jest aktualizacja modelu zgodnie ze zmieniającą się konfiguracją systemu elektroenergetycznego. Zmiany mogą być wywoływane stanami normalnej pracy jak i awariami występującymi w systemie. Przedstawiono wady i zalety stosowania obu metod.

Keywords:
dynamic thermal line rating,
blackout prevention, heat equation

Lukasz STASZEWSKI*, Waldemar REBIZANT*

BLACKOUT PREVENTION POSSIBILITY USING DYNAMIC THERMAL LINE RATING

This paper presents the Dynamic Thermal Line Rating (DTLR) application, based on the heat equations, that makes possible overhead transmission lines operation over their conservatively designed current ratings. The DTLR concept is well known – owing to the CIGRE [1,2] and IEEE [3] standards for overhead bare conductor temperature calculations. However, this phenomenon may not have been used for a purpose of increasing electrical power system stability and thus for blackout prevention. This paper is based on both CIGRE and IEEE standards and presents investigation of the current flow through various conductors. Their temperature and monitoring ambient weather conditions and thermal limits of a conductor are considered. The influence of the weather conditions on the lines flow capacities is presented as a comparison of various types of AFL 6 conductor and various weather conditions. Also the short analysis of the recent blackouts and possibilities of DTLR use are presented. Obtained results are described and conclusions are drawn.

1. LINE MONITORING APPROACH

1.1. SIGNALS AND VALUES USED FOR CALCULATIONS

The thermal rating, which is also referred to as ampacity, of an overhead line is a maximum value of the current, not causing an excessive sag, exceeding the designed, allowable conductor temperature or loosening strength of a conductor. The sag temperature is a value of temperature for which the smallest legislated clearance between ground and a conductor is met and further heating would endanger public safety. There are many factors influencing temperature of an overhead conductor: current flowing throughout the conductor, wind speed, wind direction in relation to the trans-

* Wroclaw University of Technology, Institute of Electrical Power Engineering, Wybrzeze Wyspianskiego 27, 50-370 Wroclaw, Poland.

mission line axis, ambient temperature and solar radiation. There are also others factors (e.g. altitude of a line, azimuth of the sun, type of atmosphere, type of ground under the conductor, etc.) but these will not be presented in this paper, despite of being concerned during the analysis, due to a low significance. Since weather conditions are difficult to predict and the public safety must always be ensured, very conservative assumptions must be made when designing transmission lines ampacity. This also applies to the overload protection of transmission lines. The relays settings are chosen to meet the need of switching of the line when the flowing current value is close to the one for which, during the conservatively assumed conditions, the conductor reaches its thermal limit.

The main purpose of the real time monitoring is to utilize overhead lines with their full potential and not only to their limits coming from conservative assumptions. It should be noted that with real time systems, when the external factors are favorable, the line is not operated at temperatures higher than designed but running at its designed temperature for a longer period of time. Thus the line is better utilized.

As the line is running closer to the thermal limit, one can expect the losses to increase. This should be taken into account when optimizing the network configuration and line loading. This paper shows the possibilities of DTLR usage to do so and in addition points at the possibility of using DTLR as a way of blackout prevention in some particular cases.

1.2. MATHEMATIC FORMULAE

Conductor temperature calculations according to [3] are based on the heat balance equation (1) and consider heats and losses due to flowing current and various external conditions.

$$q_c + q_r = q_s + q_i \,, \tag{1}$$

where q_c is a cooling due to convection, q_r due to radiation, and q_s and q_r are respectively heating due to solar radiation and due to Joule's law by the current flow.

Cooling due to convection is calculated from two equations (2) and (3), then the higher value is chosen.

$$q_{c1} = \left[1.01 + 0.0372 \left(\frac{D \rho_f v_w}{\mu_f} \right)^{0.52} \right] k_f K_{\text{angle}} \left(T_c - T_a \right), \tag{2}$$

$$q_{c2} = \left[1.0119 \left(\frac{D\rho_f v_w}{\mu_f} \right)^{0.6} k_f K_{\text{angle}} \left(T_c - T_a \right) \right], \tag{3}$$

where: ρ_f density of air, v_w air stream velocity at a conductor, k_f thermal conductivity of air, K_{angle} angle between the line axis and wind direction and T_c and T_a conductor and ambient air temperature, respectively.

Cooling due to radiation is usually only a small fraction of total heat balance and is calculated with:

$$q_r = 0.0178 D\varepsilon \left[\left(\frac{T_s + 273}{100} \right)^4 - \left(\frac{T_a + 273}{100} \right)^4 \right], \tag{4}$$

where: D is external diameter of the conductor, ε is emissivity.

Heating due to solar radiation is presented by:

$$q_s = \alpha Q_{se} \sin(\theta) A', \tag{5}$$

where: α is solar absorptivity, Q_{se} is the total solar and sky radiated heat flux elevation corrected, θ is effective angle of incidence of sun rays and A' is projected area of conductor per unit length.

The last term is heating due to Joule's law,

$$q_i = I^2 R(T_c) = I^2 \left(\left[\frac{R(T_{\text{high}}) - R(T_{\text{low}})}{T_{\text{high}} - T_{\text{low}}} \right] (T_c - T_{\text{low}}) + R(T_{\text{low}}) \right), \tag{6}$$

that takes into account not only the flowing current (I) but also the change of resistance (R) due to conductor temperature and where $R(T_{\text{high}})$, $R(T_{\text{low}})$ are the resistance values for high and low conductor temperatures, respectively.

2. CONDUCTOR RATINGS

2.1. VARIOUS CONDUCTOR TYPES

Particular conductors differ between each other with the percentage increase of current flow possibilities with use of Dynamic Thermal Line Rating. For this paper

purpose the AFL 6 conductor type was chosen in three versions: AFL 6 95, AFL 6 120 and AFL 6 240. The difference between these conductor types is in a cross section surface area (95, 120 and 240 mm^2, respectively). In this part of investigation these conductors are put into the tests with the same weather conditions and with different values of current: 110, 115 and 120% of rated current. Rated current value is calculated for the conservative conditions of wind speed 0.1 m/s, ambient air temperature 40°C, and for each conductor. It is a value for which the conductor reaches its thermal limit set to 80°C. The results are presented in Tab. 1, showing the temperatures of the conductors during favorable weather conditions, and in Fig. 1, presenting heating curves for each tested conductor, with respective temperatures that conductor reached for each current value. This illustrates the possibilities of exceeding rated current values while not exceeding thermal limits.

Table 1. AFL 6 conductor temperatures for various current values

Type of conductor	Rated current [A]	Conductor temperature [°C]		
		110%	115%	120%
AFL 6 95	517.1419	**81.05**	**83.16**	**85.28**
AFL 6 120	546.1467	79.68	**81.50**	**83.42**
AFL 6 240	612.8172	77.26	78.65	**80.20**

As it can be seen in above table, the thermal limits exceeding is different for each type of the conductor. And so are the possibilities of controlled overloading them. The best case is for the AFL 6 240 which can be loaded with 115% of the rated current continuously under the favorable weather conditions, and as it can be seen from Fig. 1 with 120% of rated current for about 25 minutes.

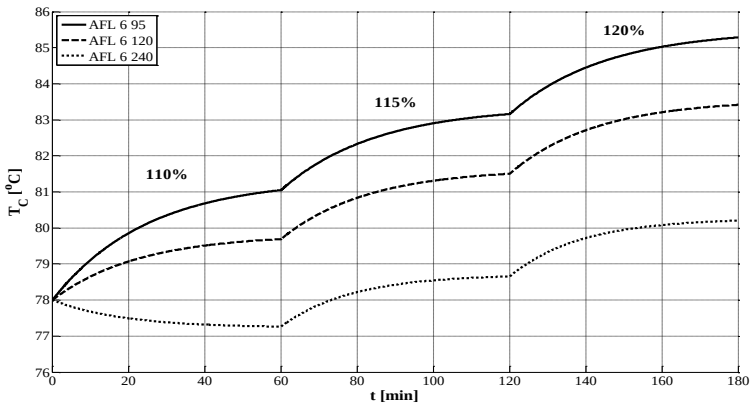

Fig. 1. Temperature of different types of conductors dependent on current values

3. BLACKOUT PREVENTION

Large-scale blackouts in North America, Europe, and other countries, such as the 1996 blackout in the U.S. [4], the 2003 blackout in North America [5], the 2003 blackout in Italy [6], and the 2006 blackout in Europe [7], are important reminders of the importance of the reliability of the electric energy infrastructure and the economic impacts of blackouts.

In order to avoid catastrophic outages, appropriate control actions to mitigate emergency conditions including overload conditions in power systems are important. The network problems including overload and voltage problems should be solved with control actions through system operation and/or emergency controls. Among them, overload is an important problem and thus control actions through the collaboration between system operation and emergency controls are vital [8]. One of the parts of the mentioned control of the system operation could be used DTLR technique, for example introducing an additional blocking signal into a protection relay – restraining it from tripping the line when needed.

In general, the sequences of events in the major blackouts followed a common process. Typically, the cascaded events were initiated by a single event or multiple events, such as the 500 kV line outage (U.S. 1996), the generator tripping and the 345 kV line outage (U.S. and Canada 2003), the line outage (Italy 2003) and the coupling operation of bus bars at a substation (Europe 2006). Following the initiating events, the cascaded events took place sequentially. One component failure may trigger another failure, which can bring successive line and/or generator tripping.

There are many causes of cascaded events which contribute to catastrophic outages. They typically include faults, unwanted relay operations (including hidden failures), equipment failures or malfunctions, communication and information failures, and operational errors. Due to the mixture of the causes, prediction of the exact sequence of cascaded events that will take place is practically impossible. However, it is important to look into the fundamental patterns of cascaded events, i.e., which event may trigger other events. Some examples of fundamental patterns of cascaded events are:

- line tripping due to overloading [4, 5, 9, 10],
- generator tripping due to over-excitation [5, 9],
- line tripping due to loss of synchronism [5, 9],
- generator tripping due to abnormal voltage and frequency condition [5,9,10],
- under-frequency/voltage load shedding [4].

From the point of view of this paper, the only one event type taken into account is the first one – line tripping due to overloads. There is a high possibility of DTLR

technique usage in that case. Considering mentioned earlier blackouts it is worth pointing some important events.

In case of November 4th, 2006 [11] two important steps of cascade can be distinguished in the whole process. The first was at 22:06, after over 30 minutes since the beginning, when the current on the line Landesbergen-Wherendorf increased from 1800 A to 1900 A within 2 to 3 minutes. Thus, the setting value for protection device (1800 A) – as specified by RWE – was exceeded on this line. And the second, when at 22:10:13, the line Landesbergen-Wherendorf was first tripped by the protection device due to overload. Then two other lines (220 kV and 380 kV) were also tripped due to overloads.

Mentioning blackout in Italy on September 28th, 2003 it is worth to say that as a result of previous events the power deficit in Italy was such that this country started to lose synchronism with the rest of Europe and the lines on the interconnection between France and Italy tripped due to distance relays (first or second step). The same happened for the 220 kV interconnection between Italy and Austria and subsequently, the 380 kV corridor between Italy and Slovenia became overloaded and it tripped too.

The blackouts in the U.S. in 1996 and in North America in 2003 were also analysed and despite that their main causes were not the line overloads, these still remained an important part of blackouts development.

Amongst many other causes and steps of blackout evolution the one, most important from the point of view of Dynamic Thermal Line Rating based on real time lines monitoring, is an overload.

As mentioned in case of Europe 2006 blackout the line overload was 1900 A that is less than 106% of its normal ampacity of 1800 A and the DTLR techniques are capable to dynamically increase the limit up to 120% for a short period of time and up to 115% constantly (Fig. 1). This observation leads to a conclusion, that probably the line could have not been tripped, as a result of the occurring overload. Of course it is difficult to assume that the most favourable situation (weather conditions) was met, at that time, to reach the 120% of the rated ampacity, but it is highly probable that the 106% overload was not a hazard to the line. Thus DTLR application might have been a great relief for the system stress and a way of avoiding further evolution of the failures. The same refers to the Italian blackout in 2003, where also an overload was one of the main causes and the DTLR application might have saved Italian system from extensive failure.

Despite that the U.S. in 1996 and in North America in 2003 blackouts did not show the possibility of DTLR use to direct restrain of failure from spreading wider, they present also the cascaded events pattern ipso facto pointing the overload as a one of possible factors to occur during the whole evolution process.

4. SUMMARY

Overloads, even if not as a main cause, still often occur as one of the factors contributing to spreading the power system outage to the wider areas. It creates the need of avoiding them and the Dynamic Thermal Line Rating makes it possible. The analysis carried out and presented above showed that the overload as an excessive current flow can be sometimes allowed. It depends on the transmission line ambient weather conditions. For favourable conditions: high wind speeds, low air temperature, etc. it is possible to provide from a few to even a few tens of minutes of an additional time to restrain standard protection from operation and to maintain the power system integrity.

REFERENCES

[1] *Mathematical model for evaluation of conductor temperature in the steady (or quasi-steady) state (normal operation)*, CIGRE, ELECTRA No. 144 Oct. 1992, 109-115.
[2] *The thermal behavior of overhead conductors*, CIGRE, ELECTRA No. 174 Oct. 1997, 59-69.
[3] *IEEE Standard for Calculating the Current-Temperature of Bare Overhead Conductors*, IEEE Std 738-2006 (Revision of IEEE Std 738-1993).
[4] WSCC, *Western Systems Coordinating Council (WSCC) Disturbance Report for the Power System Outage that Occurred on the Western Interconnection, August 10, 1996*, approved by the WSCC Operations Committee on October 18, 1996.
[5] U.S.-Canada Power System Outage Task Force, *Final Report on the August 14th blackout in the United States and Canada*, United States Department of Energy and National Resources Canada, April 2004.
[6] UCTE, *Final Report of the Investigation Committee on the 28 September 2003 Blackout in Italy*, April 2004.
[7] UCTE, *Final Report on the Disturbances of 4 November 2006*, Jan. 2007.
[8] YAMASHITA K., LI J., ZHANG P., LIU C-C, *Analysis and Control of Major Blackout Events*, Power Systems Conference and Exposition, 2009. PSCE '09. IEEE/PES
[9] BIALEK J. *Why has it happened again? Comparison between the UCTE blackout in 2006 and the blackouts of 2003*, IEEE, PowerTech 2007, Paper ID: 177
[10] ANDERSSON G., DONALEK P., FARMER R., HATZIARGYRIOU N., KAMWA I., KUNDUR P., MARTINS N., PASERBA J., POURBEIK P., SANCHEZ-GASCA J., SCHULZ R., STANKOVIC A., TAYLOR C., and VITTAL V., *Causes of the 2003 Major Grid Blackouts in North America and Europe, and Recommended Means to Improve System Dynamic Performance*, IEEE TRANSACTIONS ON POWER SYSTEMS, VOL. 20, NO. 4, NOVEMBER 2005.
[11] CHUNYAN Li, YUANZHANG Sun, XIANGYI Chen, *Analysis of the Blackout in Europe on November 4, 2006*, The 8th International Power Engineering Conference (IPEC 2007), 939-944.

ZASTOSOWANIE DYNAMICZNEJ CIEPLNEJ OBCIĄŻALNOŚCI LINII PRZESYŁOWYCH JAKO MOŻLIWOŚCI ZAPOBIEGANIA BLACKOUTOM

Artykuł przedstawia zastosowanie dynamicznej termicznej obciążalności linii przesyłowych (DTOLP) jako narzędzia umożliwiającego unikanie powstawania lub dalszego rozwoju powstałej już

awarii wielkoobszarowej systemu elektroenergetycznego. Sama idea DTOLP jest dobrze znana, dzięki standardom CIGRE i IEEE służącym do obliczeń termicznego stanu przewodu jako funkcji warunków pogodowych oraz przepływającego przez przewód prądu elektrycznego. Na potrzeby artykułu korzystano z obu standardów i zaprezentowano analizę wpływu przepływu prądu w różnych przewodach na ich możliwości przesyłowe w zależności od otaczających je warunków pogodowych. Dodatkowo artykuł podkreśla istotność przeciążeń linii przesyłowych, jako elementu wywołującego lub pogłębiającego awarie wielkoobszarowe oraz możliwość zastosowania dynamicznej termicznej obciążalności linii przesyłowych w celu zapobiegania tym zjawiskom.

Keywords:
microprocessor controller,
Programmable Logic Controller

Janusz STASZEWSKI*

MICROPROCESSOR CONTROLLERS VERSUS PLC

This paper describes microprocessor controllers and Programmable Logic Controllers for industry applications. The differences in hardware and in programming are presented.

1. INTRODUCTION

Ones upon a time… there were transistors and the first control systems with many problems, with noise and low level signals. Next were digital control systems using logical gates and memory elements like flip-flops, etc. These systems are more resistant to disturbance and signals can be sent to long distances. But there is still only one problem. Every time we want to change control system, we must add new logic elements and change connections between them. So, a man has thought "What can I do to change a control circuit without changing hardware? The solution was only one: a universal structure with many logical gates, flip-flops etc. and connections between them changed by special algorithm (program).

2. MICROPROCESSOR CONTROLLER

2.1. HARDWARE

This special programmable structure is called microprocessor. It sounds very simple but, in fact it is very complex. The typical structure of microprocessor is shown in

* Wroclaw University of Technology, Institute of Electrical Power Engineering, Wybrzeze Wyspianskiego 27, 50-370 Wroclaw, Poland.

Fig. 1. The main part CPU (Central Processing Unit) is called ALU (Arithmetic Logic Unit). In this unit all arithmetical and logical operations are executed. This, what is executed (program) is stored in the block called Memory. The Memory is connected with ALU by unidirectional Address Bus and bidirectional Data Bus. We can also use the Memory to read or write variables. Very important is a block called Input/Output. It is used for communication of ALU with external world. This block is connected with ALU in the same way as Memory. On the rising edge of the special signal called Read, when the appropriate address of external module is present on the Address Bus, all the signals on the microprocessor Inputs are read. On the rising edge of the special signal called Write, when the appropriate address of external module is present on the Address Bus, all signals from ALU are latched in the microprocessor Outputs. Signals Read and Write are the same to operate Memory and Input/Output Block. To distinguish these signals for external devices (by Input/Output Block), a special signal called Chip Enable is created. These signals (Read, Write, Chip Enable) are managed by Control Block. This block contains a crystal oscillator too. Program execution is synchronized by clock of Control Block.

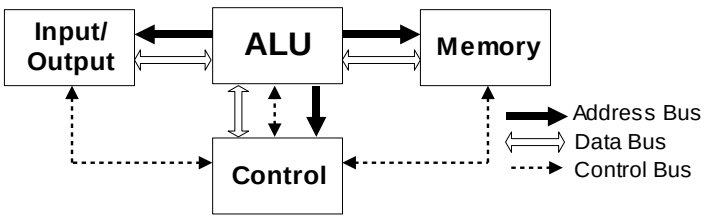

Fig. 1. The typical structure of microprocessor

2.2. SOFTWARE

First microprocessor programmes were very sophisticated. There were binary sequences (4 or 8 bits) - difficult to write and to remember. The next notation of a program is called assembler. Each binary sequence has its own mnemonic code. This code is similar to English words, for example: *move*, *ld* (load), *call*, *jmp* (jump) etc. But still programming is not so easy. There is one programme instruction for each hardware, arithmetical or logical operation. Only addition and subtraction operations are implemented in basic microprocessor. To obtain the other arithmetical operations for example multiplication, division or square rotation one must write a lot of basic instructions.

It is impossible to program well without perfect knowledge on microprocessor hardware. Many years ago somebody said: "To understand microprocessor it is necessary to know memory management and interrupt structure". And that is true. There are two popular memory architectures: von Neumann architecture and Harvard architec-

ture. The first one uses only one memory space, divided into three areas: instructions, data, and input/output. The second one uses separate memory space with almost the same addressing for instructions, data, and input/output areas, but with common memory and data buses. It means that there are three memory areas with exactly the same address. To distinguish these cells we have to use different instructions or different kinds of addressing. There are two ways of addressing: direct and indirect with many variants. For example in direct addressing we can use simply the address of register or the name of this register.

The most difficult in microprocessor management are interrupts. Interrupts service external events. The simplest example of interrupt using: we have to check voltage level of battery. Without interrupt, it is difficult to say how often we should check the voltage: once a week, but maybe once a minute. Once a week, it seems too seldom, because between two periods of checking, the battery can be discharged. Once a minute seems good, but it takes too much time of microprocessor working. Interrupt is in this example most convenient. The level of battery voltage is controlled by external analogue comparator with digital output and microprocessor is working normally without battery checking. When the voltage is too low, the comparator generates special digital signal to microprocessor interrupt system. And only now microprocessor breaks standard program to service this problem. There are many sources of interrupts and problems, when two (or more) interrupts are coming simultaneously. User should establish priority of interrupts. The interrupt service is the same like the subroutine service. So we should declare interrupt vector (assigning addresses in memory space) and write separate procedures for each interrupt. There is only one important difference: the place and time of interrupt calling are unpredictable.

2.3. INDUSTRIAL MICROPROCESSOR CONTROLLERS

Microprocessor controllers are utilized very often in industry. They are convenient and can substitute a lot of analogue control systems. They work more reliably, the construction is simpler and, finally, they are cheaper than analogue systems. But they have disadvantages too. To create even the simplest microprocessor controller, we have to know very good its hardware and software. The software is horrifying for some people. Assembler, often called “low level language”, is the difficult programming language. As a matter of fact we can use “high level languages” too, for example C language. Using of this language can simplify only arithmetical algorithms, because for example ”sine” function doesn’t exist in assembler. But the hardware programming is more difficult like in assembler, because in C language the bit operations, which are essential for input/output programming, are not implemented. And now a few words about hardware. The supply voltage is not typical, for example 3.3 V, and we have to design (or buy) special AC/DC adaptor. All digital outputs have very low level of current rating (about 1 mA), so it is impossible to operate external devices

without amplifier. Maximum level of digital input voltage is also limited, most frequently to TTL signals (5V). The hardware of microprocessor controller is very fragile and a special case resistant to atmospheric conditions is needed.

So the microprocessor controllers should be design only by specialists. And what about the other engineers?

3. PROGRAMMABLE LOGIC CONTROLLERS

The designer's answer could be only one: a special microprocessor controller adapted to industrial condition. This controller referred to as PLC (Programmable Logic Controller) is the standard microprocessor controller with special case resistant to industrial applications, with standard power supply 230 V AC or safe 24 V DC and with high level current rating outputs. There are two kinds of output: slow speed relay output with maximum current about 2…5 A or high speed open collector transistor output with maximum current about 1 A. The voltage range of digital input is also higher: 120 V AC or 24 V DC.

3.1. PLC SOFTWARE

There are more changes in software. Management of software is very simple. First of all, a user doesn't need to know controller's hardware to write a program. The main problems like memory addressing or interrupts in principle don't exist. Memory is divided into several areas. Each area has the same way of addressing, for example:

- register addressing MB23, where first letter means memory type (M – general purpose memory), the second one means size of the memory register (B – byte, W – word, D – double word). The number at the end means decimal number of memory cell.
- bit addressing Q2.6, where first letter means memory type (Q- output image register), first digit means decimal number of memory cell, the second one – number of bit in byte register.

This addressing system allows mixing different sizes of memory registers at any time (Fig. 2). The essential convenience results from available three very simple programming methods:

STL (Statement List) – very high level text language basis of mnemonic codes,

FBD (Function Block Diagram) – very high level graphical language basis of symbols like logical gates, flip-flops, etc.

LAD (Ladder Logic) - very high level graphical language based on symbols used in electrical engineering.

The third one allows direct and very easy transformation of electric circuit diagrams into PLC program implementation. The user can choose any programming language and, at any time, change it with automatic translation to new language. This is very important particularly when the program is written by many people working in interdisciplinary areas.

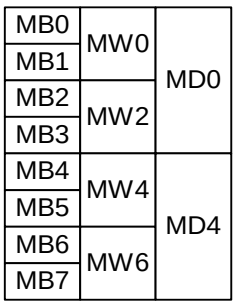

Fig. 2. PLC memory organisation

PLC executes programme in a continuous, cyclical series of tasks called a scan. The scan cycle for the CPU consists of the following tasks (Fig. 3):

- reading the inputs,
- executing the program,
- processing any communication requests,
- executing the CPU self-diagnostic test,
- writing to the outputs.

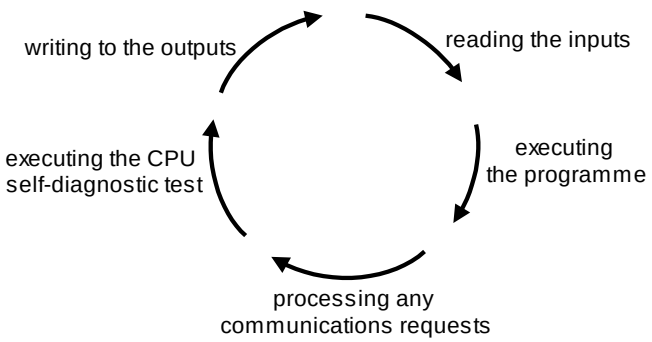

Fig. 3. Scan cycle of PLC

Self-diagnostic test, not implemented in classical microprocessor controllers, is very important. There are special immediate input/output instructions which allow direct access to the specified input or output signal excluding some scans like communication and diagnostic ones.

Power supply interruption handling is one of the biggest disadvantages of controller's operation. PLC offers three ways to avoid it. The first one is the application of the super capacitor with capacity about 1F which enables to store data in memory for about 50 hours. The second one is a dedicated lithium battery which enables to store data in memory for about 2 years. More important data can be stored in flash memory with unlimited time of data keeping. To make testing of production process without breaks possible some fragments of program can be exchanged without stopping the PLC. To test, for example, inactivated alarm system, some input or output can be frozen on specific value. PLC has possibility to communicate with external devices by a lot of standard communication protocols, for example: RS-485, Ethernet etc. The modular construction allows extending of PLC hardware very easily.

4. CONCLUSIONS

Classical microprocessor controllers are very convenient in automation process. However, very complex hardware and software discouraged potential users, in particular unskilled engineers, from applying them in industry. Very experienced specialists were needed for development and implementation of microprocessor controller programs.

Programmable Logic Controllers standardize almost all microprocessor controllers. Now even inexperienced engineer can use them.

REFERENCES

[1] KASPRZYK J., *Programowanie sterowników przemysłowych*, WNT, Warszawa, 2005.
[2] *ARM family microprocessors. User manual*, PHILIPS Publishing 2004.
[3] *Simatic S7-1200 microcontrollers. User manual*, SIEMENS Publishing 2010.

STEROWNIKI MIKROPROCESOROWE KONTRA PLC

W artykule opisano klasyczne sterowniki mikroprocesorowe oraz programowalne sterowniki logiczne PLC pod kątem ich użycia w aplikacjach przemysłowych. Zostały zaprezentowane podstawowe różnice zarówno w budowie sprzętowej jak i oprogramowaniu.

Keywords:
SF6 and vacuum circuit-breakers, small inductive currents, dielectric strength restoration, overvoltage, recovery voltage

Tahir LAZIMOV, Esam SAAFAN*

ON INTERACTION BETWEEN CIRCUIT-BREAKER AND NETWORK AT SMALL INDUCTIVE CURRENTS' SWITCHING-OFFS

Results of an investigation of interaction between circuit-breaker against its dielectric strength restoration law and parameters such as chop current and operation time (all conditioned by the circuit-breaker type and arc quenching medium) at small inductive currents' switch-offs are presented in this article. The results include curves of transitional voltages at switching under consideration and also conclusions on dependence of overvoltages and recovery voltages ratios on re-ignitions in inter-contact space. The results concerning investigation of stability are also presented. The analyzed methods were investigated from the point of view of stability in wide range of simulation parameters.

1. INTRODUCTION

Interaction between circuit-breaker and network means, in general, influence of circuit-breaker characteristics on transitional processes which may occur at circuit-breakers' switching. The minded problem has been investigated since 1970's of the last century (e.g. see [1, 2]). Note that the first researchers were mainly interested in the circuit-breakers design and construction in the view of transitional processes rather than in the influence of circuit-breakers themselves on the transient processes may take place in electric networks.

Switching-offs the small inductive currents in power systems were investigated for no-load transformers of rated voltage 110 kV. The equivalent networks used for the problem under consideration (e.g. see [3, 4]) have no great differences. The one presented in [4] and shown in Fig. 1 has been used in the analysis.

* Electric Supply and Insulation Chair, Azerbaijan Technical University, AZ1009, Baku, Azerbaijan.

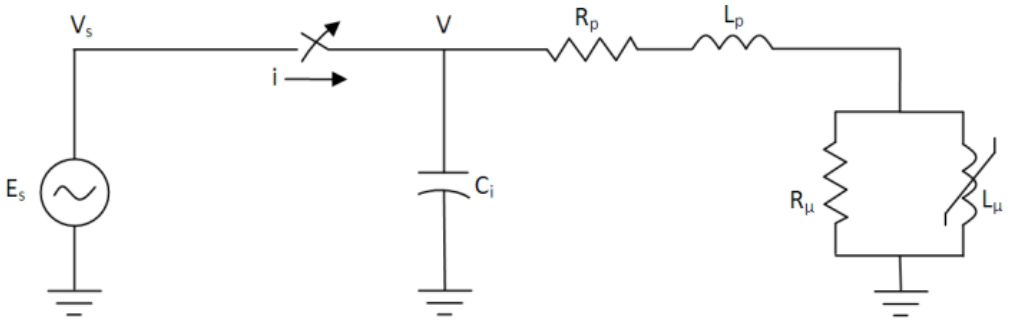

Fig. 1. Equivalent network

In Fig. 1 R_p is the transformer's primary resistance; L_p is the transformer's primary inductance; R_μ is the transformer's core resistance; L_μ is the transformer's core inductance; C_i is the transformer's input capacitance.

The maximum values of the chop current for SF6 circuit-breakers were determined depending on switched currents values in accordance with [5]. For vacuum circuit-breakers the maximum chop current given in [6] was used. This is due to that unlike auto-compression circuit-breakers vacuum ones have the chop current which does not depend on switched currents

For the modeling of dielectric properties of the inter-contact spaces the following laws have been used:

- the co-sinusoidal law of dielectric strength restoration in auto-compression (SF6) circuit-breakers presented in [7],
- the logarithmic law of dielectric strength restoration in vacuum circuit-breakers, as in [8].

For computer simulation of transitional processes conditioned by 110 kV no-load transformers switching-offs the MATLAB ode 23tb method and also 23t and 15s methods (see also [9]) have been mostly used. As it was stated earlier the ode 23tb method has given the best solutions from the point of view of stability for the problem considered in the article [9].

The parameters of the computer simulation such as initial step size, absolute and relative tolerances were chosen under the necessity to provide stability of the solution got. As it was shown in [9, 10] this is conditioned by stiffness of differential equations formalized currents and voltages and their first temporal derivatives for the transitional regimes of electric networks. The investigation of stability of computations is presented further.

Note that alike capacitive currents switching-offs the same commutation of small inductive currents is one of the most dangerous regimes from the point of view of influence on insulation of electric systems and circuit-breakers themselves.

2. RESULTS OBTAINED AND DISCUSSION

Numerous runs of computer simulations of no-load transformer (autotransformer) switching-off process realized the known models described in [3, 4] for the cases of switched current less or equal to chopping current of circuit-breaker have been carried out. Description of the gotten results follows.

The greatest ratios of overvoltages and recovery voltages take place at absence of repeated re-ignitions in inter-contact space during the contacts separation time. It means that maximum values of overvoltages and recovery voltages at switching-off small inductive current may depend just on the circuit-breaker chop current and transformer input capacitance and no-load regime inductance. Note that for capacitive currents switching-off there is more complicated dependence of overvoltages and recovery voltages on appearance and number of repeated re-ignitions which causes overvoltages [3, 11]. In the same time too great number of repeated re-ignitions may even limit the overvoltage ratios at switching-off capacitive currents of capacitor banks [12].

In Fig. 2 and Fig. 3 the calculated curves of transitional voltages at switching-off the transformer (ТД type, rated apparent power 31.5 MVA, rated voltage of switched winding 110 kV) by the SF6 circuit-breaker with chop current 6.11 A and vacuum circuit-breaker with chop current 5 A (for chrome-copper contacts) are presented, respectively. As it seems from the obtained results there takes place greater values of overvoltage and recovery voltage for the SF6 circuit-breaker. It is conditioned by the greater value of the chop current for the SF6 circuit-breaker in the network under consideration in comparison with vacuum ones equipped with chrome-copper contacts [5]. If accept the same values of chop current for either kind of circuit-breaker we would get the strongly same ratios at absence repeated re-ignitions. Also for the vacuum circuit-breakers with copper-bismuth contacts one will get greater overvoltages and recovery voltages than for SF6 circuit-breakers [5]. It is conditioned by the minded fact on correspondence of maximum overvoltages and recovery voltages to the condition of absence of repeated re-ignitions. As a result, a transitional process at maximum V and ΔV does not depend on dielectric strength restoration law which is the most important factor determining interaction between a circuit-breaker and a network. In Fig. 4 the calculated curves of transitional voltages for the switching-off process accompanied with repeated re-ignitions (at SF6 circuit-breaker use) are presented. Note that for all the cases accompanied with repeated re-ignitions ratios of overvoltages and recovery voltages are less than the ones presented in Fig. 2 and Fig. 3. One may also conclude that use of vacuum circuit-breakers with copper-bismuth contacts for switching of transformers and autotransformers is not expedient.

Value of the chop current has generally a significant influence on ratios of overvoltages and inter-contact recovery voltages at switching-offs small inductive currents of no-load transformers and autotransformers. In Fig. 5 the calculated curves of transi-

tional voltages at switching-off the 110 kV winding of the ТД type transformer of apparent rated power 31.5 MVA by the SF6 circuit-breaker with chop current 4 A for the case of absence of repeated re-ignitions (i.e. for the worst case) are given. Comparing curves of V and ΔV presented in Fig. 2 and Fig. 5 one can state that less value of chop current causes less magnitudes of overvoltage and inter-contact recovery voltage. The differences are equal to 24% for V and 38% for ΔV. Remind that values of chop current depend on circuit-breaker camera's construction and contacts' material [13] (see also the previous conclusion). For auto-compression SF6 circuit-breakers it also depends on amplitude of switched-off current [5].

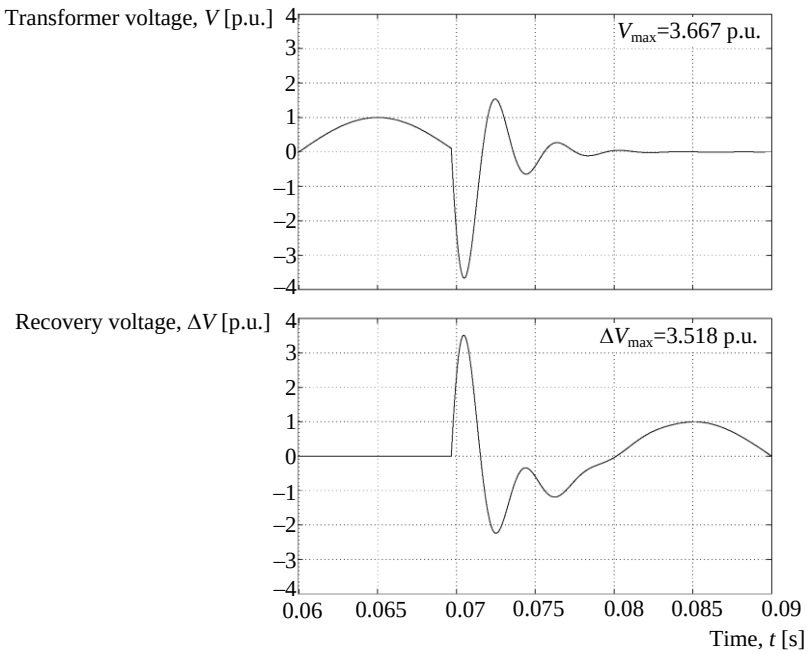

Fig. 2. Transient voltages at switching-off transformer of 31.5 MVA, 110 kV by SF6 circuit-breaker (with no repeated re-ignitions)

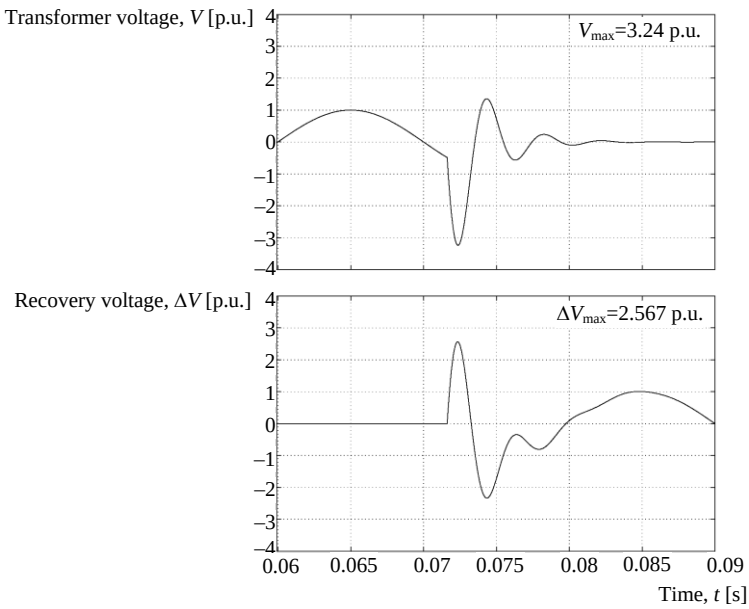

Fig. 3. Transient voltages at switching-off transformer of 31.5 MVA, 110 kV by vacuum circuit-breaker (with no repeated re-ignitions)

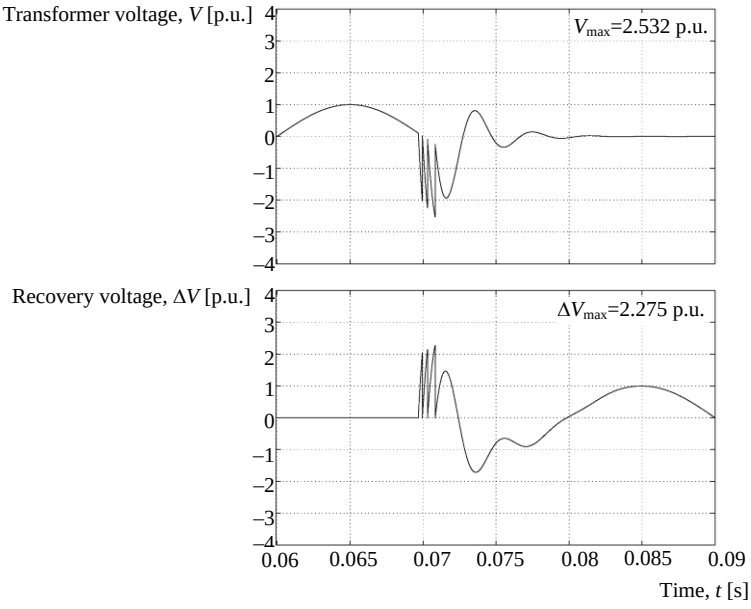

Fig. 4. Transient voltages at switching-off transformer of 31.5 MVA, 110 kV by SF6 circuit-breaker (with repeated re-ignitions)

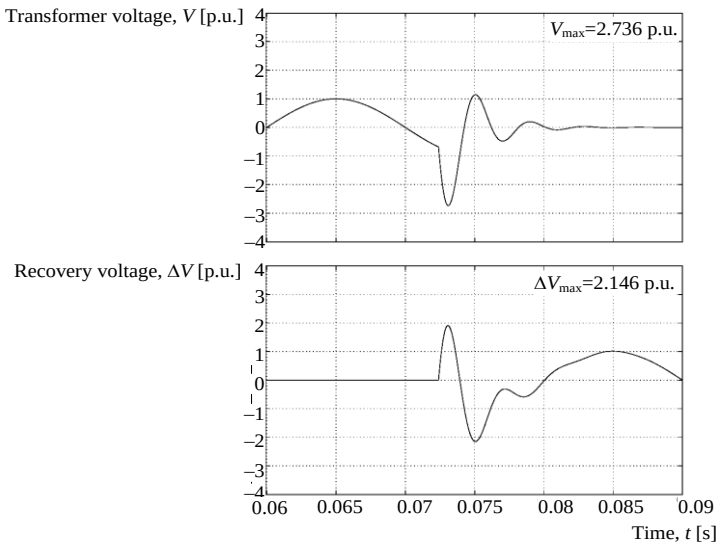

Fig. 5. Transient voltages at switching-off transformer of 31.5 MVA, 110 kV by SF6 circuit-breaker with less chop current (with no repeated re-ignitions)

As it was stated earlier the ratios of overvoltages while switching-off small inductive currents of no-load transformers and autotransformers of rated voltages 110-220 kV do not exceed triple value [4]. However, our last research led for transformers and autotransformers of wide range apparent powers has let us to find out that in only case for the ТД type (Ukraine produced) transformer of 31.5 MVA, 110 kV the overvoltage ratio has prevailed triple value of rated voltage. These cases are presented in Fig. 2 and Fig. 3. Note that both overvoltage ratio and inter-contact recovery voltage of the considered transformer may exceed the allowable voltage of high voltage networks. It is conditioned by relatively little value of no-load inductance of this type of transformer and correspondingly by relatively great free frequency and free oscillations of transitional voltages. For the considered cases of relatively small chopping currents (less or equal to chopping current of circuit-breaker) an interruption takes place at equality of chopping current and amplitude of switched current.

3. INVESTIGATION OF STABILITY

Computer simulation of transitional processes in electrical systems is based on solution of differential equations systems. Switching conditions is usually given due to logical conventions. Both differential equations and logical conventions form mathematical model of problem under consideration [4].

As it is known differential equations formalized mathematically transitional processes in electrical systems concern to the class of so called "stiff" differential equations [10]. Obtaining solutions of "stiff" differential equations and their systems may face with stability problems because that, just for this kind of equations the minded problem is serious enough [13, 14].

The calculated ratios of overvoltages and recovery voltages for the case of absence repeated re-ignitions corresponded to Fig. 2 for wide ranges of tolerance and initial step size are given in Tables 1, 2 and 3. In the tables results obtained at use of the ode23tb, ode23t and ode15s methods are presented, respectively.

Analyzing computer simulation results from the computational point of the following remarks have been stated.

All the methods used give the same stable values of V and ΔV at the initial step size equal to 0.1 μs. The maximum deviations (by modules) from stable solution for all the ranges of tolerance and initial step size are less than 2% by overvoltages and less than 3% by recovery voltages. The least deviation from the stable solutions took place at use the ode23tb method (less than 0.5% by V and less than 1.8% by ΔV). The greatest deviations took place for the initial step size 0.1 ms.

Behavior of recovery voltage is less stable in comparison with overvoltage function and calculated values of ΔV have greater deviation in comparison with V. It means that at computer simulation of transitional processes under consideration stability of whole problem must be evaluated by stability of recovery voltage function.

Change of calculated values V and ΔV is more uniform at fixed initial step size and tolerance varied than at fixed tolerance. This may be taken into account at computer simulation. Note that the same conclusion were presented in [9] for the problem of capacitive currents switching-off.

The carried out investigations have shown that realization of simulation at appearance of arc repeated re-ignitions becomes more difficult from the point of view of stability. E.g. realization of the ode15s method for initial step size 10^{-4} s becomes impossible, deviations of V and ΔV from their stable values become greater for all the considered methods.

Table 1. Calculated ratios of overvoltages (V) and recovery voltages (ΔV) for wide ranges of tolerance and initial step size at use ode23tb, $V/\Delta V$

Step size	Tolerance			
	10^{-6}	10^{-5}	10^{-4}	10^{-3}
10^{-7}	3.667/3.518	3.667/3.518	3.667/3.518	3.667/3.518
10^{-6}	3.667/3.518	3.668/3.518	3.668/3.517	3.668/3.517
10^{-5}	3.675/3.504	3.671/3.512	3.677/3.498	3.677/3.498
10^{-4}	3.669/3.514	3.680/3.489	3.679/3.485	3.677/3.455

Table 2. Calculated ratios of overvoltages (V) and recovery voltages (ΔV) for wide ranges of tolerance and initial step size at use ode23t, $V/\Delta V$

Step size	Tolerance			
	10^{-6}	10^{-5}	10^{-4}	10^{-3}
10^{-7}	3.667/3.518	3.667/3.518	3.667/3.518	3.667/3.518
10^{-6}	3.668/3.518	3.668/3.517	3.668/3.517	3.667/3.518
10^{-5}	3.669/3.515	3.669/3.514	3.675/3.501	3.667/3.504
10^{-4}	3.607/3.449	3.672/3.506	3.667/3.513	3.675/3.467

Table 3. Calculated ratios of overvoltages (V) and recovery voltages (ΔV) for wide ranges of tolerance and initial step size at use ode15s, $V/\Delta V$

Step size	Tolerance			
	10^{-6}	10^{-5}	10^{-4}	10^{-3}
10^{-7}	3.667/3.518	3.667/3.518	3.667/3.518	3.667/3.518
10^{-6}	3.668/3.517	3.668/3.517	3.668/3.518	3.668/3.519
10^{-5}	3.673/3.504	3.674/3.499	3.677/3.496	3.668/3.513
10^{-4}	3.661/3.427	3.681/3.419	3.672/3.486	3.675/3.440

4. CONCLUSIONS

This paper presents results of computer simulation of transitional processes at small inductive currents switching-offs.

It was stated that at switching-off of no-load inductive currents (less than circuit-breaker chopping current) the greatest overvoltages and recovery voltages take place at absence of arc repeated re-ignitions. There was shown that for only kind of transformer (ТД type of 31.5 MVA, 110 kV) ratios of overvoltages and recovery voltages at switching under consideration can exceed the triple value i.e. permissible level although for all the other types the minded level is not exceeded.

Concerning to stability it was stated that all the methods of computer simulation provide stable results at initial step size 0.1 μs and worst results at 0.1 ms. It was also found that recovery voltage is more sensitive to variations of simulation parameters and recommended to evaluate solutions' stability by the stability of recovery voltage.

REFERENCES

[1] KLAUS RAGALLER, *Current interruption in high voltage networks*, Plenum Press, New-York, 1978.

[2] EL-AKKARI F. R., TUMA D. T., *Simulation of transient and zero current behavior of arcs stabilized by forced convection*, IEEE Transaction on PAS, 1977, vol. 96, No. 6, 1784–1788.

[3] VAN DER SLUIS L., *Transients in power systems*, New-York: John Wiley & Sons, 2001.

[4] LAZIMOV T. M., AKHUNDOV S. A., *Research on influence of high voltage circuit-breakers' characteristics on switching overvoltages and overcurrents*, Proceedings of the Third International Conference on Electrical and Electronics Engineering ELECO'2003, Bursa, Turkey, 2003, 1–4.
[5] RUBEN D. GARZON, *High voltage circuit breakers design and applications*, New-York: Marcel Dekker, 2002.
[6] YEVDOKUNIN G. A., TILER G., *Modern vacuum switching apparatus for medial voltages*, M.P. Sizov publisher, Sankt-Petersburg, 2002 (in Russian).
[7] LAZIMOV T. M., AKHUNDOV S. A., *Modeling of electrical strength of high voltage circuit-breakers*, Proceedings of the International Symposium SIEMA'2001, Kharkov, Ukraine, 2001, 112–-114 (in Russian).
[8] MAMMADOV H., LAZIMOV T., IMANOV S., *Improved model of vacuum circuit-breaker's dielectric strength restoration*, Proceedings of the ELECO'09 International Conference on Electrical and Electronic Engineering, Bursa, Turkey, 2009.
[9] LAZIMOV T.M., IMANOV S.V., *On stability while simulating the switching-offs the capacitive and small inductive currents*, Proceeding of the MEPS'06 International Symposium. Wroclaw, Poland, 2006, 407–410.
[10] LAZIMOV T., AKHUNDOV S., *Peculiarities of transients' simulation in electrical circuits*, Proceedings of the Republican Conference on IT, Baku, Azerbaijan, 2003.
[11] BICKFORD J. P., MULLINEUX N., REED S. R., *Computation of power system transients*, Peter Peregrinus Ltd. England, 1976.
[12] MIRONOV G. A., JAFAROV E. M., LAZIMOV T. M., et al. *Overvoltages conditioned by switching-offs of capacitor banks equipped by protecting devices*, Electricity, 1979, No. 11(in Russian).
[13] SHAMPINE L. F., *Numerical solutions of ordinary differential equations*, Chapman and Hall, New-York, 1994.
[14] HAIRER E., NORSETT S. P., WANNER G., *Solving ordinary differential equations*, Part 1, Springer-Verlag, Berlin, Heidelberg, New-York, London, Paris, Tokyo, 1987.

O WZAJEMNYM ODDZIAŁYWANIU WYŁĄCZNIKA I SIECI PODCZAS WYŁĄCZEŃ MAŁYCH PRĄDÓW INDUKCYJNYCH

W artykule przedstawiono rezultaty badania wzajemnego powiązania rodzaju wyłącznika oraz prawa odbudowy wytrzymałości dielektrycznej i jego parametrów (determinowanych rodzajem wyłącznika oraz zastosowanym medium gaszenia łuku), takich jak prąd ucięcia oraz czas wyłączenia podczas wyłączania małych prądów indukcyjnych. Badania dotyczyły określania napięć przejściowych podczas rozważnych operacji łączeniowych oraz zależności przepięć i napięć powrotu na ponowne zapłony w przestrzeni między biegunami wyłącznika. Przedstawiono również rezultaty badań stabilności obliczeń, przeprowadzonych w szerokim zakresie parametrów symulacji.

Keywords:
current differential criterion,
current transformer, fuzzy logic, saturation

Krzysztof SOLAK*, Waldemar REBIZANT*

DIFFERENTIAL PROTECTION WITH BETTER STABILIZATION FOR EXTERNAL FAULTS

This paper presents a new differential protection scheme for transmission lines with application of fuzzy signal processing and support of phase comparison criterion. Traditional differential relays may have problems with proper classification of external faults with CT saturation. Better protection stabilization for such cases is obtained with support of fuzzy signal processing. In proposed solution the input signals as well as the standard percentage characteristic are fuzzified. The performance of presented fuzzy protection scheme has been tested with the signals generated with use of EMTP-ATP program and compared to the traditional solution.

1. INTRODUCTION

Current differential protection is one of the first relays that were developed and put into service. Its main advantage is reliable and fast detection of internal faults. Therefore, it is used to protection of various elements in power systems, i.e. power transformers, generators, busbars and transmission lines. The zone of action of differential relay embraces only protected object, which means that differential relay should trip for internal faults only and restrain for all external disturbances. This is the main requirement differential protection must meet.

The basic operating principle of current differential criterion (in accordance with the Kirchhoff's current law) is to compare currents flowing into the object with the currents flowing out of the object at the other end(-s) [1]. Generally in standard solution the current differential signal is calculated according to following formula [2]:

* Wroclaw University of Technology, Institute of Electrical Power Engineering, 50-370 Wroclaw, Wybrzeze Wyspianskiego 27, krzysztof.solak@pwr.wroc.pl, waldemar.rebizant@pwr.wroc.pl.

$$I_d = |\underline{i}_1 + \underline{i}_2 + ... + \underline{i}_k| \tag{1}$$

where: $\underline{i}_1$, ..., $\underline{i}_k$ –secondary current phasors (from CTs) measured at *k*-terminals, I_d – amplitude of differential current.

The value of differential current amplitude for internal faults is much greater than zero, while for external faults and normal operation of protection object should be negligible. This case is purely theoretical. In practice, the value of differential current amplitude may also be greater than zero for external faults which may lead to protection maloperation. This situation is caused by CT errors which are due to high value of fault current amplitude or/and decaying DC components in fault currents. To improve the selectivity of protection operation for external faults with CTs saturation the restraint current (4) and stabilized characteristic is used. Fig. 1 presents the typical two-segment stabilized characteristic which can be described by (2) and (3) [2]. The first section of this characteristic (k_1) is responsible for detecting of internal faults (especially via high resistance). However, the second part of characteristic (k_2) is used to improve protection stability for external faults with CT saturation [2]. In standard solution the trajectory of differential/bias currents is tracked with respect to the relay characteristic to determine whether or not to trip the transmission line. The tripping command is initiated if:

$$|I_d| \geq I_{op} = k_1 \cdot |I_{st}| + I_{d0} \quad \text{for} \quad |I_{st}| \leq I_{s2} \tag{2}$$

$$|I_d| \geq I_{op} = k_2 \cdot |I_{st}| - (k_2 - k_1) \cdot I_{s2} + I_{d0} \quad \text{for} \quad |I_{st}| \geq I_{s2} \tag{3}$$

$$I_{st} = \sum_{j=1}^{k} |\underline{i}_j| \tag{4}$$

where: I_{st} – amplitude of restraint current, I_{d0} – minimum pick-up level of the protection, I_{s2} – the threshold value determines which part of characteristic k_1 or k_2 is used, k_1 – the lower percentage restraint setting, k_2 – the higher percentage restraint setting.

Generally, CT errors due to saturation should be compensated for by conventional stabilized characteristic with adequate slope setting. However, when there is a mismatch in CTs' load or they have non-identical magnetizing characteristics or/and residual flux, a possibility still exists that one of the CTs may saturate and not the other, which may lead to protection malfunction.

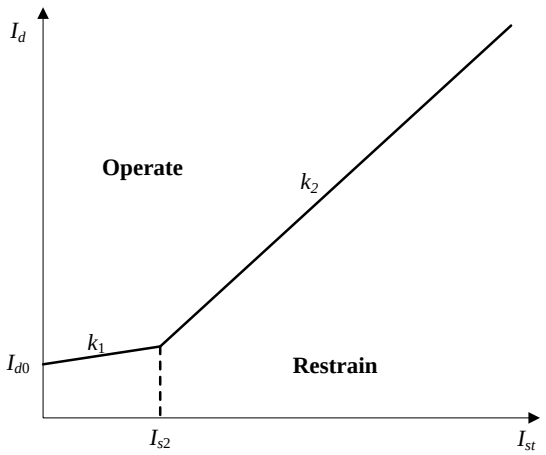

Fig. 1. Stabilized characteristic of the current differential relay

Several approaches may be found in the literature, that according to the authors, should improve performance of the line differential relays. The solution presented in [1] is based on the so called phaselets ("partial" Fourier signals) and variable window Fourier transform as well as variance-based measurement confidence calculation that is used for dynamical adaptation of the relay percentage restraint, which should bring improvement in sensitivity. The other idea described in [4] makes use of adaptive time-dependent restraint coefficients that define the shape of percentage differential curve. A method based on zero-sequence component for detection of current transformer saturation is proposed in [9]. In order to better improve stabilization of the differential protection harmonics of differential current may be used (e.g. second and/or fifth) [5] or a method which identifies CTs saturation (i.e. employing second or third derivative of secondary current) [6]. Since also the cited solutions do not guarantee proper operation of the relay for all fault cases, new protection ideas are still needed to fulfill the gap, especially if the CT saturation evoked errors are concerned.

Therefore, there is a need for an improved algorithm for protecting transmission lines with better stabilization for external faults cases, yet with maintained sensitivity and operation speed for internal faults requiring prompt tripping. Therefore, the authors of this paper focused on the development of the new algorithm (described in section II) that improves the performance of differential protection for external faults with CTs saturation.

2. STABILIZATION SCHEME FOR DIFFERENTIAL PROTECTION

Classical (Boolean) logic based on the concept of truth/falsity cannot effectively cope with the many ambiguities that arise during operation of the power system. Therefore, fuzzy logic is increasingly being used in decision-making, whereas the

criteria signals are described by membership functions. The use of fuzzy logic increases the confidence of the decision-making within an area of uncertainty, since the fuzzy logic can deal better (as compared to Boolean logic) with suspense and missing data. In addition, inferencing with multiple objectives in such systems is a natural way of processing information – it is therefore utterly possible to use numerous criteria in parallel.

Fig. 2 presents the structure of the new fuzzy protection. The main idea of action relies on fuzzification of differential current I_d that is further compared with fuzzy setting obtained on the basis of the stabilized characteristic (Fig. 1). Additionally, the criterion of phase difference is introduced, value of which affects the degree of fuzziness of fuzzy setting. Below the various blocks of scheme from Fig. 2 are described in detail.

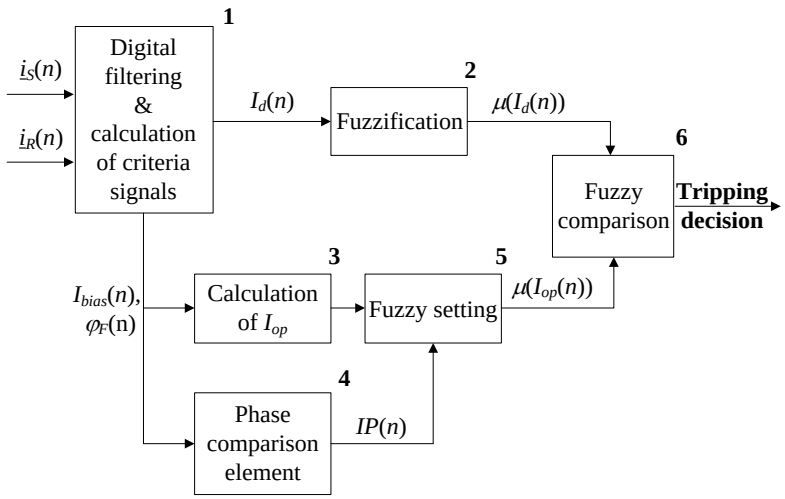

Fig. 2. Block scheme of the fuzzy adaptive differential protection of transmission line

Digital filtering and calculation of criteria signals (block 1) – here the main criteria signals (differential current I_d (3), bias current I_{bias} (3) and phase difference φ_F) are calculated with use of full cycle Fourier filters. The variable φ_F can be expressed by the formula based on negative sequence currents from both line terminals:

$$\varphi_F = 180^{\circ} - \left| \arg \frac{\underline{i}_{2S}}{\underline{i}_{2R}} \right| \tag{5}$$

which is well suited for effective discrimination of asymmetrical faults [7].

Unfortunately, the negative sequence current cannot provide identification of three-phase faults. Therefore, for symmetrical faults the phase difference φ_F is calculated on the basis of positive sequence current as follows:

$$\varphi_F = 180^o - \left| \arg \frac{\underline{i}_{1S}}{\underline{i}_{1R}} \right|. \tag{6}$$

A three-phase fault is detected using overcurrent element tracking the level of restraint currents in all phases.

Symmetrical components of the signals can be calculated according to the well known matrix formula:

$$\begin{bmatrix} \underline{i}_{0S(R)} \\ \underline{i}_{1S(R)} \\ \underline{i}_{2S(R)} \end{bmatrix} = \frac{1}{3} \begin{bmatrix} 1 & 1 & 1 \\ 1 & a & a^2 \\ 1 & a^2 & a \end{bmatrix} \begin{bmatrix} \underline{i}_{L1S(R)} \\ \underline{i}_{L2S(R)} \\ \underline{i}_{L3S(R)} \end{bmatrix}, \tag{7}$$

where: a=exp(j2π/3), $i_{0S(R)}$, $i_{1S(R)}$, $i_{2S(R)}$ – zero, positive, negative sequence currents at the *S* and *R* ends, $i_{L1S(R)}$, $i_{L2S(R)}$, $i_{L3S(R)}$ – phase currents at the *S* and *R* ends of the line.

Measuring of phase difference is initiated when the differential current is greater than or equal to I_{d0} in any phase.

Fuzzification (block 2) – magnitude of differential current (3) is fuzzified, which means that triangular membership functions is formed by using minimum I_{min}, average I_{av} and maximum I_{max} values of differential current (it was assumed that these values were calculated for a quarter of fundamental frequency cycle):

$$I_{\min}(n) = \min_{k=0 \div (N/4)-1} \{I_d\ (n-k)\} \tag{8}$$

$$I_{av}(n) = \frac{1}{N/4} \sum_{k=0}^{(N/4)-1} I_d\ (n-k) \tag{9}$$

$$I_{\max}(n) = \max_{k=0 \div (N/4)-1} \{I_d\ (n-k)\} \tag{10}$$

here: N – number of samples per cycle of the fundamental harmonic (here N=20).

An example of how the fuzzification of differential current proceeds is shown in Fig. 3. Based on five samples of magnitude of differential current (Fig. 3(a)) the adequate values are calculated according to equations (8), (9) and (10). Next, the triangle membership function is formed as shown in Fig. 3(b).

Calculation of I_{op} (block 3) – the value of operation current is calculated according to equations (2) and (3) – based on restraint current I_{st}.

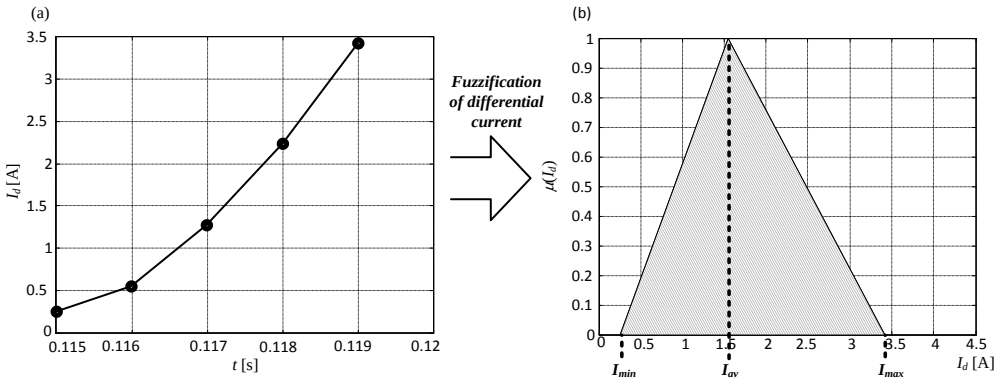

Fig. 3. Fuzzification of differential current:(a) magnitude of differential current, (b) fuzzy differential current

Phase comparison element (block 4) – here the calculated phase difference, (5) or (6), is compared with the operation characteristic (see Fig. 4(b)). The adequate threshold values of the characteristic have been set according to the statistical information gained through analysis of generated simulation signals. One can see (Fig. 4(a)) that basing on this criterion signal it is possible to define two regions: operation and restraint. The output value *IP* from phase comparison element influences fuzzification of the operation current. If the output value is close to 1.0 it indicates an external fault. Otherwise (internal fault cases) the output is close to 0.

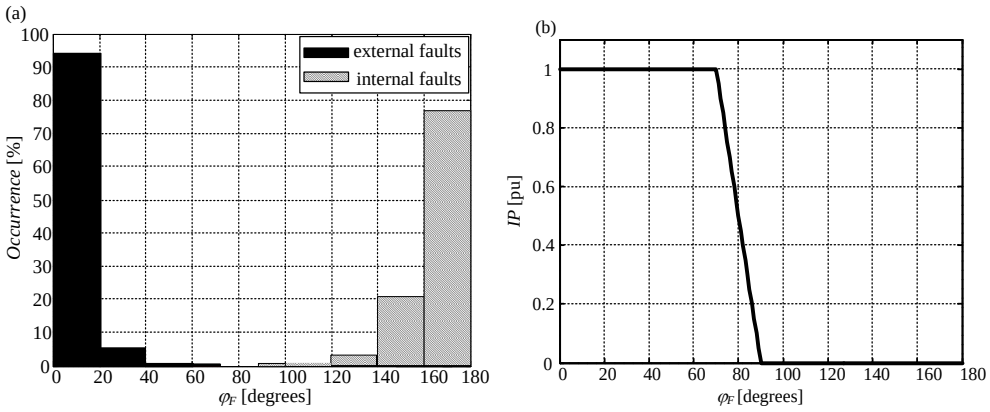

Fig. 4. Statistical information (a) and operation characteristic (b) for phase difference

Fuzzy setting (block 5) – based on the actual value of operation current and information from phase comparison block the fuzzy setting is formed as it is illustrated in Fig. 5(a). The parameters δ_1 and δ_2 determine the shape of membership function of fuzzy setting, being calculated according to:

$$\delta_1 = IP \cdot I_{st} + 0.1 \qquad \delta_2 = 1.5 \cdot IP \cdot I_{st} + 0.3 \tag{11}$$

The values of parameters in (10) are small (δ_1=0.1 and δ_2=0.3) for *IP*=0 (this value indicates internal fault) which means that membership function is slightly fuzzy. When *IP*=1 (this value indicates external fault) both parametres are high and the membership function of fuzzy setting is quite broad.

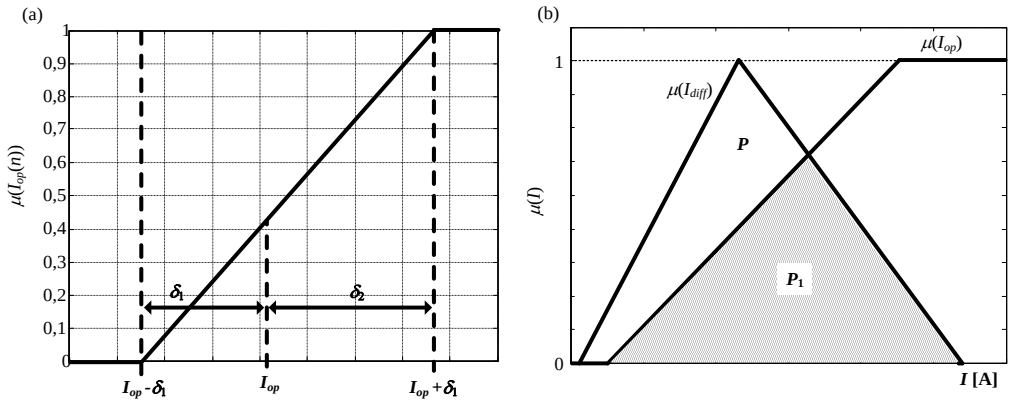

Fig. 5. Formation of fuzzy setting (a) and fuzzy comparison illustration (b)

Fuzzy comparison (block 6) – in this block both membership functions fuzzy differential current $\mu(I_d)$ and fuzzy setting $\mu(I_{op})$ are compared with each other (Fig. 5(b)). The value of fuzzy comparison is determined by:

$$P_d = \frac{\int \min[\mu(I_d), \mu(I_{op})] dI}{\int \mu(I_d)\, dI} = \frac{P}{P_1} \tag{12}$$

where P - the area under the membership function of differential current $\mu(I_{\mathrm{d}})$ and P_1 - surface area (hatched) under both the fuzzy setting $\mu(I_{\mathrm{op}})$ and $\mu(I_{\mathrm{d}})$, [8].

The final decision to trip a protected transmission line is taken when the value of index P_d is greater than threshold 0.7.

Below testing results of two different types of protection versions (standard differential relay [2] and fuzzy adaptive scheme proposed) are presented.

3. TESTING OF DEVELOPED FUZZY PROTECTION SCHEME

The tests were performed on the ATP-EMTP model as shown in Fig. 6. It consists of two 5P30 20VA 1000/1A CTs which were modeled using the TYPE-96 pseudo-nonlinear element [3]. In this model there is a possibility to set the residual flux in the CT core, which is very important for studying CT saturation effects [9]. It was assumed that CT_A is the reference CT (never saturated) and CT_B is the saturable CT.

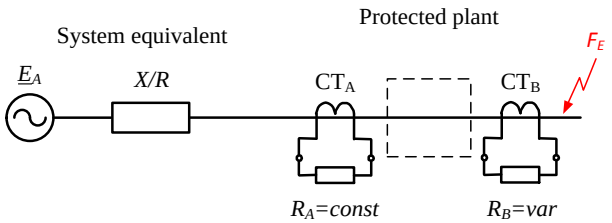

Fig. 6. ATP-EMTP test model

The adequate value of the CT knee voltage can be calculated according to the following equation [5]:

$$V_k > K \cdot I_s \cdot \left(1 + \frac{X}{R}\right) \cdot Z \tag{13}$$

where: I_s – nominal secondary current, K – multiples of secondary current (fault level), system X/R ratio, Z – current transformer burden.

In some cases (for high value X/R ratio and fault level), the fulfilment of this condition is impossible (very high value of knee voltage) because it would imply the CT with large core diameter, which is uneconomical. Therefore, it is important that differential protection works properly even when the CTs saturate.

This test was to prove that the new method is more immune to CT saturation than the standard relay. In the test the following parameters that affect the saturation of CT were being changed:

- system X/R ratio ($X/R = 10 \div 120$),
- multiples of secondary current ($K = 5 \div 35$),
- burden of CT_B ($R_B = 1 \div 25\Omega$),
- point on wave (maximum current offset).
- residual flux in the CT core (0 or ±0.7 of saturation flux).

The testing results proved that the proposed scheme is stable for external faults (zero percent of incorrect operation). Contrary, the standard protection failed for a few percent of external fault cases. Figs. 7-8 present an extreme example generated for the

following parameters assumed: K = 35, RB=25 Ω, X/R = 120. As one can see the CTB gets deeply saturated, especially in phase L1 (Fig. 7(a)) and the standard protection based on the stabilized characteristic with fixed settings maloperates, since the differential-restraining trajectory (phase L1) enters the tripping zone (Fig. 7(b)), thus the trip command is sent to the circuit breakers (Fig. 8(c)). For this case the phase comparison element output was high (Fig. 8(a)) since the value of calculated phase difference was low (not greater than 40 degrees), which implies an external fault. The response of the phase comparison element affected the shape of fuzzy setting membership function, which became much broader. As one can see the proposed algorithm remained fully stable here, without issuing false tripping command (Fig. 8(d)).

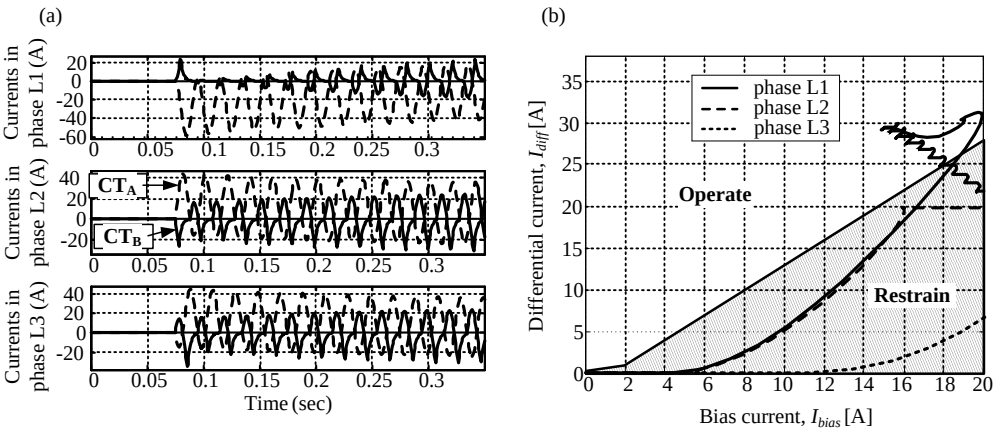

Fig. 7. Testing example: (a) line terminal current waveshapes, (b) protection stabilized characteristic and I_d-I_{st} trajectory

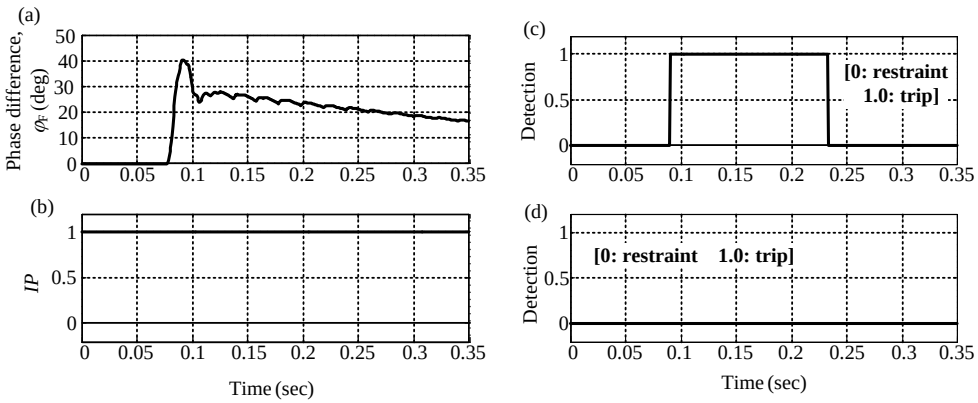

Fig. 8. Testing example: (a) calculated phase difference φ_F, (b) phase comparison element response, (c) standard differential protection response, (d) fuzzy differential protection response

4. CONCLUSIONS

The solution for improvement of the line differential protection operation for external fault cases with possible CT saturation is described in the paper. For better stabilization under external faults a method employing fuzzy signal processing and phase comparison element is proposed to be used. The tests performed prove that the developed algorithm remains stable for external faults under all conditions, including heavily saturated current transformers. This method can also be used for protection of other power system elements, e.g. busbars or generators.

REFERENCES

[1] ADAMIAK M.K., PREMERLANI W., *A New Approach to Current Differential Protection for Transmission Lines*, GE publication GER-3981, 1998.
[2] AREVA. *P54x Application Guide*, 2005.
[3] DOMMEL H.W., *Electromagnetic Transients Program. Reference Manual (EMTP theory book)*, Bonneville Power Administration, Portland 1986.
[4] GANG W., BAOJI Y., JIALI H., LI K.K., *Implementation of Adaptive Dispersed Phase Current Differential Protection for Transmission Lines*, Proceedings of the 5th International Conference on Advances in Power System Control, Operation and Management, APSCOM 2000, Hong Kong, October 2000, pp. 64–69.
[5] IEEE C.37.110, *IEEE guide for the application of current transformers used for protective relaying purposes*, 2007.
[6] KANG Y., KANG S., CROSSLEY P., *An algorithm for detecting CT saturation using the secondary current third-derivative function*, Proceedings of the IEEE Bologna PowerTech Conference, 23–26 June 2003, pp. 320–326.
[7] KASZTENNY B., VOLOH I., UDREAN E.A., *Rebirth of the Phase Comparison Line Protection Principle*, 59th Annual Conference for Protective Relay Engineers, 4-6 April 2006, pp. 193–252.
[8] REBIZANT W., WISZNIEWSKI A., SCHIEL L., *Acceleration of Transformer Differential Protection with Instantaneous Criteria*, Proceedings of International Conference on Advanced Power System Automation and Protection, Korea, 24–27 April 2007, CD-ROM, paper 505.
[9] VILLAMAGNA N., CROSSLEY P.A., *A CT Saturation Detection Algorithm Using Symmetrical Components for Current Differential Protection*, IEEE Transactions on Power Delivery, Vol. 21, No. 1, JANUARY 2006, pp. 38–45.
[10] WARD S., ERWIN T., Current Differential Line Protection Setting Considerations, RFL Electronics Inc, 2005.

ZABEZPIECZENIE RÓŻNICOWE Z LEPSZĄ STABILIZACJĄ DLA ZWARĆ ZEWNĘTRZNYCH

W artykule zaprezentowano nowe zabezpieczenie różnicowe, w którym zastosowano rozmyte przetwarzanie sygnałów oraz dodatkowe kryterium porównawczo-fazowe. Proponowane zabezpieczenie jest bardziej odporne na zwarcia zewnętrzne z nasyceniem przekładników prądowych, co potwierdziły przeprowadzone testy. Proponowany algorytm testowany był na sygnałach pochodzących z symulacji w EMTP-ATP, a wyniki porównano ze standardowym przekaźnikiem różnicowym.

Keywords:
fault detection, modelling of induction motor,
transient simulation, internal turn to turn fault

Maciej WIECZOREK*, Eugeniusz ROSOLOWSKI*

SIMULATION ANALYSIS OF INDUCTION MOTOR TURN-TO-TURN FAULTS IN STATOR WINDINGS

Accurate and flexible computer model of an induction motor is a very important tool for diagnosis and fault protection algorithms investigation. This paper presents a new method for internal inter-turn faults in an induction motor stator windings. General approach to inter-turn faults representation in such machines is discussed. The simulation model is implemented in ATP-EMTP programme by using of Type-94 element. The aim of the provided simulation is to investigate new algorithms for induction motor internal fault protection under different conditions. Included examples demonstrate basic characteristics of the proposed model and its application for internal fault analysis in the complex system included motor, load and a supplying network.

1. INTRODUCTION

Damage of stator insulation is the most frequent failure in electrical motor. Protection of the induction motor against different internal faults would limit the fault duration and prevent motor from substantial damage, what is particularly important for higher motor ratings. Diagnosis of faults in electrical motors is a very important function, which enables to protect the motor against the results of disruptions. In order to design an algorithm, which will effectively eliminate this kind of disruptions; it is necessary to make a proper model of the motor.

Traditional models of electrical machines are based on electrical circuit equations and equations of motion (circuit model). Mathematical model of induction motor described in this way is composed of differential and algebraic equations. Generally, it is an arrangement of high order set of equations containing nonlinear functions. The

* Wroclaw University of Technology, Institute of Electrical Power Engineering, Wybrzeze Wyspianskiego 27, 50 – 370 Wroclaw, maciej.wieczorek@pwr.wroc.pl, rose@pwr.wroc.pl

model is extremely hard to use directly [10].

Loss of power in one of the phases is often caused by mechanical tension and vibrations. Vibrations can lead to loosening of the screws on the machine's terminal or mechanical tensions, consequently leading to the loss of power in one of the phases. Turns to turn faults are caused by different factors affecting stator directly. For example, mechanical tensions during assembly or while machine is working, and also by partial discharges caused by high voltage among the turns, can cause damage to the insulation, and in consequence the flow of short circuit current. Various solutions are available in literature for detection of internal faults [1]-[5], [9], [10]. Efficient motor protection should detect all possible faults and isolate the motor in order to minimize the damage size. Common method for investigation of the process involved is based on application of suitable computer models.

Widely used computer models have a close connection with mathematical models. Obtained results based on these models of computer simulation are more and more reliable and because of that, play an important part in designing and testing of the devices themselves, and also relating to them automatics systems.

The squirrel cage motor was chosen for further investigation. The model was prepared in the ATP – EMTP simulation program [6]. Included examples demonstrate basic characteristics of the proposed model and the detection results obtained using the proposed protection algorithm.

2. SIMULATION OF TURN TO TURN FAULTS IN STATOR WINDINGS

Let us consider turn-to-turn fault on phase A. Winding in this phase is divided on two parts – un – faulted turns winding section μ_{us} and shorted turns winding μ_{sh}, as in Fig. 1. Phase B and C have the same number of turns as the phase A.

If the number of turns in all three stator phases is the same, we can apply basic model to describe a mathematical model of induction motor with turn-to-turn fault [12].

The model of a faulty motor can be derived from standard relations (1). Flux equations of induction motor with turn-to-turn fault in *abc* system take the following form [11]:

$$\begin{aligned}
\frac{d\boldsymbol{\phi}_{sABC}}{dt} &= \mathbf{u}_{sABC} - \mathbf{r}_s\left(\mathbf{i}_{sABC} - \boldsymbol{\mu}_{ABC} i_f\right) \\
\frac{d\boldsymbol{\phi}_{rABC}}{dt} &= -\mathbf{r}_r\,\mathbf{i}_{rABC} \\
\boldsymbol{\phi}_{sABC} &= \mathbf{L}_s\left(\mathbf{i}_{sABC} - \boldsymbol{\mu}_{ABC} i_f\right) + \mathbf{L}_m(\theta)\mathbf{i}_{rABC} \\
\boldsymbol{\phi}_{rABC} &= \mathbf{L}_m^T(\theta)\left(\mathbf{i}_{sABC} - \boldsymbol{\mu}_{ABC} i_f\right) + \mathbf{L}_r\mathbf{i}_{rABC}
\end{aligned} \tag{1}$$

where vectors $\mathbf{u}_{sABC}$, $\mathbf{i}_{sABC}$ and $\boldsymbol{\lambda}_{sABC}$ represent stator voltages, currents and flux. $\mathbf{i}_{rABC}$ and $\boldsymbol{\lambda}_{rABC}$ are currents and flux of rotor. As a symmetrical machine is considered, it is assumed: $\mathbf{r}_s = r_s\mathbf{I}$ and $\mathbf{r}_r = r_r\mathbf{I}$, where $\mathbf{I}$ is identity matrix. $\boldsymbol{\mu}_{ABC} = [\mu_{sh}\ 0\ 0]^{\mathrm{T}}$ is a vector representing position of turn-to-turn fault in the stator circuit.

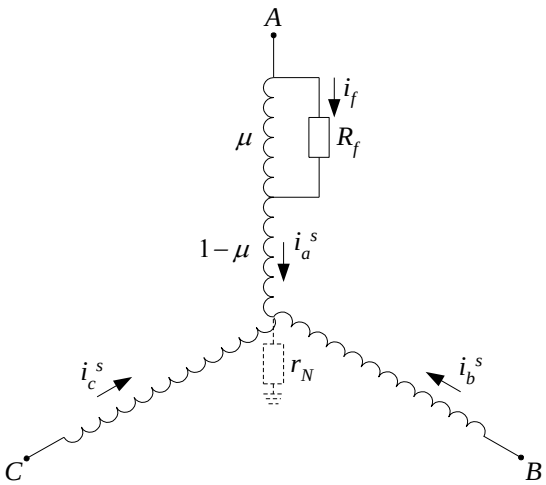

Fig. 1. Three phase stator winding with turn to turn fault in phase A

The flux in circuited part of winding *A* can be calculated according to the following equation:

$$\frac{d\phi_{sha}}{dt} = R_f i_f - \mu_{sh} r_s (i_{sA} - i_f) \tag{2}$$

where i_f – short-circuit current (Fig. 1).

Transforming above equations into $\alpha\beta 0$ coordinates, with taking into consideration of (2), one can obtain:

$$\begin{aligned}
\frac{d\boldsymbol{\phi}_{s\alpha\beta 0}}{dt} &= \mathbf{u}_{s\alpha\beta 0} - \mathbf{r}_s \left(\mathbf{i}_{s\alpha\beta 0} - \mathbf{T}_{\alpha\beta 0}\boldsymbol{\mu}_{\alpha\beta 0} i_f\right) \\
\frac{d\boldsymbol{\phi}_{r\alpha\beta 0}}{dt} &= -\mathbf{r}_r \mathbf{i}_{r\alpha\beta 0} + z_p \omega_r \mathbf{K}\boldsymbol{\phi}_{r\alpha\beta 0} \\
\frac{d\phi_{sh\alpha}}{dt} &= R_f i_f - \mu_{sh} r_s (i_{s\alpha} - i_f)
\end{aligned} \tag{3}$$

where fluxes are given by:

$$\begin{aligned}
\boldsymbol{\phi}_{s\alpha\beta 0} &= \mathbf{L}_s\left(\mathbf{i}_{s\alpha\beta 0} - \mathbf{T}_{\alpha\beta 0}\boldsymbol{\mu}_{\alpha\beta 0} i_f\right) + \mathbf{L}_m \mathbf{i}_{r\alpha\beta 0} \\
\boldsymbol{\phi}_{r\alpha\beta 0} &= \mathbf{L}_m\left(\mathbf{i}_{s\alpha\beta 0} - \mathbf{T}_{\alpha\beta 0}\boldsymbol{\mu}_{\alpha\beta 0} i_f\right) + \mathbf{L}_r \mathbf{i}_{r\alpha\beta 0} \\
\phi_{sh\alpha} &= \mu_{sh} l_{ls}\left(i_{s\alpha} - i_f\right) + \mu_{sh} L_m\left(i_{s\alpha} + i_{r\alpha} - \frac{2}{3}\mu_{sh} i_f\right)
\end{aligned} \tag{4}$$

and: $\boldsymbol{\mu}_{\alpha\beta 0} = [\mu_{sh}\ 0\ 0]^{\mathrm{T}}$, $\mathbf{u}_{s\alpha\beta} = [u_{s\alpha}\ u_{s\beta}\ u_{s0}]^{\mathrm{T}}$, $\mathbf{i}_{s\alpha\beta} = [i_{s\alpha}\ i_{s\beta}\ i_{s0}]^{\mathrm{T}}$, $\boldsymbol{\phi}_{s\alpha\beta} = [\phi_{s\alpha}\ \phi_{s\beta}\ \phi_{s0}]^{\mathrm{T}}$, and $\mathbf{i}_{r\alpha\beta} = [i_{r\alpha}\ i_{r\beta}\ i_{r0}]^{\mathrm{T}}$, $\boldsymbol{\phi}_{r\alpha\beta} = [\phi_{r\alpha}\ \phi_{r\beta}\ \phi_{r0}]^{\mathrm{T}}$ are adequately voltages, currents, flux matrix of stator and currents, flux matrix of rotor [7]; $\mathbf{r}_s$, $\mathbf{r}_r$, $\mathbf{L}_s$, $\mathbf{L}_r$, $\mathbf{L}_m$ are diagonal matrix at the size of (2 x 2); $\mathbf{K} = \begin{bmatrix} 0 & -1 & 0 \\ 1 & 0 & 0 \\ 0 & 0 & 0 \end{bmatrix}$.

Mechanical part of induction motor in $\alpha\beta 0$ system is described by:

$$J\frac{d\omega_r(t)}{dt} = T_{em} - T_m \tag{5}$$

$$T_{em} = \frac{3}{2} z_p\left(\phi_{s\alpha} i_{s\beta} - \phi_{s\beta} i_{s\alpha}\right) - z_p \mu_{sh} \phi_{s\alpha} i_f \tag{6}$$

Intensity level of turn to turn faults in this model can be adjusted through the change of number of shorted turns and resistance (r_f), limiting short current.

3. TURN – TO – TURN FAULTS PROTECTION ALGORITHM

3.1. ISOLATED STAR POINT OF STATOR WINDINGS

Proposed protection algorithm is based on the information contained in the symmetrical components – especially negative sequence component of current and difference angle of space vectors (α and β) voltages and currents of stator. Negative sequence components of current gives information that the modeled system state is not allowed. However, this component occurs when the fault is both external and internal. Therefore, it additionally uses information that comes from impedance angle, which is calculated from the spatial vectors voltages and current of stator.

Transforming the phase currents and voltages to a stationary system of coordinates $\alpha\beta$ is realized by:

$$i_{s\alpha} = \frac{2}{3} i_{sA} - \frac{1}{3}\left(i_{sB} + i_{sC}\right)$$
$$i_{s\beta} = \frac{1}{\sqrt{3}}\left(i_{sB} - i_{sC}\right) \tag{7}$$

$$u_{s\alpha} = \frac{2}{3} u_{sA} - \frac{1}{3}\left(u_{sB} + u_{sC}\right)$$
$$u_{s\beta} = \frac{1}{\sqrt{3}}\left(u_{sB} - u_{sC}\right) \tag{8}$$

where: i_{sA}, i_{sB}, i_{sC} – currents of stator in phase A, B, C; u_{sA}, u_{sB}, u_{sC} – phase voltages; $i_{s\alpha}$, $i_{s\beta}$ – stator current space vector components and $u_{s\alpha}$, $u_{s\beta}$ – supplying voltage space vector components.
The impedance angle is obtained from:

$$\underline{Z} = \frac{\underline{U}}{\underline{I}} \Rightarrow |Z| e^{j\varphi_z} = \frac{|u_{\alpha\beta}| e^{j\varphi_u}}{|i_{\alpha\beta}| e^{j\varphi_i}} = \frac{|u_{\alpha\beta}|}{|i_{\alpha\beta}|} e^{j(\varphi_u - \varphi_i)} \tag{9}$$

$$\varphi_z = \varphi_u - \varphi_i \tag{10}$$

where: $\varphi_u = \arg(u_\alpha, u_\beta)$, $\varphi_i = \arg(i_\alpha, i_\beta)$, $\underline{U} = u_\alpha + j u_\beta$, $\underline{I} = i_\alpha + j i_\beta$.

During symmetrical steady-state the impedance angle φ_z is close to 0, otherwise this angle carries the following information:

$$\varphi_z \Rightarrow \begin{cases} > \varphi_0 \text{ then internal fault} \\ < -\varphi_0 \text{ then external fault} \end{cases} \tag{11}$$

where: φ_0 - a threshold value.

3.2. EARTHED STAR POINT OF STATOR

In this case it is proposed to apply the zero-sequence of motor voltage and current at the motor terminal. The fault in this power network is identified by the appearance of zero sequence components of stator voltage u_0. But the voltage u_0 occurs when the fault is both external and internal. Therefore, additionally uses information that comes from current angles of symmetrical components (negative and zero).

Zero sequence component of stator voltage and angles of symmetrical components are calculated by:

$$u_0 = \frac{1}{3}\left(u_{sA} + u_{sB} + u_{sC}\right) - u_N \tag{12}$$

$$\varphi_{I_2} = \arg\left(\mathrm{Im}(I_2), \mathrm{Re}(I_2)\right)$$
$$\varphi_{I_0} = \arg\left(\mathrm{Im}(I_0), \mathrm{Re}(I_0)\right) \tag{13}$$

Proper combination of pairs of angles, allows to identify the type of faults. If $\varphi_{I_2} \in \left(-\frac{\pi}{2}, 0\right)$ and $\varphi_{I_0} < \frac{\pi}{2}$ then fault is internal. In the other cases, the damages (faults, voltage unbalance, open phase) are external.

4. SIMULATION RESULTS

The squirrel cage induction motor was used in the simulation tests. That was the motor of 2 MW power with supply voltage 10 kV and electrical parameters: stator resistance r_s = 0.3607 Ω, stator inductance x_{ls} = 0.011482 Ω, rotor resistance, r_r = 1.1685 Ω, rotor inductance x_{lr} = 0.011482 Ω, mutual inductance x_m = 0.494 Ω. Structure of simulation model is presented in Fig. 5.

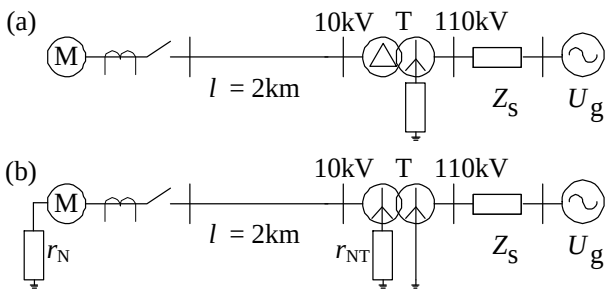

Fig. 2. Structure of simulation model (a) isolated star point of stator, (b) earthed star point of stator

The aim of simulation was to verify the given assumptions and to check the obtained results with a similar data available from the literature. It is considered to further use of this model for investigation of protection algorithms. Selected waveforms obtained during simulations are presented below.

In the first part of simulations the inter-turn fault was considered, in the system with isolated of the star point of stator. Simulation parameters r_f = 0.1 Ω, $T_m = T_N$. Some results can be track at Figs. 3–6. The fault included 1%, 5% and 50% of stator phase A winding was introduced at t = 0.04 s. Fig. 3. shows very interesting case because number of shorted turns is equal 1% and voltage (Fig. 3(a)) and current waveshapes (Fig. 3(b)) do not carry information, that fault in the motor has occurred. It is well known that appearance of the negative sequence current at the supplied current is a good detector of an turn - to - turn fault. However, this information is not sufficient,

because the external faults would be detected. Therefore the algorithm additionally uses information that comes from φ_z. This case presents a challenge for designer of protective algorithm, because despite this fault is very difficult to detect.

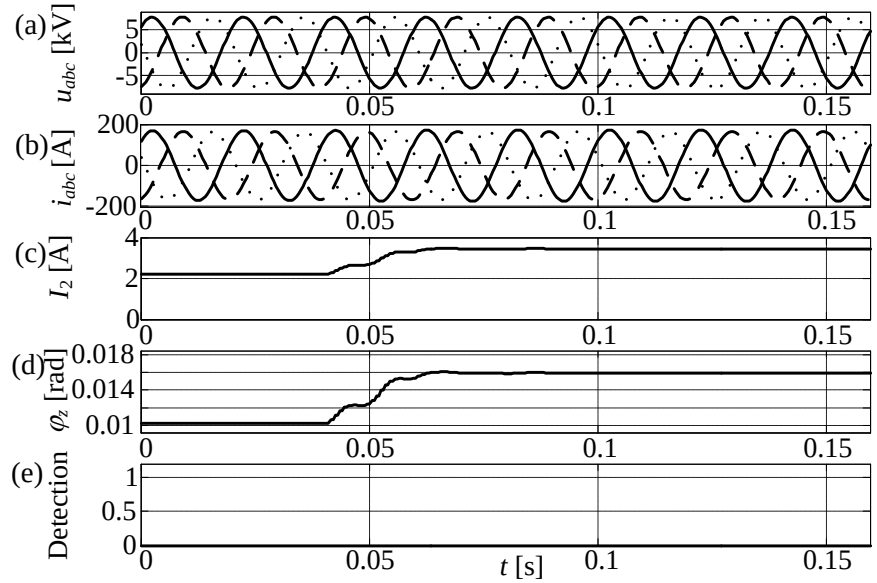

Fig. 3. Turn to turn fault in the stator, isolated star point of stator, μ = 1%, (a) voltages of stator, (b) currents of stator, (c) negative sequence component of current, (d) impedance angle, (e) detection efficiency

Figs. 4-5 present other fault situations. It can be seen, that with an increase in the number of shorted turns, criteria signals I_2 and φ_z can effectively eliminate these faults.

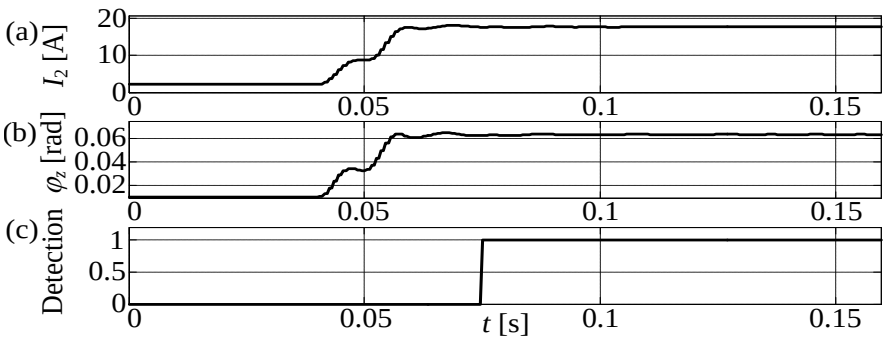

Fig. 4. Turn to turn fault in the stator, isolated star point of stator, μ = 5%, (a) negative sequence component of current, (b) impedance angle, (c) detection efficiency

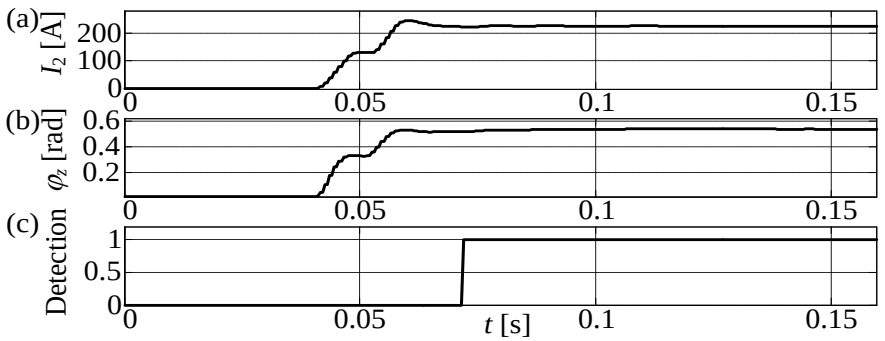

Fig. 5. Turn to turn fault in the stator, isolated star point of stator, μ = 50%, (a) negative sequence component of current, (b) impedance angle, (c) detection efficiency

Fig. 6 shows external fault. At the time of fault, angle φ_z is less than zero, but after inception of disturbance its value is fixed (Fig. 6(b)) over 1.5 period. This situation prevents proper working of the protection. Therefore, the detection time delay introduced - 30 ms.

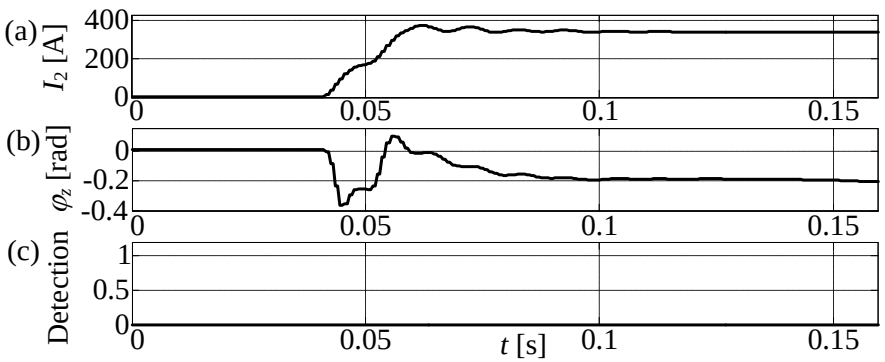

Fig. 6. External fault, isolated star point of stator, r_f = 1 Ω, (a) negative sequence component of current, (b) impedance angle, (c) detection efficiency

In the second part of simulations the inter–turn fault was considered, in the system with earthed of the star point of stator. Simulation parameters r_f = 0.1 Ω, r_N = 10 Ω, $T_m = 0.5T_N$. Some results can be track at Figs. 7 – 10. The fault included 1%, 5% and 50% of stator phase A winding was introduced at t = 0.04 s. Criteria signals used in the algorithm U_0, φ_{I2}, φ_{I0}, give information that effectively detects internal faults (Fig. 7(c), 8(c), 9(c)) simultaneously block external faults (Fig. 10(c)). Time delay (20 ms) was introduced – (as above) because of the transient state in the waveform angle φ_{I2} occurred (Fig. 10(b)).

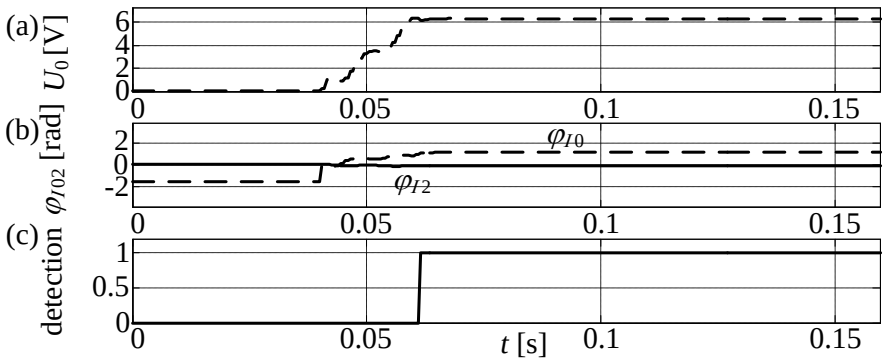

Fig. 7. Turn to turn fault in the stator, earthed star point of stator, r_f = 0.1 Ω, μ = 1%, (a) negative sequence component of current, (b) impedance angle, (c) detection efficiency

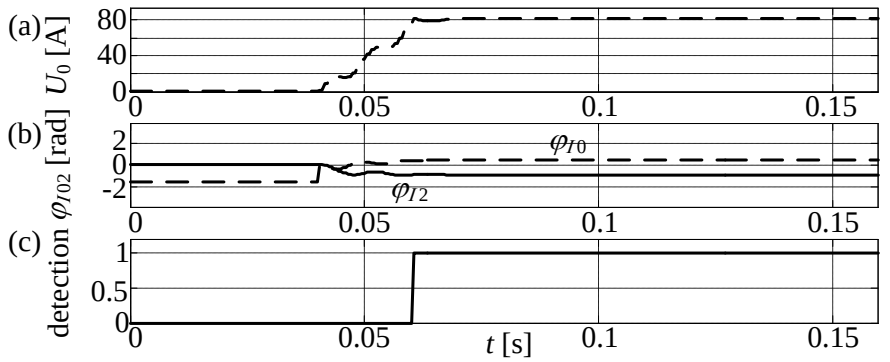

Fig. 8. Turn to turn fault in the stator, earthed star point of stator, r_f = 0.1 Ω, μ = 5%,(a) negative sequence component of current, (b) impedance angle, (c) detection efficiency

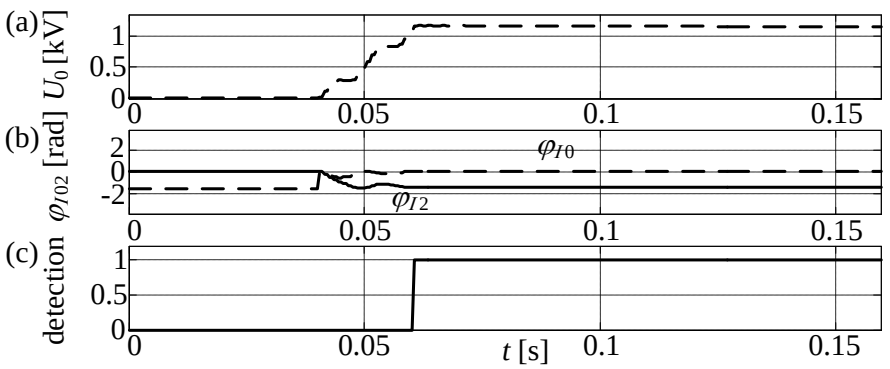

Fig. 9. Turn to turn fault in the stator, earthed star point of stator, r_f = 0,1Ω, μ = 50%, (a) negative sequence component of current, (b) impedance angle, (c) detection efficiency

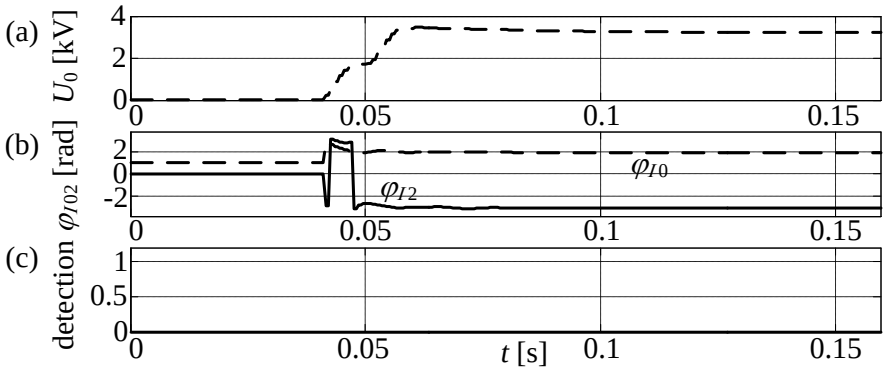

Fig. 10. External fault, earthed star point of stator, r_f = 1Ω, (a) negative sequence component of current, (b) impedance angle, (c) detection efficiency

5. CONCLUSIONS

The problems related to modelling of turn - to - turn faults in induction motors, and their detection are presented in the paper. The fault model was prepared by using of the ATP – EMTP program. Protection algorithm was tested also by using of the ATP – EMTP. Included simulation results show its fundamental properties during transients. It can be concluded that the proposed method gives a handy to use tool which enables to analyse the fault induced transients in induction machines. The future works will focus on improvement the effectiveness of the protection algorithm by choosing new criteria signal or new decision making method.

REFERENCES

[1] ARKAN M., PEROVIC D. K., UNSWORTH P. J., *Modelling and simulation of induction motors with inter-turn faults for dignostics*, Electric Power Systems Research 75, 2005, pp.57–66.

[2] ARKAN M., PEROVIC D. K., UNSWORTH P. J., *Online stator fault diagnosis in induction motors*, IEDEE proceedings on electrical power applications, Vol. 148, No. 6, 2001, pp.537–547.

[3] BRIZ F., DEGNER M. W., ZAMARRON A., GUERRERO J. M., *On-line stator winding fault diagnosis in inverter-fed ac machines using high frequency signal injection*, 37th IAS Annual Meeting and World Conference on Industrial applications of Electrical Energy, 2002, pp.2094–2101.

[4] CRUZ S. M. A., CARDOSO A. J. M., *Stator winding fault diagnosis in three-phase synchronous and asynchronous motors, by extended park's vector approach*, IEEE Transaction on Industrial Applications, Vol. 37, No. 5, 2001, pp.1227–1233.

[5] CASH M. A., HABETLER T. G., KLIMAN G. B., *Insulation failure prediction in induction machines using line-neutral voltages*, IEEE Industry Applications Conference, Thirty-Second IAS Annual Meeting, IAS '97, 1997, pp.208–212.

[6] DOMMEL H. W., Electromagnetic Transients Program Reference Manual. BPA, Portland, Oregon, 1986.

[7] DUBÉ L., *How to use MODELS-based User-defined network components in ATP*. EEUG News, No. 1, vol. 3, Feb. 1997, pp. 43-51.
[8] ESZTERGALYOS J., KOSTEREV D., DUBÉ L., *The application of user defined induction machine models in EMTP*, IPST'99 – International conference of power system transient, Budapest – Hungary 1999, pp.247–252.
[9] GARCIA P., BRIZ F., DENGER M. W., DIEZ A. B., *Diagnostics of induction machines using the zero sequence voltage*, Proceedings of the IEEE 39th IAS Annual Meeting, Seattle, Washington, 2004, pp.34–41.
[10] LEE S. B., TALLAM R. M., HABETLER T. G., A robust, on-line turn-fault detection technique for induction machines based on monitoring the sequence component impedance matrix, IEEE Transactions on Power Electronics, Vol. 18, No. 3,2003, pp.865–872.
[11] TALLAM R. M., HABETLER T. G., HARLEY R. G., Transient model for induction machines with stator winding turn faults, IEEE Transactions on Industry Applications, Vol. 38, No 3 2002, pp.632–637.
[12] THOMSEN J. S., KALLESOE C. S., Stator fault modelling of induction motors International Symposium on Power Electronics, Electrical drives, Automation and motion, Speedam 2006, pp.6–11.
[13] WIECZOREK M., ROSOŁOWSKI E., Modelling of induction motor for simulation of internal faults, Modern Electrical Power System MEPS, Wroclaw 2010.

ANALIZA SYMULACYJNA ZWARĆ ZWOJOWYCH W UZWOJENIU STOJANA SILNIKA INDUKCYJNEGO

W artykule przedstawiono propozycje dwóch algorytmów detekcji zwarć wewnętrznych zwojowych w silnikach indukcyjnych średniego napięcia. Analizę przeprowadzono z użyciem cyfrowego modelu zawierającego model silnika, umożliwiający symulowanie zwarć wewnętrznych. Przedstawiono także wpływ charakteru uziemienia punktu gwiazdowego stojana na skuteczność detekcji tego rodzaju zakłóceń. Zamieszczono przykłady symulacji zwarć wewnętrznych zwojowych zawierających różną liczbę zwojów objętych zwarciem w sytuacji, kiedy punkt gwiazdowy jest izolowany lub uziemiony. Model symulacyjny jak i proces testowania algorytmów zabezpieczeniowych zostały wykonane w programie ATP/EMTP.

Keywords: phase-locked loop, orthogonal signal generator, frequency estimation, phase-angle detection, power electronics controller

Michal WYSZOMIRSKI*, Eugeniusz ROSOLOWSKI*

PHASE-LOCKED LOOP TECHNIQUE SYSTEM WITH ORTHOGONAL SIGNAL GENERATOR FOR POWER ELECTRONICS CONTROLLERS

This paper presents a Phase-Locked Loop (PLL) scheme with Orthogonal Signal Generator (OSG). The proposed technique enables to eliminate the influence of distortions from the observed signal on proper determination of its parameters as a phase, magnitude or frequency. A simulation model of the system is developed and results of investigation are provided. Some recommendations on the scheme settings for elimination of harmonic and inter-harmonic components are also included. It was verified that the proposed PLL with OSG system can be considered as an useful and effective tool in implementations that require a great accuracy of the phase angle and frequency estimation. The system could be applied in three-phase power systems control units such as FACTS converters or doubly-fed induction generators control scheme. Simulation results demonstrate the effectiveness and robustness of the proposed solution.

1. INTRODUCTION

Almost all power electronic converters such as FACTS have indispensable component called a Phase-Locked Loop (PLL). IEEE defined the Flexible Alternating-Current Transmission Systems (FACTS) as "ac transmission systems incorporating power electronics-based and other static controllers to enhance controllability and increase power transfer capability" [2]. A most often structure PLL used in power electronics converters is the three-phase PLL based on dq-frame signals. For distortion-free input signal, this PLL estimates the input phase-angle without any double-

* Wroclaw University of Technology, Institute of Electrical Power Engineering, Wybrzeze Wyspianskiego 27, 50 – 370 Wroclaw, michal.wyszomirski@pwr.wroc.pl, rose@pwr.wroc.pl

frequency ripple in the loop. When the input is unbalanced or distorted the three-phase PLL does not provide the proper phase-angles.

Conventional single-phase PLL suffers from the presence of second-harmonic ripples. Such distortions do not appear for three-phase PLL due to the symmetry of the dq transformation for balanced signals. When input signals are unbalanced the three-phase PLL suffers from double-frequency ripples like for conventional single-phase PLL. The second-order harmonics can effectively be eliminated by included filters but this delaying the time response. An alternative PLL system that does not generate any double-frequency ripple was introduced in [4]. The paper presents an interesting scheme that is not based on the PLL at all [5], [6]. However, this method is vulnerable to inaccuracy due to the voltage disturbance.

This paper proposes a novel structure of the PLL scheme with the orthogonal signal generator which is tolerable under input signal disturbances. Generally, the proposed solution is based on schemes presented in [1], [7] but the new structure has essentially better characteristics. This new system may be used to estimate phase-angles of individual phases in case of unbalanced inputs.

The paper is organized as follows. First, a review of the PLL technique applied to signal estimation is presented. Then the proposed solution is presented in details. It was shown that it is capable to fundamentally remove all the impacts of harmonic/inter-harmonic components. Simulations compare the structures and verify performance of proposed structures. Finally, some concluded remarks are stated.

2. BASIC SCHEME CONSTRUTION OF PHASE-LOCKED LOOP

Principle of the PLL with reference to harmonic signals is well-known in the radio-engineering and the telecommunication [3]. The conventional scheme of the PLL is shown in Fig. 1. Phase Detector (PD) is composed of a multiplier block, which realizes of the following operation:

$$u_d = K_d \cdot u_1 \cdot u_2 = \frac{K_d U_1 U_2}{2} \sin\left(\theta_1(t) - \theta_2(t)\right) + \frac{K_d U_1 U_2}{2} \sin\left(2\omega t + \theta_1(t) + \theta_2(t)\right) \quad (1)$$

where: $u_1 = U_1 \sin\left(\omega t + \theta_1(t)\right)$, $u_2 = U_2 \cos\left(\omega t + \theta_2(t)\right)$, K_d - gain coefficient.

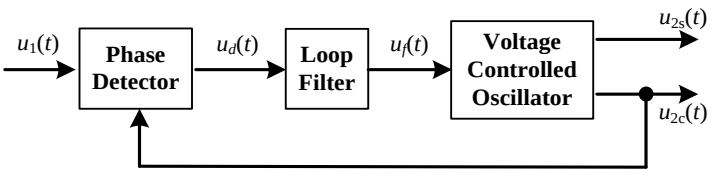

Fig. 1. Conventional PLL system

It can be seen from (1) the output of PD consist of two signals from which the first describes a function of a phase shifting between the input signals, while the second part depicts an oscillatory component of double frequency. This component is next filtered-out in a low-pass Loop Filter (LF) has a low-pass characteristic. Remaining dc component of the form:

$$u_f(t) = \frac{K_d U_1 U_2}{2} \sin\left(\theta_1(t) - \theta_2(t)\right) \tag{2}$$

is delivered to the Voltage Controlled Oscillator (VCO) which generates the harmonic orthogonal signals $u_{2c}(t)$ and $u_{2s}(t)$ of the unity magnitude and the frequency:

$$\omega_c = \omega_0 + K_v u_f(t) \tag{3}$$

where Kv is a gain and ω_0 is a nominal (reference) frequency.

The signal u_f (t) is called a VCO control signal. According to (3) the relation $\omega_c = \omega_0$ occurs if the signal u_f (t) is equal to zero (full synchronization).

Instantaneous phase of the PLL output signal can be determined according to the following expression:

$$\theta_2(t) = 2\pi K_v \int_0^t u_f(t)dt \tag{4}$$

Range of changes in the output waveform with respect to the central pulse of generator ω_0 for which synchronization is achieved is called the capture range. If the pulsation of the input signal exceeds the pulsation range of capture, the loop is not able to bring to the synchronous state of two waveforms.

Basic dependencies of the conventional PLL are used to create new systems that estimate the input phase-angle without any double-frequency ripple in the loop. Single-phase system with such properties is the PLL magnitude estimator [5], [6] and the PLL with orthogonal signal generator (OSG) [1]. PLL with magnitude estimator is shown in Fig. 2. This system combines conventional PLL and the magnitude estimator

in the external feedback loop. More detailed description of the system shown in Fig. 2 can be found in [5], [6], [7].

Phase Locked Loop can be also combined with an Orthogonal Signal Generator (GSO) as in Fig. 3. This system is composed of conventional PLL and the orthogonal signal generator.

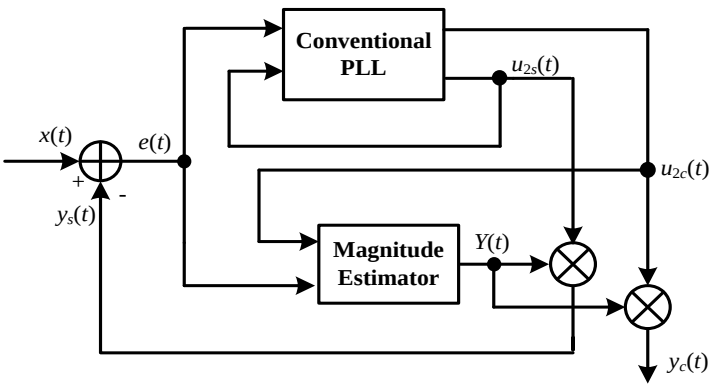

Fig. 2. PLL with magnitude estimator [5], [6], [7]

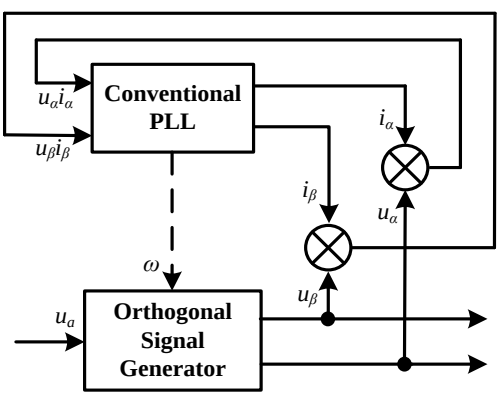

Fig. 3. PLL with orthogonal signal generator [1], [7]

Frequency from the conventional PLL is used in GSO. Structure of GSO is shown in Fig. 4. This scheme is based on the second order generalized integrator (SOGI) [1]. It can be seen that the system has a simple structure. Moreover, it is also independent on changing of the grid frequency.

Waveforms in Fig. 5 illustrate superiority of the PLL with magnitude estimator and the PLL with OSG over the conventional PLL. The last one could not remove a double-frequency component from the input signal. Input signal have 50 Hz fundamental frequency with no distortion in Fig. 5(a) and 5(b) with 55 Hz fundamental fre-

quency and no distortion. Fundamental frequency in VCO in all system is equal to 50 Hz. Magnitude of input signal is equal to one. The input signal is the same in all considered schemes. Parameters of conventional PLL in three models are the same. When changing the frequency from 5 Hz shown in Fig. 5(b) arrangement with OSG has the greatest momentum.

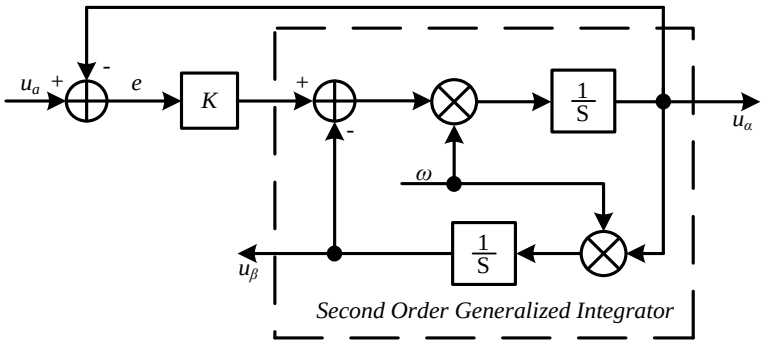

Fig. 4. Orthogonal signal generator based on Second Order Generalized Integrator

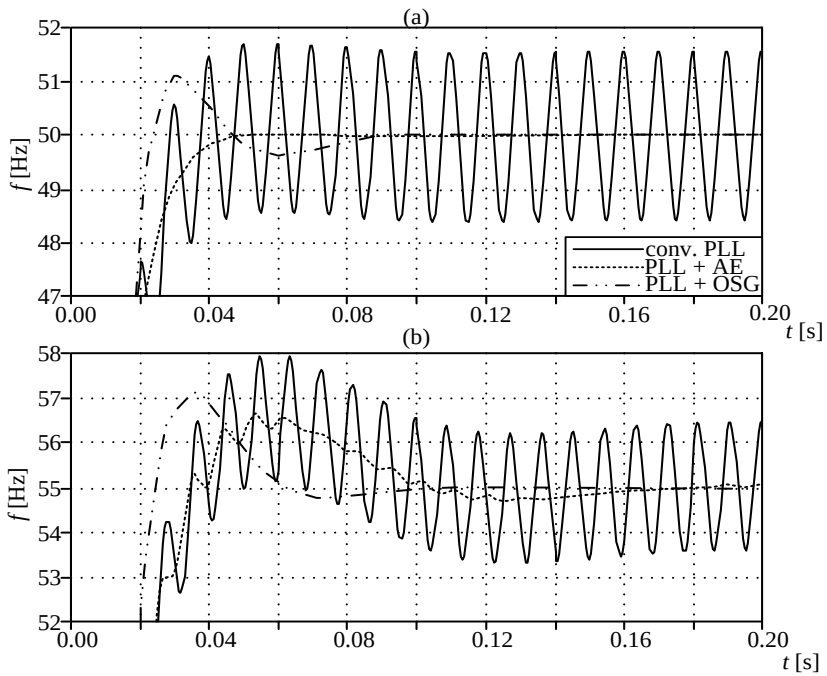

Fig. 5. Performance of the PLL systems in removing double-frequency ripples: (a) estimated frequencies of the conventional PLL, PLL with magnitude estimator and PLL with OSG for input frequency equal to 50 Hz and (b) for input frequency equal to 55 Hz

The PLL with magnitude estimator and OSG remove the double-frequency ripple and provide an error-free estimation of the phase angle and frequency when input signal is pure sinusoidal signal. Usually measurements of the voltage or current signals are corrupted by high-frequency distortions and noise. The case when signal is corrupted with 30% of the second harmonic (a) – and a 30% of the third harmonic (b) has been shown on Fig. 6. In such cases, the PLL with magnitude estimator and system with OSG cannot remove the harmonics either the conventional PLL.

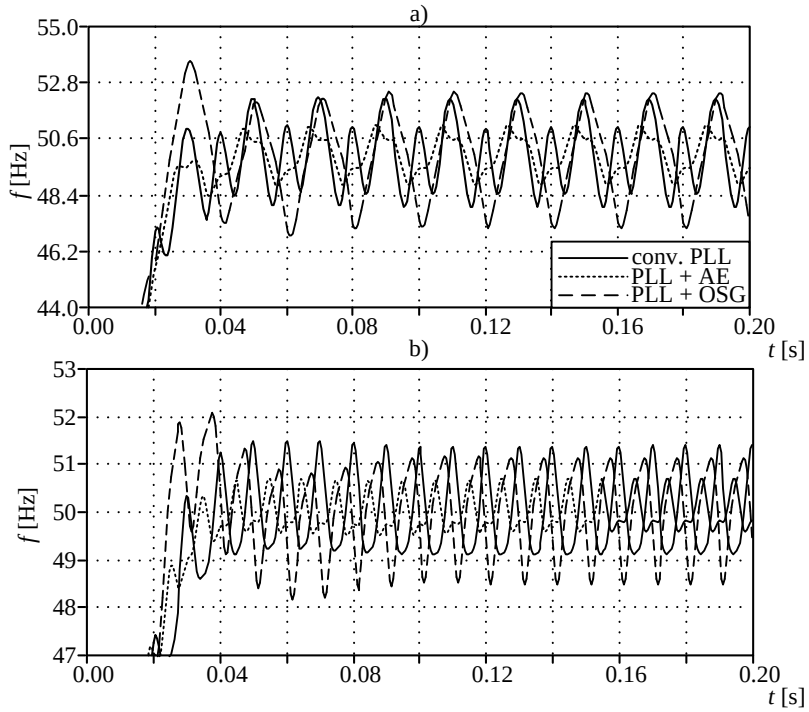

Fig. 6. Performance of the PLL systems when the input signal is distorted: estimated frequencies for (a) 30% of the second harmonic and (b) 30% of the third harmonic

All PLL systems can not remove error from frequency measurement when input signal is corrupted by high-frequency distortion and noise. The purpose of this paper is to overcome this drawback of the conventional PLL and the PLL with magnitude estimator and PLL with OSG which is sensitivity to the presence of harmonics. A developed structure is based on the system of PLL [4] with magnitude estimator and new PLL with OSG [1], [7] which is able to completely remove impacts of harmonics.

3. DISTORTION-FREE PHASE LOCKED LOOP SYSTEMS

Structure of the system is based on multiple units of the PLL with magnitude estimator and units of the PLL with OSG. First possible scheme is shown in Fig. 7 for PLL with magnitude estimator [4] and in Fig. 8 for PLL with OSG. Unit 1 (with shown details) is intended to the fundamental component of frequency 50 Hz. Unit 1 in both cases are the open loop part of PLL as shown in Fig. 7 and 8. The errors of signals in new systems depend on all units. Unit 1 to Unit N have similar but operate within a pre-specified frequency range. Each pre-specified frequency range is primarily determined by the value of the nominal frequency of its VCO. Unit 2 has frequency $2\omega_0$, Unit 3 - $3\omega_0$ and Unit N - $N\omega_0$. More details can be find in [4].

Examples of performance of the proposed system from Figs. 7 and 8 are presented in Fig. 9. It was considered two different input signals were considered: first one with 30% of the second harmonic and the second - with 30% of the third harmonic. In each case the proposed PLL has $N = 3$ units with adequate nominal frequency of each unit. It can be seen that the frequency of the input signal is estimated with no error.

Two proposed PLL systems provides absolutely error-free estimate of the phase-angle and frequency if the harmonic components of the input signal are all detected by the units. This is the case when the number of units is no fewer than the number of harmonics presented in the signal. In practice, signals are contaminated with a wide

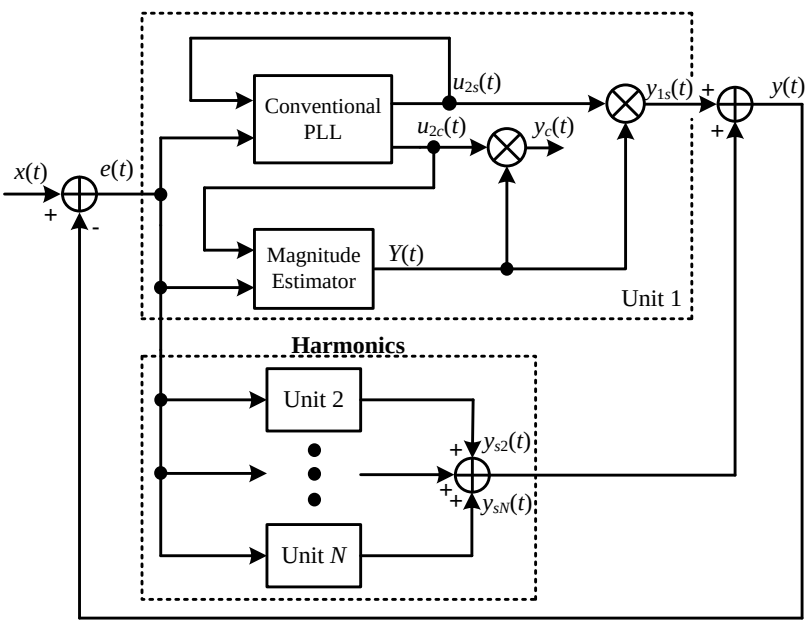

Fig. 7. PLL system with magnitude estimator from [4]

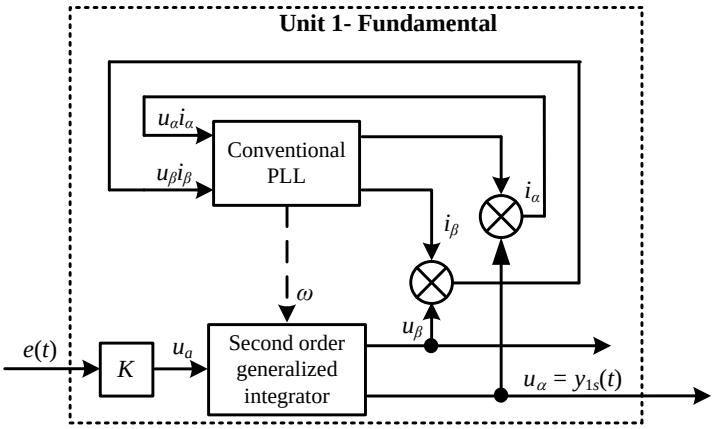

Fig. 8. Structure of Unit 1 in the proposed PLL system with OSG

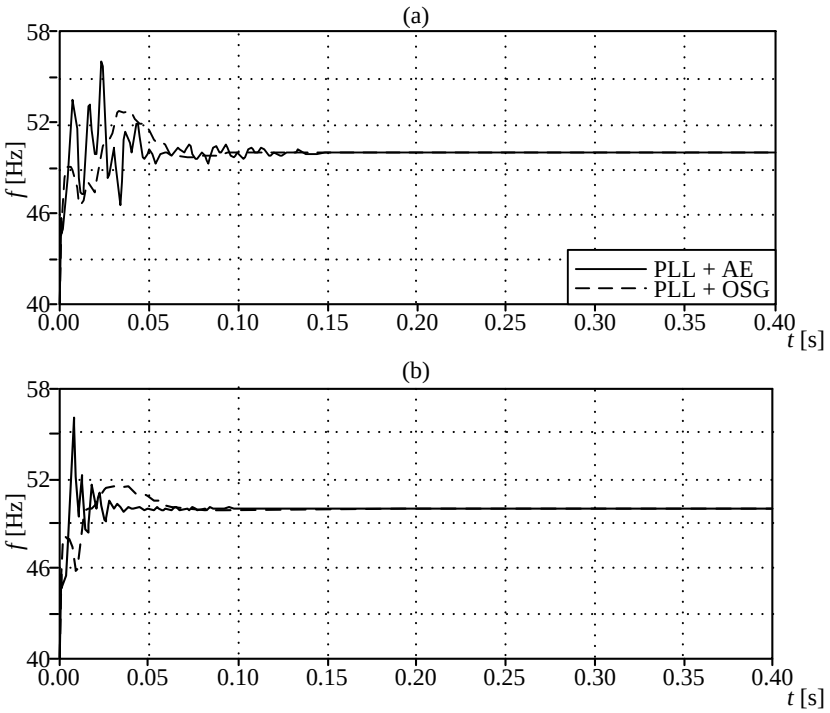

Fig. 9. Performance of PLL system of Fig. 7 and Fig. 8 when the input signal is distorted: estimated frequency for (a) 30% of the second harmonic and (b) 30% of the third harmonic

range of harmonics from low-frequency range to high frequencies. The error will decrease with increasing the number of applied units.

4. SIMULATION STUDY

The proposed PLL schemes from Figs. 7 and 8 were examined by simulation against the input signal contamination. Tested systems were represented in ATP-EMTP program. The parameters of systems with OSG and the magnitude estimators were chosen independently. Parameters of tested schemes were selected to adjust to the input signal harmonics and inter-harmonics and to immune to the fundamental frequency deviation with the range of 5 Hz. More details regarding the selection of parameters can be read in [1], [4], [5], [6], [7]. For the examples considered in this section, $N = 5$ units are taken each of which is set to operate in the frequency range of $[k\omega_0 - \omega_0/2, k\omega_0 + \omega_0/2]$, $k = 1\ldots5$ with $\omega_0 = 100\pi$ s^{-1}.

For the first case study, the input signal is comprised of 40% of the second harmonic and 10% of fifth harmonic, i.e.:

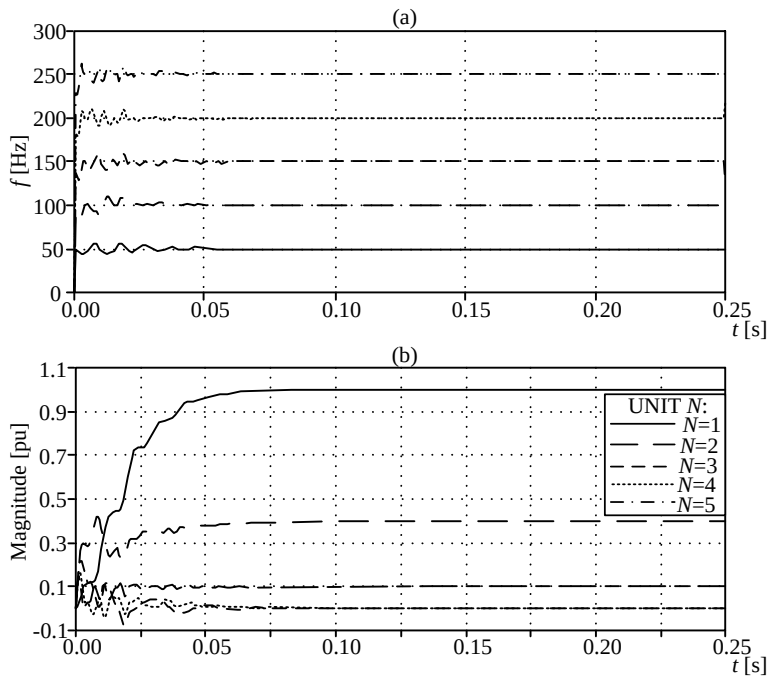

Fig. 10. Performance of PLL system with amplitude estimator with $N = 5$ Units as in Fig. 7 for input signal (5): (a) estimated frequencies, and (b) estimated magnitudes

$$u(t) = \sin(\omega_0 + \delta_0) + 0.4\sin(2\omega_0 + \delta_2) + 0.1\sin(5\omega_0 + \delta_5) \tag{5}$$

where the initial phase-angles, δ_i's, are chosen randomly between -2π and 2π.
Figs. 10 and 11 show the estimated frequencies and magnitudes by the units of PLL system with the amplitude estimator and OSG. In two cases estimated magnitudes Fig. 10(b) and Fig. 11(b) take the following values 1 for fundamental unit and 0.4, 0, 0, 0.1 for successive units $k = 1 \ldots 5$. The frequencies of fundamental, second and the fifth are estimated with no error for both systems. The third and forth harmonic is estimated but the amplitude of this signals is equal zero. The results confirm the correctness of both systems in the measurement of signal (5).

Comparing the results of two analyzed schemes (Figs. 10 and 11) one can see that the PLL system with OSG has considerable better dynamics in the frequency estimation while the time delays for magnitude estimation are similar end equal to 0.05 s.

One of the important characteristics of the considered estimators is the ability to deal with inter-harmonics. The proposed structures have its adaptive properties and there are able to detect inter-harmonics in the frequency range of units in the system. The signal components can be determined without error when the frequency of inter-

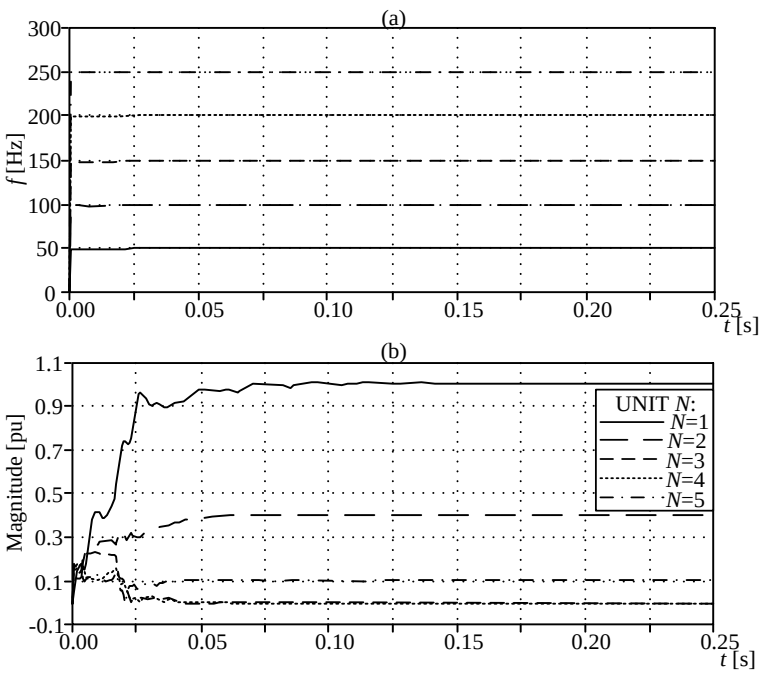

Fig. 11. Performance of PLL system with OSG as in Fig. 8 with $N = 5$ Units for input signal (5): (a) estimated frequencies, and (b) estimated magnitudes

harmonic is in the capture range of loops located in units of the system. Results of measurement of the signal having inter-harmonic component are shown in Fig. 12 - for the system with the amplitude estimator and in Fig. 13 - for the system with OSG. The input signal comprises three components at the fundamental frequency of 50 Hz, an inter-harmonic component at 130 Hz, and fifth harmonic. The magnitudes of these components are the same as in the previous example. For smoothing out of the input signal the LPF is included at the input of PLL. It can be seen that the magnitudes and frequencies are accurately estimated in both systems. The inter-harmonic component falls within the range of the third unit and is detected by that unit. Time of reaching a steady state in measurement of inter-harmonic frequency is worse than that in the estimation of the harmonic frequency. This delay is related to the synchronization time of PLL. However, for both systems for inter-harmonic measurements are successful. There are some insignificant differences in the output waveforms but, generally, both systems have the similar response.

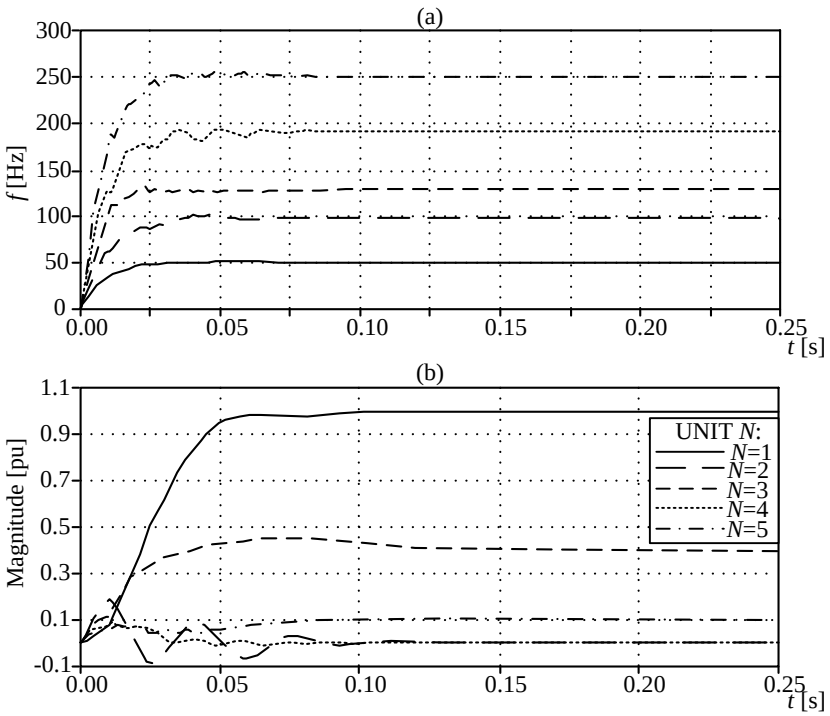

Fig. 12. Performance of PLL scheme for amplitude estimator as in Fig. 7 with $N = 5$; input signal has 40% of 30 Hz component and 10% of fifth harmonic: (a) estimated frequencies; (b) estimated magnitudes

The last example of simulation shows the effect of reducing number of units in the system for quality of the frequency estimation. The input signal is described by the equation:

$$u(t) = \sin(\omega_0 + \delta_0) + 0.4\sin(2\omega_0 + \delta_2) + 0.1\sin(5\omega_0 + \delta_5) + 0.4\sin(7\omega_0 + \delta_7) \qquad (6)$$

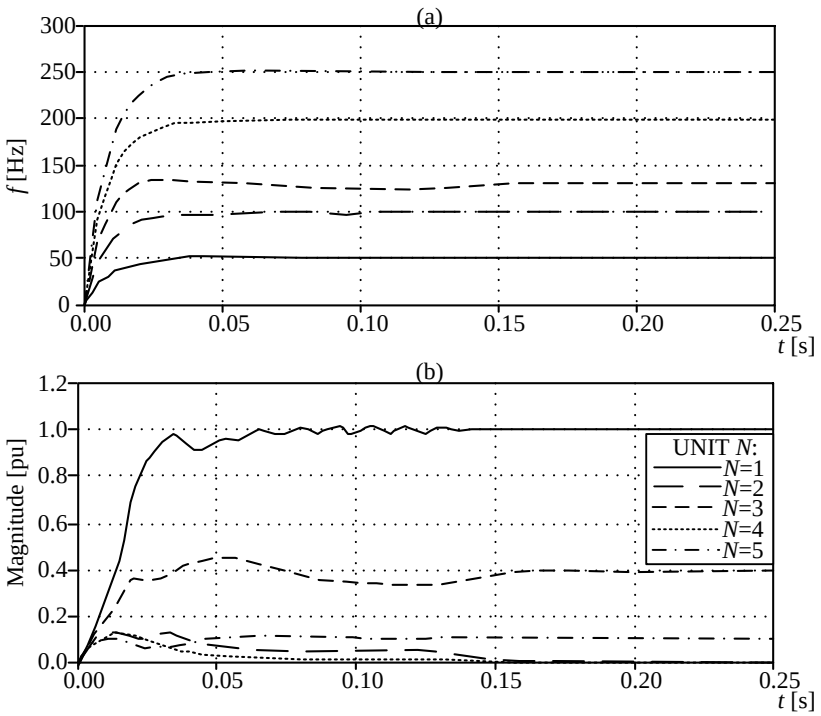

Fig. 13. Performance of PLL with OSG system as in Fig. 8 with 5 Units; input signal has 40% of 30 Hz component and 10% of fifth harmonic: (a) estimated frequencies, and (b) estimated magnitudes

Fig. 14(a) shows the input signal. The measured signal is applied to the proposed PLL schemes (Figs. 7 and 8). Figs. 14(b) to 14(d) show results of the frequency measurements for different number of applied units. It can be seen that the measurement accuracy dramatically decrease if N is reduced from $N = 5$ to $N = 1$.

The reduction of unit numbers causes much deterioration in the quality of the measurement. This behavior is visible in both considered systems: with amplitude estimator and with added OSG. The conclusion for this example is that the more units in the system, the better quality and range for frequency measurement.

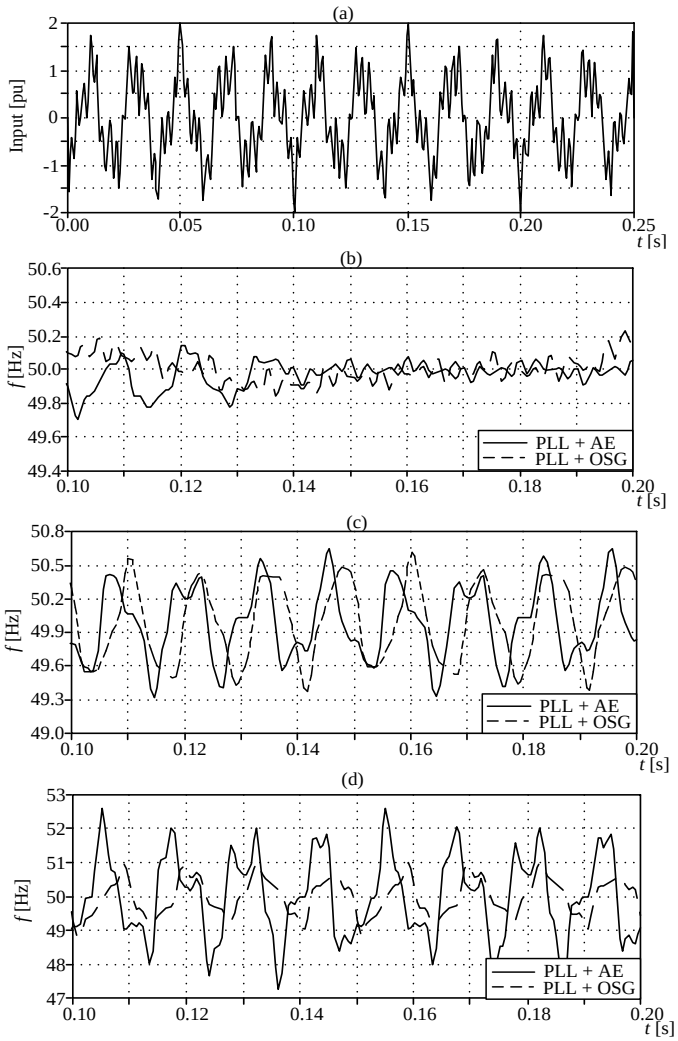

Fig. 14. Results of frequency estimation: input signal (a); results for system with units number $N = 5$ (b); $N = 2$ (c) and $N = 1$ (d)

5. CONCLUSIONS

The proposed PLL scheme with OSG obviates the fundamental drawback of the conventional single phase PLL system which has double-frequency ripples in the output and is sensitive to harmonics. The considered circuit is as reliable as the structure presented in [4] with amplitude estimator. Thus, the proposed PLL provides errorless estimate of the phase-angle and frequency in the presence of harmonic and inter-

harmonic components. Performed simulation studies have shown the performance of the proposed system. Multiple generic units can compose a complex scheme which can be applied to estimate the phase-angles of the individual phases of a multi-phase unbalanced system. PLL with OSG can also be successfully adapted for amplitude estimation without any double-frequency ripples at the output.

REFERENCES

[1] CIOBOTARU M., TEODORESCU R., AGELIDIS V. G., *Offset rejection for PLL based synchronization in grid-connected converters.*
[2] EDRIS A. A., *Proposed terms and definitions for flexible ac transmission system (FACTS)*, IEEE Trans. on Power Delivery, vol. 12, no. 4, Oct. 1997.
[3] HOROWITZ P., HILL W., *Sztuka elektroniki*, T. 2. WKŁ. Warszawa 2006.
[4] KARIMI-GHERTEMANI M., *A distortion-free phase locked loop system for FACTS and power electronics controllers*, Electrical Power Systems Research 77 (2007) 1095-1100 .
[5] KARIMI-GHARTEMANI M., IRAVANI M. R., *A nonlinear adaptive filter for online signal analysis in power systems: applications*, IEEE Trans. Power Del. 17 (1) (2002) 617-622.
[6] KARIMI-GHARTEMANI M., ZIARANI A. K., *Periodic orbit analysis of two dynamical systems for electrical engineering applications*, J. Eng. Math. 45 (2) (2003) 135-154.
[7] ROSOŁOWSKI E., WYSZOMIRSKI M., *Zastosowanie analogowej Pętli Synchronizacji Fazowej do pomiarów w automatyce elektroenergetycznej,*. Automatyka Elektroenergetyczna 1/2011 (70).

WYKORZYSTANIE UKŁADU PĘTLI SYNCHRONIZACJI FAZOWEJ Z ZASTOSOWANIEM GENERATORA SYGNAŁÓW ORTOGONALNYCH W ENERGOELEKTRONICZNYCH UKŁADACH STEROWANIA

W artykule przedstawiono układ pętli synchronizacji fazowej (PSF) z generatorem sygnałów ortogonalnych (GSO). Proponowana technika umożliwia wyeliminowanie wpływu zakłóceń zanalizowanego sygnału na określenie jego parametrów takich jak faza, amplituda czy częstotliwość. Przedstawiono model symulacyjny proponowanego układu i zaprezentowano wyniki doświadczeń. Zawarto także niektóre z zalecanych konfiguracji schematu w celu eliminacji składowych harmonicznych i interharmonicznych sygnału. Dowiedziono, że proponowany system PSF z GSO może być rozpatrywany jako użyteczne i efektywne narzędzie w implementacjach wymagających dużej dokładności estymacji fazy i częstotliwości. Proponowany system może być stosowany w układach sterowania trójfazowych systemów takich jak FACTS lub w układach sterowania generatorów indukcyjnych dwustronnie zasilanych (DFIG). Wyniki symulacji wskazują na skuteczność i poprawność działania zaproponowanego rozwiązania.

Keywords: wind generation, doubly-fed induction generator,
active and reactive power control,
stator flux reference frame

Leszek JEDUT*, Eugeniusz ROSOLOWSKI*

COMPARATIVE ANALYSIS OF POWER CONTROL SCHEMES IN DFIG FOR WIND ENERGY GENERATION

This paper describes two algorithms applied for active and reactive power control in wind turbine driven doubly fed induction generator (DFIG). The first proposed method applies the PI controllers for regulation of DFIG power and the rotor current while the second one utilizes a difference approximation of a given flux derivative. Both algorithms are based on the model description with reference to the stator flux linkage frame. General description of the analyzed methods is delivered and some results of simulations are included.

1. INTRODUCTION

The growing penetration of wind power on the electrical system and the increasing of the generating units rated power bring new challenges to the engineers. The wind-powered electricity generation grows rapidly because of the advantages of the active and reactive power regulate independently capacity and excitation converters requires small capacity, the doubly fed induction generator (DFIG) has been widely used in the wind power system. Due to an increase in the separate unit and total power of wind turbine installations, the utilities and the local network dispatchers request that wind supplied generators support the grid following different kind of disturbances.

Wind energy systems, generally, are based on variable-speed turbines. From among different alternatives to work with variable speed, the system based on the DFIG has been commonly employed for the recently build wind farms. In such a system the machine stator is directly connected to the grid and the rotor is connected via slip rings to a variable frequency inverter. To cover a wide range rotor speed - from

* Wroclaw University of Technology, Institute of Electrical Power Engineering, Wybrzeze Wyspianskiego 27, 50 – 370 Wroclaw, leszek.jedut@pwr.wroc.pl, rose@pwr.wroc.pl

subsynchronous to supersynchronous – the power converter needs to operate with power flowing in both directions (back-to-back inverter). For analyzing the mutual interaction between aforementioned wind generator and the utility network a simulation and modeling technique may be applied.

Traditionally, DFIG control is achieved by vector control (VC) [2], [4], which decouples the rotor currents into active power (or torque) and reactive power (or flux) components, and adjusts them separately in a reference frame fixed to either the rotor flux [4], the stator flux [7], [8], magnetizing flux [5] or voltage [4]. The rotor flux reference is calculated using the reactive power/power factor reference. Since the rotor supply frequency, can become very low, rotor flux estimation is significantly affected by the machine parameter variations. Recently, a direct power control strategy based on the estimated stator flux was proposed. Since the stator (network) voltage is relatively harmonic-free with fixed frequency, a DFIG's estimated stator flux accuracy can be guaranteed. The control system is very simple, and the machine parameters' impact on system performance was found to be negligible [7], [8]. The controller directly calculates the required rotor voltage within each fixed time period based on the stator flux, the rotor position, and the values of active and reactive powers and their errors. The very similar scheme based on the stator flux reference frame was proposed in [5]. The rotor current in *x*-*y* coordinates is used to control the stator reactive and active powers. The resulting control chain is composed of two control loops with two pairs of independent PI regulators: the inner one stabilizes the rotor current and the outer loop controls the value of active and reactive power.

In the paper two selected schemes for DFIG control are investigated by using of ATP-EMTP [1] and MATLAB-SIMULINK [3] models. Details of the proposed procedures are presented in the paper. Some results of simulations are also included.

2. DFIG MODEL DESCRIPTION

Considering the equivalent scheme of DFIG presented in Fig. 1 one can write the following relations for the stator and rotor voltages [6], [8]:

$$\underline{U}_s = -R_s \underline{I}_s + \frac{d\underline{\Psi}_s}{dt} + \mathrm{j}\omega_1 \underline{\Psi}_s \tag{1}$$

$$\underline{U}_r = R_r \underline{I}_r + \frac{d\underline{\Psi}_r}{dt} + \mathrm{j}\omega_{sl} \underline{\Psi}_r \tag{2}$$

where: ω_1 – angular velocity of the supplying voltage; $\omega_{sl} = \omega_1 - \omega_r$ – angular slip velocity; $\underline{U}_s = U_{sd} + \mathrm{j}U_{sq}$ and similarly for other vectors with:

$$\underline{\Psi}_s = L_m \underline{I}_r - L_s \underline{I}_s = L_m \underline{I}_m \tag{3}$$

$$\underline{\Psi}_r = L_r \underline{I}_r - L_m \underline{I}_s \tag{4}$$

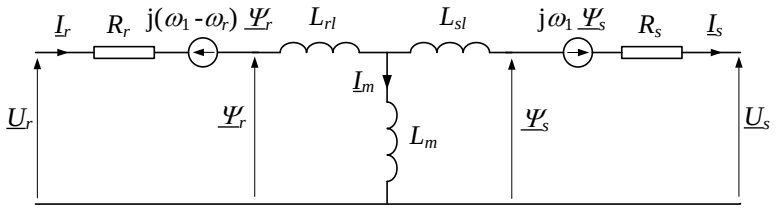

Fig. 1. Equivalent scheme of DFIG in synchronous *d-q* reference frame

The DFIG model defined by (1) and (2) in *d-q* reference frame is very important for further derivation because it assures the stator active and reactive power separate control by directing the current fed into the rotor windings [4], [7]. Let us track down the procedure to obtain the proper relations.

Neglecting of a zero-sequence component, the rotor and stator variables can be represented in their natural α-β frames by applying Clarke transformation:

$$\mathbf{X}_{\alpha\beta} = \mathbf{C}_1 \mathbf{X}_{\mathrm{ABC}} \tag{5}$$

where: $\mathbf{C}_1 = \frac{2}{3}\begin{bmatrix} 1 & -1/2 & -1/2 \\ 0 & \sqrt{3}/2 & -\sqrt{3}/2 \end{bmatrix}$, $\mathbf{X}_{\alpha\beta} = \begin{bmatrix} X_\alpha & X_\beta \end{bmatrix}^{\mathrm{T}}$, $\mathbf{X}_{\mathrm{ABC}} = \begin{bmatrix} X_A & X_B & X_C \end{bmatrix}^{\mathrm{T}}$.

In particular, the rotor current phasor components related to the rotor α-β frame are calculated as follows:

$$\mathbf{I}^r_{\mathrm{r}\alpha\beta} = \mathbf{C}_1 \mathbf{I}_{\mathrm{rABC}} \tag{6}$$

Therefore, the phasor $\underline{I}^r_{\mathrm{r}\alpha\alpha} = I^r_{r\alpha} + \mathrm{j}I^r_{r\beta}$ rotates in the angular velocity ω_r – the same as the rotor. It can be next transformed to the stator reference frame:

$$\underline{I}^s_{\mathrm{r}\alpha\beta} = \underline{I}^r_{\mathrm{r}\alpha\beta} \cdot \mathrm{e}^{\mathrm{j}\theta_r} \tag{7}$$

where θ_r is an angle between the rotor and the stator.

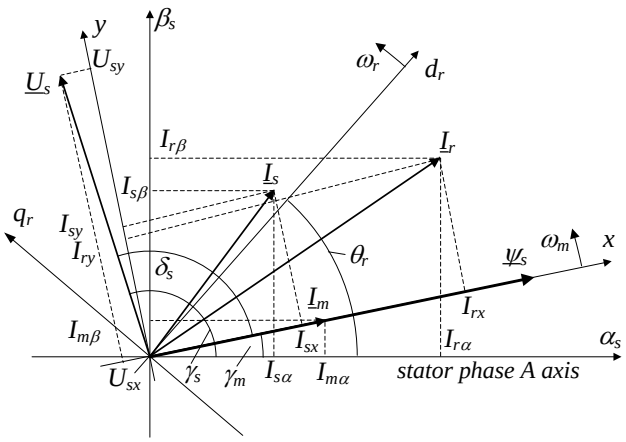

Fig. 2. Stator and rotor vectors

Having also the stator current determined in α-β coordinates (which can be calculated similarly as in (6)), a magnetizing current phasor can be given by [5]:

$$\underline{I}_{\mathrm{m}\alpha\beta} = \underline{I}^{s}_{r\alpha\beta} - \frac{L_s}{L_m}\underline{I}^{s}_{\mathrm{s}\alpha\beta} = I_{m\alpha} + \mathrm{j}I_{m\beta} = \left|I_m\right| \cdot \mathrm{e}^{\mathrm{j}\gamma_m} \tag{8}$$

where: $\gamma_m = \arctan\dfrac{I_{m\beta}}{I_{m\alpha}} = \displaystyle\int_0^t \omega_m dt + \gamma_{m0}$.

It can be noted that the angular velocity ω_m of the stator flux-linkage frame is practically the same as the velocity of the stator frame: $\omega_m \approx \omega_1$. The insignificant difference occurs only during a transient state and can be neglected. Therefore, the magnetizing current $\underline{I}_m$ in Fig. 1 is obtained from:

$$\underline{I}_m = \underline{I}_{\mathrm{mdq}} = \underline{I}_{\mathrm{m}\alpha\beta} \cdot \mathrm{e}^{-\mathrm{j}\gamma_m} \tag{9}$$

In fact, the stator flux-linkage frame is depicted as *x*-*y* frame, so similarly to (8) can be also transformed other variables of the DFIG model, e.g. transformation of the rotor current to the flux-linkage frame is given by:

$$\underline{I}_{\mathrm{rxy}} = \underline{I}^{s}_{\mathrm{rm}\alpha\beta}\mathrm{e}^{-\mathrm{j}\gamma_m} \tag{10}$$

It is interesting to note that in steady-state all variables related to the stator flux-linkage frame (*x*-*y* frame) take constant values.

To derive the rotor voltage control principle let us consider the flux linkage related to the *x-y* frame:

$$\underline{\Psi}_{xy} = L_m \underline{I}_{\mathrm{sxy}} = \underline{\Psi}^{s}_{\mathrm{sm}\alpha\beta} \mathrm{e}^{-j\gamma_m} \tag{11}$$

By definition the flux real component Ψ_x determines the 0*x* axis what gives:

$$\Psi_x = L_m I_{rx} - L_s I_{sx} = L_m \left|\underline{I}_m\right| \tag{12}$$

$$\Psi_y = L_m I_{ry} - L_s I_{sy} = 0 \tag{13}$$

It follows from (12), (13) that $I_{my} = 0$, $I_{mx} = \left|\underline{I}_m\right|$ and:

$$I_{sx} = \frac{L_m}{L_s}\left(I_{rx} - \left|I_m\right|\right), \quad I_{sy} = \frac{L_m}{L_s} I_{ry} \tag{14}$$

Substituting (11) – (14) into (2) and after adequate transformation yields:

$$\begin{aligned} U_{rx} &= U_{\mathrm{prx}} + U_{\mathrm{drx}} \\ U_{ry} &= U_{\mathrm{pry}} + U_{\mathrm{dry}} \end{aligned} \tag{15}$$

where:

$$\begin{aligned} U_{\mathrm{prx}} &= R_r I_{rx} + \sigma L_r \frac{dI_{rx}}{dt} \\ U_{\mathrm{pry}} &= R_r I_{ry} + \sigma L_r \frac{dI_{ry}}{dt} \end{aligned} \tag{16}$$

$$\begin{aligned} U_{\mathrm{drx}} &= -\omega_{sl} \sigma L_r I_{ry} \\ U_{\mathrm{dry}} &= \omega_{sl}(1-\sigma) L_r \left|I_m\right| + \omega_{sl} \sigma L_r I_{rx} \end{aligned} \tag{17}$$

and $\sigma = 1 - \dfrac{L_m^2}{L_s L_r}$.

The element $(1-\sigma)L_r\left(d\left|I_m\right|/dt\right)$ in (15) was omitted because changing of the magnetizing current magnitude is very small even during big disturbances [5].

It can be seen from (16), (17) that individual rotor voltage components depend on separate components of the rotor current. Expressions (16) represent differential equations which can be described in the Laplace transform notation:

$$I_{rx}(s) = \frac{1/R_r}{1+\sigma T_r s} U_{\text{prx}}(s)$$
$$I_{ry}(s) = \frac{1/R_r}{1+\sigma T_r s} U_{\text{pry}}(s) \tag{18}$$

where: $T_s = \frac{L_s}{R_s}$, $T_r = \frac{L_r}{R_r}$.

Adequate tuning of the rotor current components can be achieved by application of a PI regulator as in Fig. 3 [7]. Control schemes for both components are the same.

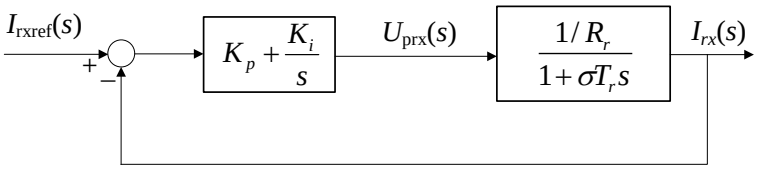

Fig. 3. Control scheme for adjusting the current I_{rx}

Settings of the PI controller in Fig. 3 can be calculated under the assumption that both coefficients K_p, K_i are related according to the rule:

$$K_p = \frac{K_i \sigma L_r}{R_r} \tag{19}$$

Under this condition the transfer function of the scheme from Fig. 3 is reduced to

$$G_{rx}(s) = \frac{I_{rx}(s)}{I_{\text{rx ref}}(s)} = \frac{1}{\tau_i s + 1} \tag{20}$$

where $\tau_i = R_r / K_i$ is a given time constant of the equivalent scheme from Fig. 3.

Starting from a given time constant τ_i the tuning PI controller coefficients are then determined as follows:

$$K_p = \frac{\sigma L_r}{\tau_i}, \quad K_i = \frac{R_r}{\tau_i} \tag{21}$$

The reference currents $I_{\text{rx ref}}, I_{\text{ry ref}}$ are defined by active and reactive powers control chain. Detailed formulas can be received on the basis of the stator:

$$P_s = \frac{3}{2}\left(U_{sx}I_{sx} + U_{sy}I_{sy}\right) \approx \frac{3L_m}{2L_s}\left|\underline{U}_s\right| I_{ry}$$
$$Q_s = \frac{3}{2}\left(U_{sy}I_{sx} - U_{sx}I_{sy}\right) \approx \frac{3L_m}{2L_s}\left|\underline{U}_s\right|\left(I_{rx} - \left|I_m\right|\right) \tag{22}$$

and the rotor power components:

$$P_r = -\frac{3}{2}\left(U_{rx}I_{rx} + U_{ry}I_{ry}\right)$$
$$Q_r = -\frac{3}{2}\left(U_{ry}I_{rx} - U_{rx}I_{ry}\right) \tag{23}$$

Total power components delivered to the network are:

$$P_n = P_s + P_r, \quad Q_n = Q_s + Q_r \tag{24}$$

Proceeding similarly as for the current control loop the following transfer function for equivalent active power control chain may be obtained (Fig. 4):

$$G_P(s) = \frac{P_n(s)}{P_{\text{nref}}(s)} = \frac{\dfrac{K_{1p}}{\tau_i}\left(s + \dfrac{1}{\tau_i}\right)}{s^2 + \dfrac{1 + K_{1p}B_s}{\tau_i}s + \dfrac{K_{1i}B_s}{\tau_i}} \tag{25}$$

where $B_s = \dfrac{3L_m U_s}{2L_s}$ is the scaling factor.

Transfer function (25) can also be reduced to the first order element under the assumption: $K_{1p} = K_{1i}\tau_i$. Then (25) is simplified to:

$$G_P(s) = \frac{P_n(s)}{P_{\text{nref}}(s)} = \frac{1}{\tau_i B_s\left(s\tau_1 + 1\right)} \tag{26}$$

For a given time constant τ_1 the PI_1 controller parameters are as follows:

$$K_{1i} = \frac{1}{B_s\tau_1}, \quad K_{1p} = \frac{\tau_i}{B_s\tau_1} \tag{27}$$

It can be noted that the gain in the equivalent control loop as in Fig. 4 is equal to: $k=(1/B_s\tau_i)$ (26). This derivation can be repeated for reactive power control loop receiving the same results. Time constant τ_i and τ_1 should be selected small to obtain fast response but not too very small to avoid a noise influence.

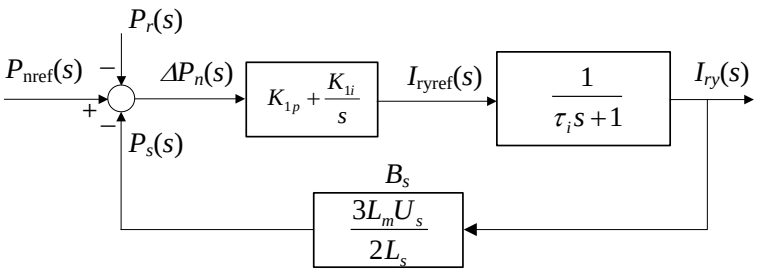

Fig. 4. Control loop for the active power adjusting the current I_{rx}

Relations (15)-(17) with the PI controllers description define the first considered algorithm for DFIG control.

The second regarded algorithm is based on the assumption that the integration operation in the PI controller is replaced by adequate difference calculus [8], [9]. Considering the formula (2) with respect to the flux derivative one can write the following change of this flux during sampling period T_s:

$$\Delta\underline{\Psi}_r=(\underline{U}_r-R_r\underline{I}_r-\mathrm{j}\omega_{sl}\underline{\Psi}_r)T_s \tag{28}$$

The stator power can be determined from the relation:

$$P_s-\mathrm{j}Q_s=\frac{3}{2}\underline{U}_s\underline{I}_s^* \tag{29}$$

Taking into account (3) and (4) and neglecting the voltage drop on the stator and rotor resistances the above expression may be written in the forms:

$$P_s=k_\sigma\left(\Psi_{sd}\left(\Psi_{rq}-\frac{L_r}{L_m}\Psi_{sq}\right)-\Psi_{sq}\left(\Psi_{rd}-\frac{L_r}{L_m}\Psi_{sd}\right)\right) \tag{30}$$

$$Q_s=k_\sigma\left(\Psi_{sd}\left(\Psi_{rd}-\frac{L_r}{L_m}\Psi_{sd}\right)+\Psi_{sq}\left(\Psi_{rq}-\frac{L_r}{L_m}\Psi_{sq}\right)\right) \tag{31}$$

where: $k_\sigma = \dfrac{3L_m\omega_1}{2\sigma L_s L_r}$.

Rearranging of (30), (31) leads to:

$$\Psi_{rd} = \frac{1}{k_\sigma \left|\underline{\Psi}_s\right|^2}\left(\Psi_{sd}Q_s - \Psi_{sq}P_s\right) + \frac{L_r}{L_m}\Psi_{sd} \tag{32}$$

$$\Psi_{rq} = \frac{1}{k_\sigma \left|\underline{\Psi}_s\right|^2}\left(\Psi_{sq}Q_s + \Psi_{sd}P_s\right) + \frac{L_r}{L_m}\Psi_{sq} \tag{33}$$

Changing of active and reactive powers on ΔP_s, ΔQ_s values, respectively, results in adequate changing of the rotor fluxes:

$$\Delta\Psi_{rd} = \frac{1}{k_\sigma \left|\underline{\Psi}_s\right|^2}\left(\Psi_{sd}\Delta Q_s - \Psi_{sq}\Delta P_s\right) \tag{34}$$

$$\Delta\Psi_{rq} = \frac{1}{k_\sigma \left|\underline{\Psi}_s\right|^2}\left(\Psi_{sq}\Delta Q_s + \Psi_{sd}\Delta P_s\right) \tag{35}$$

Adequate substitution of components from (28) into (34) and (35), with application of (32) and (33) gives similar relations as in (15):

$$\begin{aligned} U_{rd} &= U_{\mathrm{prd}} + U_{\mathrm{drd}} \\ U_{rq} &= U_{\mathrm{prq}} + U_{\mathrm{drq}} \end{aligned} \tag{36}$$

where:

$$\begin{aligned} U_{\mathrm{prd}} &= \frac{1}{k_\sigma \left|\underline{\Psi}_s\right|^2 T_s}\left(\Psi_{sd}\Delta Q_n - \Psi_{sq}\Delta P_n\right) \\ U_{\mathrm{prq}} &= \frac{1}{k_\sigma \left|\underline{\Psi}_s\right|^2 T_s}\left(\Psi_{sq}\Delta Q_n + \Psi_{sd}\Delta P_n\right) \end{aligned} \tag{37}$$

$$\begin{aligned} U_{\mathrm{drd}} &= -\omega_{sl}\left(\frac{1}{k_\sigma \left|\underline{\Psi}_s\right|^2}\left(\Psi_{sq}Q_n + \Psi_{sd}P_n\right) + \frac{L_r}{L_m}\Psi_{sq}\right) + R_r I_{rd} \\ U_{\mathrm{drq}} &= \omega_{sl}\left(\frac{1}{k_\sigma \left|\underline{\Psi}_s\right|^2}\left(\Psi_{sd}Q_n - \Psi_{sq}P_n\right) + \frac{L_r}{L_m}\Psi_{sd}\right) + R_r I_{rq} \end{aligned} \tag{38}$$

Relations (36) – (38) constitute the considered second algorithm. It is demonstrated in the next section that both considered algorithms have almost the same characteristics.

3. EXPERIMENTAL RESULTS

Simulations were provided by utilizing of ATP-EMTP [1] and MATLAB – SIMULINK [3]. In the last case also AC/DC/AC SVM electronic converter was included. Parameters of the investigated DFIG are presented in Table 1.

Table 1. DFIG parameters

Parameter	Description	Value
R_s	stator resistance	1.717 mΩ
R_r	rotor resistance	5.563 mΩ
L_s/ L_r	stator/rotor inductance per phase	2.409 mH
L_m	magnetizing inductance	2.354 mH
p	number of pole pairs	2
$\|U_s\|$	stator voltage peak value	690√2/√3
S_n	nominal power	2.5 MVA

Some results of simulations of the considered DFIG with utilizing ATP-EMTP model (without electronic converters) are presented in Figs. 5 and 6. Parameters of PI controllers are assumed as follows: τ_i = 0.02s and τ_1 = 0.03s. The given powers: P_{nref} and Q_{nref} are abruptly changed as in Fig. 5. It can be seen that the obtained powers accurate tracing the given waveforms – both algorithms give almost the same results. The accompanying rotor phase current waveforms are presented in Fig. 6. These waveforms are almost the same for both analyzed algorithms.

In Fig. 7, the typical connection scheme is presented. The stator windings are directly connected to the line grid, while the rotor windings are supplied by a bidirectional power converter. The aim of the rotor side converter is to control independently active and reactive power on the grid and grid side converter has to keep the dc link capacitor voltage at the set value.

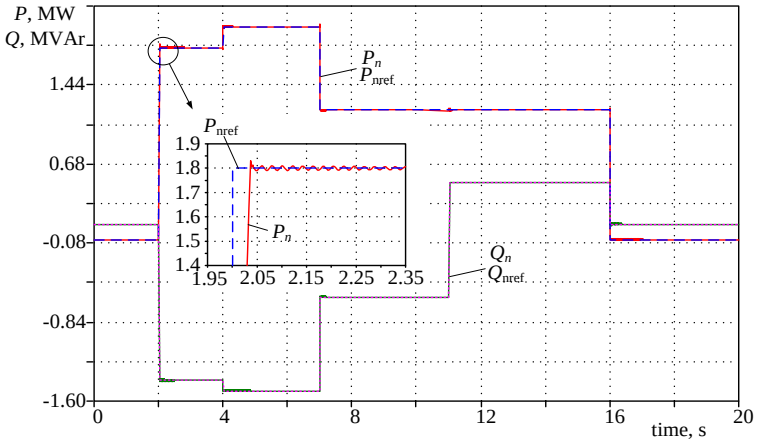

Fig. 5. Changing of active and reactive power in ATP-EMTP model

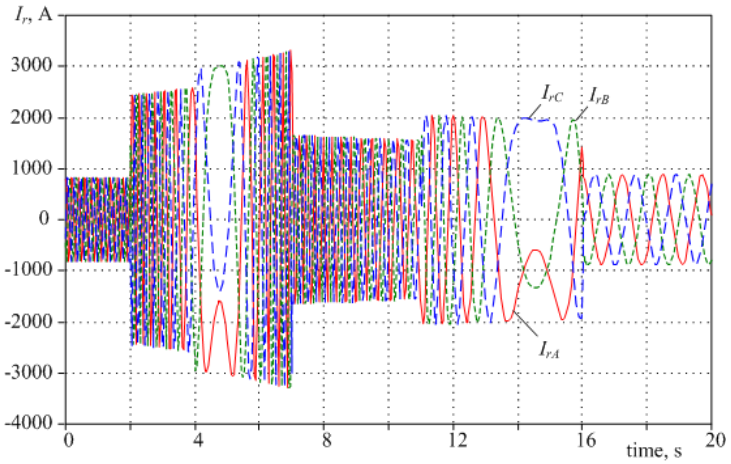

Fig. 6. The rotor current waveforms during test as in Fig. 5

Figs. 8-10 present some results of simulation which was executed in Matlab/Simulink. The model consist of full electronics converter (grid-side converter - GSC and rotor-side converter - RSC), so one can see small differences between settings value of P_{nref} and Q_{nref} and that obtained at the output of the machine: active power P_n and reactive power Q_n.

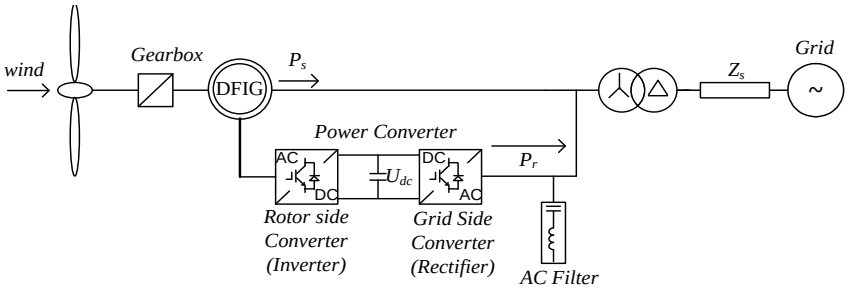

Fig. 7. Scheme of wind generation unit with DFIG

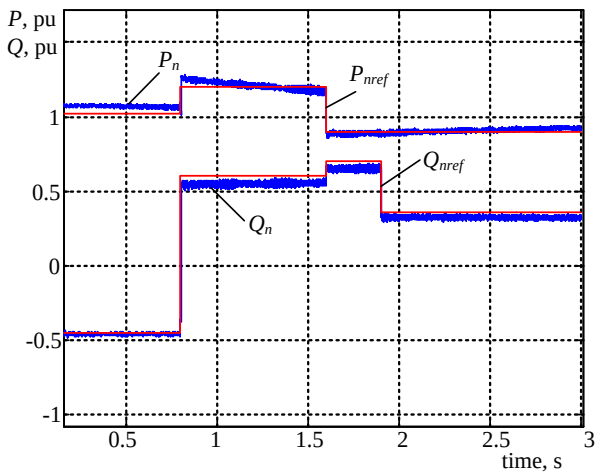

Fig. 8. Changing of active and reactive power in MATLAB/SIMULINK model

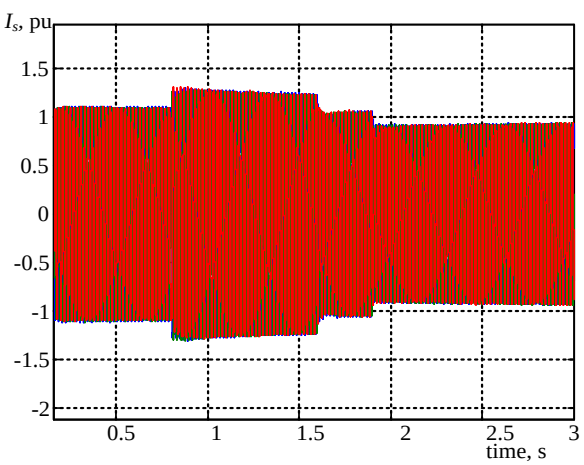

Fig. 9. The stator current waveforms during test as in Fig. 8

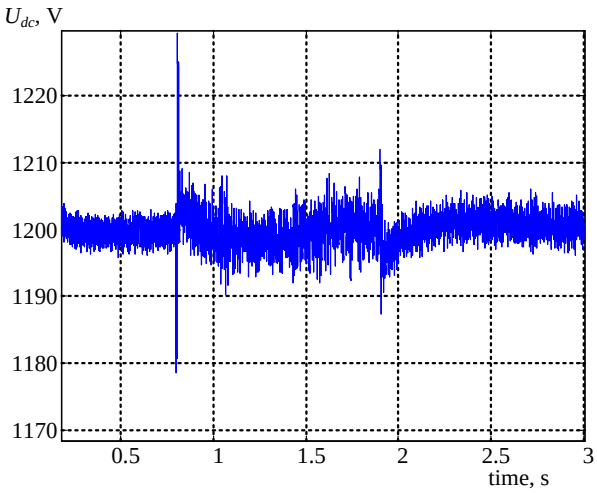

Fig. 10. Voltage U_{dc} waveform during test as in Fig. 8

Analyzing results from Figs. 8 and 9 one can observe that they follow the DFIG mathematical model: according to (14), the stator current are proportional to rotor current and rotor current depends on active and reactive power as in (22). When active and reactive powers increase, stator current raises too. Regulator of grid side converter (not describing here) keeps dc link in the constant value even during severe changing of power. Nominal voltage for dc link is equal to 1200 V.

4. CONCLUSIONS

A control structure and design of active and reactive power controllers applied in wind turbine driven DFIG was presented. The proposed schemes apply well-known linear control techniques. The algorithms were implemented in simulation models prepared in ATP-EMTP and MATLAB/SIMULINK programs. For simplicity the ATP-EMTP model was reduced: voltage sources in the rotor circuit were represented by controlled voltage. In MATLAB/SIMULINK program there was applied full power converter. Results of simulation confirm that both analyzed methods operate correctly and give similar results.

ACKNOWLEDGMENT

This work has been supported by the government of the Republic of Poland, Research Project No N N5111 352237.

REFERENCES

[1] DOMMEL H., *Electro-Magnetic Transients Program*, BPA, .Portland, Oregon, 1986
[2] MALINOWSKI M., JASINSKI M., KAZMIERKOWSKI M.P., *Simple direct power control of three-phase PWM rectifier using space-vector modulation (DPC-SVM)*. IEEE Trans. Ind. Electron, Vol. 51, no. 4, pp. 447–454, Apr. 2004.
[3] MATHWORKS, *Simulink 7.2*. Available in: http://www.mathworks.com/products/simulink/
[4] PENA R., CLARE J.C., ASHER G.M., *Double fed induction generator using back-to-back PWM converter and its application to variable- speed wind-energy generation.* IEE Proc.-Electr. Power Appl., Vol. 143, no. 3, pp. 231–241, 1996.
[5] TAPIA A., TAPIA G., OSTOLAZA J.X., SAENZ J.R., *Modeling and Control of a Wind Turbine Driven Doubly Fed Induction Generator*. IEEE Trans. Energy Convers., Vol. 18, No. 2, pp. 194–204, June 2003.
[6] TAPIA G., SANTAMARIA G., TELLERIA M., SUSPERREGUI A., *Methodology for Smooth Connection of Doubly Fed Induction Generators to the Grid*. IEEE Trans. Energy Convers., Vol. 24, No. 4, pp. 959–971, December 2009.
[7] VAS P., *Sensorless Vector and Direct Torque Control*. Oxford University Press, Oxford, U.K., 1998.
[8] XU L., CARTWRIGHT P., *Direct active and reactive power control of DFIG for wind energy generation.* IEEE Trans. Energy Convers., Vol. 21, No. 3, pp. 750–758, September 2006.
[9] ZHI D., XU L., *Direct power control of DFIG with constant switching frequency and improved transient performance.* IEEE Trans. Energy Convers., Vol. 22, No. 1, pp. 110–118, March 2007.

ANALIZA PORÓWNAWCZA METOD STOSOWANYCH DO REGULACJI MOCY CZYNNEJ I BIERNEJ W DWUSTRONNIE ZASILANYM GENERATORZE INDUKCYJNYM

W artykule przedstawiona jest analiza dwóch algorytmów stosowanych do regulacji mocy czynnej i biernej w elektrowniach wiatrowych z dwustronnie zasilanymi generatorami indukcyjnymi. W pierwszej rozważanej metodzie stosowane są regulatory PI do kontroli mocy i prądu wirnika, podczas gdy w drugiej - całkowanie ciągłe jest aproksymowane za pomocą zależności przyrostowych. W obu algorytmach model maszyny jest zapisany względem układu współrzędnych związanych ze strumieniem stojana. Zamieszczony jest opis rozważanych modeli oraz wyniki przeprowadzonych symulacyjnych testów.

Keywords:
power transmission line,
lightning discharge, lightning days

Arif M. GASHIMOV*, Fakhraddin L. KHIDIROV*, Aytek R. BABAYEVA*

LIGHTNING DISCHARGE DENSITY ON THE TERRITORY OF AZERBAIJAN

Hydro meteorological information about lightning days and period of lightning days, on the supports of OVL 110, 220, 330 kV and high objects on the territory of the republic (on the radio-television tower and lighting conductors) on the basis of statistic material, a map of lightning strokes about constant lightning strokes on the territory of the republic during a year on the 1 km2 surface was compiled. The drawn up map can be used in power engineering and other objects projecting.

1. INTRODUCTION

Enhancement of the protection reliability of different objects against lightning is impossible without knowing exactly whether the territory of these objects is exposed to lightning or not. On the specified territory activation of lightning as meteorological characteristics during one year, number of lightning days and during lightning seasons the number of lightning hours are calculated. However, to assess probability of the objects exposition to lightning, the calculation of middle annual lightning discharge is taken into account. Therefore, it would be necessary to provide with regulators which will give information about lightning stroke on the considered territory. This method with radio engineering equipment intends to record lightning discharge, a lightning recorder and a lightning territory record system are involved. Nowadays, to obtain information about the number of lightning discharge in our country the main system intended in SİQRE lightning recorders are considered.

* Azerbaijan Scientific – Research and Design- Prospecting Institute of Power Engineering LTD 94 H. Zardabi avenue, Baku, AZ 1012, Azerbaijan, Phone/Fax:+(994-12)432- 80 – 76

Currently, in some countries (USA, Japan, France, German, etc) maps showing the intensity of the lightning discharge were achieved to define lightning in a diversified system of production according to certain standard.

By means of this system, kind of lightning (inside and between clouds) can be distinguished; polarization and amplitude of lightning current between cloud and ground can also be identified.

Since September of the year 1991 technical system BLİDS by SİEMENS company is used to identify lightning stroke of on all territory of Germany and it helps to distinguish inside and between clouds kinds of clouds and polarization and amplitude of lightning between cloud and ground. Using BLİDS system, taking measurements on the territory of Germany 12 plants were used, and these plants were 200-300 km far from each other. In this area measurement accuracy was 250 m, to the direction of its borderline was 1000 m. The efficiency of lightning on the surface ground reaches 98% [1].

As a result of lightning stroke direct on the OVL supports or on the lines, switching off of the line which in some cases cause interruptions in power supply of consumers. To reduce such interruptions it would be useful to have information about lightning strokes and its parameters. It is known that in operating process to provide reliable operation of power engineering and other objects, besides other information, to protect the object from lightning the territory of the object, information about intensity of lightning is used.

2. ANALYSIS

As it was stated in [2] and in other sources related to this sphere intensity of lightning on the territory where is the object is identified according to record of the number of lightning days and duration of lightning days and when it is known a special number of lightning strokes on the surface ground on 1 km^2 (unit surface) is expressed. According to the information recorded in hydro meteorological plants and stations situated on the territory of the republic (over 20-50 years) the first two parameters shown here can be identified using special drawn up maps. According to the recordings (in hydro meteorological plants) the drawn up map about duration of lightning days on the territory of the republic was given in [3]. Using this map is possible to calculate the number of lightnings on the territory of surface ground on 1km^2.

Under field conditions identification of these parameters can be defined in different ways: by means of plengasion net of electromagnetic field formation as the result of lightning discharge; by counters registering lightning discharges, etc.

Currently, in some countries over the world forming plengasion net within certain radius, registration of lightning discharge is carried out. In most cases identification of

lightning strokes on the surface ground is difficult. Amplitude-frequency characteristics of receiving devices used in such nets is difficult to keep identically in other devices. It is difficult to use these nets in different countries. To define a number of lightning strokes on the surface ground according to CİGRE is recommended to register electromagnetic field with frequency 10 kHz.

OVL is considered to be one of the objects covering more surface ground. It is also known that ETL on the certain territory of OVL attracts lightning strokes (approx. $6h$ length, h-height of the support). This characteristic is also referred to certain high objects on the surface ground.

As it was mentioned above to record a number of lightning strokes on the surface ground and their parameters, rigid or flexible ferromagnetic registers are located on HVL supports on the certain distance.

As it was mentioned, ETL and its supports exposed to lightning strokes. A number of lightnings on the line from one side depends on potential of leader channel, amplitude value of lightning current, height of wire.

In different sources the length of area $10 \cdot h_{a.h}$ [4], $6h_{a.h}$ [2,5,7], $8h_{a.h}$ [6] and $(4h_{a.h} + b)$ was taken [8]. Here - $6h_{a.h}$ is average height of protection line or wire dip, in meters, *b*- is distance between lines and wires.

So, these values are very different from each other. It can be considered that in comparison of some values which were defined according to this model to the result of research under field conditions causes false results. Especially in reports, during one lightning day or one lightning hour, a special number of lightning strokes on the surface ground is taken as one unit value excluding mountains, foothills and plain areas.

Taking into account what was mentioned above the length l direct to OVL is calculated by the formula:

$$N = S \cdot n \cdot n_{l.h}. \tag{1}$$

Here $n_{l.h}$ – is duration of lightning days during a year [hours]; n - special number of lightning strokes for ground surface 1km^2 during one hour and a value for plain regions is 0,06 [4], 0,067 [2, 5], for mountain regions is 0,01-0,02 [4]. It is recommended to calculate a quantity value in the mentioned map. S - is an area which attracts lightning strokes of OVL, km^2.

$$S = (6-10)h_{a.h} \cdot l \cdot 10^{-3}. \tag{2}$$

Here l [km] - is a part of the line length; $h_{a.h}$ - protection from lightning, is a height of wire dip on the surface ground, in meters. Average height of lines on the surface is calculated by the following formula:

$$h_{a.h} = h - \frac{2}{3} f \ . \tag{3}$$

Here h [m] – is dip height of the line on the support; f – is dip axis of the line (wire).

Dip axis of the line can be defined in different ways. According to the value of dip axis especially depending on voltage line, between supports, span length (distance between supports) on the affect of the speed of the wind to line (wire), sleet load, etc the design influences of the line is determined. As a result of line weight formed load is determined as follows [4]:

$$g_1 = \frac{G}{1000F}, \left[\text{kg/m} \cdot \text{mm}^2\right]. \tag{4}$$

Here G – 1 km length of the line weight [kg], F-cross-section of the line [mm^2].

Depending on the affect from the load of wind speed $(v = 10\, m/s)$ special value is determined as follows:

$$g_2 = \frac{6{,}25 \cdot C_x d}{1000F} \ , \quad \left[\text{kg/m} \cdot \text{mm}^2\right]. \tag{5}$$

Here C_x – accepted for lines (wire) with aerodynamic efficiency and diameter $D \geq 20\,\text{mm}$.

In this case the special burdens arising from weight of the line and affect of the wind are possible to calculate with the following formula.

$$g_3 = \sqrt{g_1^2 + g_2^2} \ , \ \left[\text{kg/m} \cdot \text{mm}^2\right]. \tag{6}$$

Thus, it is possible to set axis dip for the same kinds of lines (wires)

$$f = \frac{g_3 \cdot l^2}{8\sigma}, \text{[m]}. \tag{7}$$

Here l – span length, σ – force influences on the line under lightning conditions $\left[\text{kg/mm}^2\right]$. By this method, e.g. by calculation performed with 220 kV voltage, span length 400 m line and *C-70* line, f=3.6 m was determined.

It is also possible to calculate it by identifying span length line and value of distance between wires.

In case when no information about axis dip is available, its approximate price can be calculated by using Table 19 [9]divide into 2.5. Span length of 100 m in the middle

of span distance between line and wire is at least 2 m, if 150 m – 3.2 m is accepted, 200m -2 m, 300 m- 5.5 m and 400 m-7 m is accepted.

Research works conducted by this method for parts of OVL and the results was calculated from the number of lightning stroke and obtained results as a result of the research was compared with the actual materials.

To compare the actual value received for registration account during 100 lightning hours on the territory 100 km is calculated by the following formula:

$$N = (6 \div 8) h_{a.h} \cdot L \cdot n_{l.h} \cdot n \cdot 10^{-1} \quad \left[1/\text{km}^2 \cdot \text{year}\right]. \tag{8}$$

Actual materials were obtained by registration ferromagnit method conducted more than 10 years on the supports of OVL parts. During report about lightning days and lightning hours average values covering more than 40 years of one circuit were taken from meteriological information.

As mentioned above, a number of the lightning stroke to the surface ground and the lightning current parameters identification by means of ferromagnetic recorders was carried out during the years of 1964-1976 and 1987-1988 on OVL supports and during 1971-1982 on the basis of research work on the radio-television towers and lightning conductors situated on the territory of the republic.

Here as in OVL the number of lightning strokes of separate objects is calculated as follows:

$$N = n \cdot S \,. \tag{9}$$

Here *n*- certain parts of the surface ground at certain time (for 1 hour) is a special number of lightning stroke and *n*=0.067, *S*- is a place of the object [km^2] which attracts lightning stroke. For separate objects:

$$S = \pi R_{ekv}^2 \,. \tag{10}$$

Here R_{ekv} – is a equivalent height which attracts a leader of lightning discharge of the object.

Thus,

$$N = \pi n R_{ekv}^2 \tag{11}$$

As it was given in [11] $R_{ekv.}=3h$ was considered for small objects with a height of 150 m and smaller, but lightning channel directed to the object with height $H_0=5h$. Here *h* – is height of the object [m].

If the object is on the surface ground the height of lightning discharge to the object, i.e. from which height the leader of the object which attracts the equivalent value of radius given in [12] is determined by the given formula:

$$R_{ekv} = \sqrt{h^{/}\left[h^{/} + 2a\exp\left(bm + b^2\frac{\sigma^2}{2}\right)\right]} \tag{12}$$

Here a and b are constant values, and a = 10, b = 0.65; m, and σ – is average value of lightning current amplitude; m = 3,14, σ = 1.11 were taken. $h^{/} = h + \Delta h$ - the effective height of the object, h - the height of the object, Δh - is length of the leader from the object to the direction to lightning discharge and its value depends on potential of lightning leader channel.

Taking into account the above-mentioned research on the basis of the registered lightning strokes to the surface ground during a year, a number of lightning strokes can be calculated by the following formula:

$$n = \frac{N}{N_{r.p} \cdot S \cdot 10^{-3}}, \left[\frac{\text{lg.strokes}}{\text{km}^2, \text{year}}\right] \tag{13}$$

Here N is a number of lightning strokes registered during research; $N_{r.p}$ – a number of the research period.

All reports about insensity of lightning on the territory of the republic were conducted on the basis of information given in [13]. As it was mentioned above, on the territory of the Republic lightning strokes 110 ÷ 330 kV on OVL, along with recordings on the radio-television and lightning conductors to research intensity of lightning, special counters were made in the laboratories and they were installed on the territory of 12 meteriological plants and 5 different objects of the Republic on the different heights of sea levels (27 m ÷ +1550 m) [14]. The effective radius of counters is 15 km and during 1973-1974 a total amount of lightning discharge in the same area, i.e. lightning discharge between clouds and the ground along with lightning discharge between inside and different load clouds were registered. From the obtained results it was determined that during one lightning day a number of lightning discharge on plains (27 ÷ +300 m on the sea level), as well as on the mountain areas (800 ÷ 1500 m) in compared with the foothill areas (300÷800 m) was quiet a lot.

According to the research conducted by optical and oscillographic method near Shusha town, lightning discharge between clouds and clouds and the ground was determined 4:1 ratio [10]. The value of this parameter especially depends on physical-geographical and climatic characteristics of the research district. Therefore, the value of this parameter which depends on the location of the research district in the moun-

tainous, foothill or plain areas and passing of frontal or local lightning clouds at the same area is shown differently in different sources. According to the information given in [15], lightning discharge from frontal type of lightning clouds only 31% reaches the surface ground.

The results of the investigation carried out by ferromagnetic registration on ETL of 110, 220, 330 kV on different heights above sea level, as well as in radio-television towers and lightning conductors, and the results received from counters during 2 years which were installed in hydro meteorological and other objects on the territory of Republic were carried out according to the above-mentioned method and on the basis of these results a map of lightning strokes density was compiled (Fig. 1).

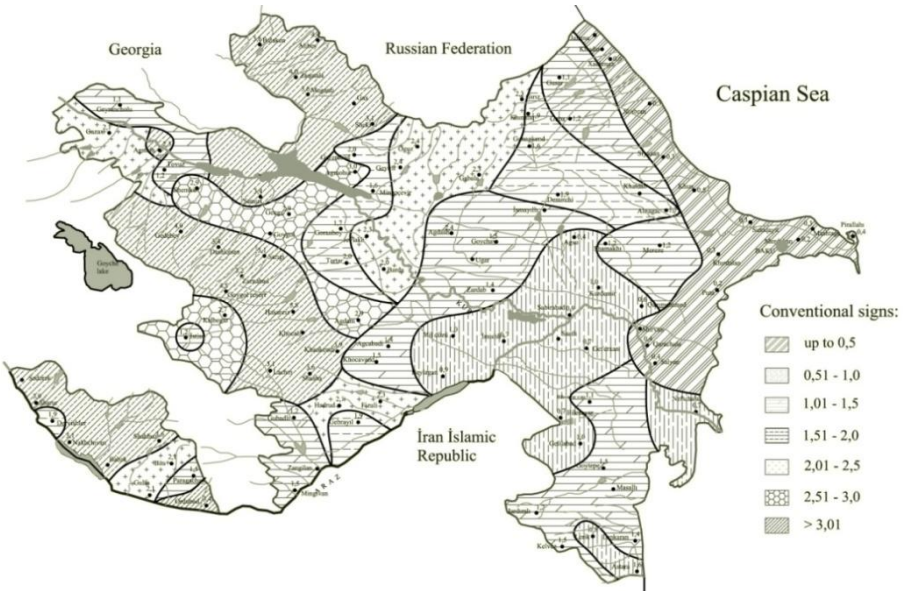

Fig. 1. The map of lightning strokes about constant lightning strokes on the territory of the republic during a year on the 1 km2 surface

From the drawn up map to the direction of Kur-Araz lowland special density reduction of lightning but in foothill and mountain areas its increasing is observed. Average calculation of a special number of lightning strokes during a year in the certain parts of the surface ground was shown in the map, in the same way as in the maps drawn up before (the average number of lightning days and average period of lightning days), as well as on the areas of meteriological plants.

CONCLUSION

The drawn up map can be used during lightning protection projecting as initial material for new construction of power engineering and other objects.

REFERENCE

[1] Qorbatenko V.P. About dependence of lightning discharge density on the ground on intensity of thunderstorm activity. Electrical, №7, 2001,p.16-21 (in russian).
[2] Guidance on power network protection 6-1120 kV from lightning surge and internal overvoltage. 153-34.3-35.125-99. S-Pt:, 1999, 355 p. (in russian).
[3] Gashimov A.M, Yusifbayli N.A, Khıdırov F.L,Babayeva A.R. Intensity of lightning on the territory of Azerbaijan republic. Baku.: Problems of Engineering, 2010, №1, 28-34 p. (in azeri).
[4] Dulzon A.A., Kalyaskiy I.I. Lightning protection of power network. Tomsk: Tomsk University, 1965, 203p. (in russian).
[5] Technics of high voltage, /under redaction Razevig D.V. M.: Ed. Power, 1976, 288p. (in russian).
[6] Dolginov A.I. Technics of high voltage in power engineering. M.: Power, 1968, 464 p. (in russian).
[7] Zakarukin V.N. Technics of high voltage. Irkutsk: 2005. 137p. (in russian).
[8] Investigation of Lightning Protective Metods for Distribution Circuits. Pt. II. Application and Evaluation. - IEEE Trans. Power Appar. and Syst. 1969, vol.88, p. 1239-1245 (Discuss 1245-1247).
[9] Rules of electrical installation devices. M.: 1986 (6-edition.), 645p. (in russian).
[10] Khidirov F.L. Lightning characteristics for lightning protection of power engineering objects, situated till 1500m above sea level on the basis of complex nature measurements. Abstract of dissertation. On research of candidate of science, M.:, 1987, 20 p. (in azeri).
[11] Bazelan E.M., Gorin B.N., Levitov V.I. Physical and Engineering basis of lightning protection. L.: 1978, 223 p. (in russian).
[12] Rakov V.A., Luc A.O. To the estimation of lightning discharge radius tighten to the object. Electricity, 1988, №9, 64-67p. (in russian).
[13] Analysis of atmosphere and sswitching surge and its protection tasks. First report, 2009, 38 p. (in azeri).
[14] Alizadeh A.A., Gadzhiyev G.A. Lightning discharge frequency – main index for lightning store estimation. For technical progress, 1976, №7, 26-30 p. (in russian).
[15] Chalmers J.A., Atmosphere electricity. L.: 1974, 420 p.

CZĘSTOŚĆ WYŁADOWAŃ ATMOSFERYCZNYCH NA TERYTORIUM AZERBEJDŻANU

Hydro meteorological information about lightning days and period of lightning days, on the supports of OVL 110, 220, 330 kV and high objects on the territory of the republic (on the radio-television tower and lightning conductors) on the basis of static material, a map of lightning strokes about constant lightning strokes on the territory of the republic during a year on the 1 km2 surface was compiled. The drawn up map can be used in power engineering and other objects projecting.

Keywords:
digital data transmission,
line differential protection

Miroslaw LUKOWICZ*

NEW METHOD OF DATA TRANSMISSION DELAY ESTIMATION FOR FEEDER DIFFERENTIAL PROTECTION

This paper is concerned with the problem of accurate aligning of digital data for purpose of feeder differential current protection. The method proposed makes use of knowledge of line susceptance for estimating the communication channel propagation time. The performance of the method is investigated under variable operational conditions of the 400 kV overhead transmission line. The outcomes show high efficiency of the approach allowing for essential improvement of sensitivity of a percentage differential protection.

1. INTRODUCTION

The requirement of the optimal operation of the systems is common in all fields of engineering. It relates mainly to the efficiency expressed in the real profits. Since the system is expected to give maximal profits under minimal yet necessary investments all its components tends to work in or above their nominal conditions. Such circumstances relates to contemporary power systems, as well. Limited investments resulting from different reasons cause that power systems are operated close to their stability margins.

To maintain safe state of a power system, limited but indispensable investments are required to allow for high speed fault clearing. A number of protection concepts are involved in relaying of power systems, yet the most effective are conceptions related to as unit protection. Such approach results in individual protection of sections of a power system. One of the most frequently used unit protection systems is differential current relaying. Its principle is to sense the difference between the incoming and out-

* Wroclaw University of Technology, Institute of Electrical Power Engineering, Wybrzeze Wyspianskiego 27, 50-370 Wroclaw, Poland.

going terminal currents of the protected section. The method is used for protection of power transformers, generators, generator-transformer units, motors, busbars and feeders.

The last enumerated element of the power system is distinctive from others by its longitudinal size. The essential difference in application of the method to feeder protection is that because of long distances between terminals the extra media for information interchange is required. Such a protective relaying is known as a digital/numerical current differential protection.

1.2. SENSITIVITY DETERIORATION FACTORS

The fundamental conditions required for maximal sensitivity of digital current differential protections are as follows:

- linear transformation of current transformers (CTs) in full range of prospective fault currents (composite error of 0%),
- no in zone leakage currents due to e.g. capacitance of the transmission line or installed compensating inductors,
- perfect transposition of the line (the symmetry of the line is unfeasible in faulty conditions),
- ideal synchronization of sampling at both terminals,
- no time delay of data transmission from the opposite relay.

The last effect is the most essential for stability of feeder differential protection. Considering ideal conditions except the last enumerated, one can assess delay in time domain or angular error for the transmission line of length l under assumed digital signal transmission propagation time. In practice, the velocity of transmission is in the range of 70% to 100% of the light velocity, for a strand wire and a light fiber based systems, respectively. Additionally, propagation time in electronic components should be concerned. Practically in 50 Hz power system, for a short line of 50 km length delay can reach 1.7 ms (i.e. 2) and for a long line of 500 km it is an angular lag of 40°. Now, one can compute apparent differential current for normal conditions and for external faults. Apparent differential current is a function of the through current according to fundamental formula:

$$I'_d = \sqrt{(I_S)^2 + (I_R)^2 - 2I_S I_R \cos\varphi} \tag{1}$$

where I_S, I_R are currents in sending and receiving terminal and φ is the angular lag. If both current are assumed to be equal $\underline{I}_S = -\underline{I}_R = \underline{I}_{SR}$, eq. (1) changes into the formula

$$I'_d = \sqrt{2} I_{SR} \sqrt{1-\cos\varphi} \tag{2}$$

For restraint current I_r defined as mean magnitude of incoming and outgoing currents it is possible to assess minimal necessary slope of the characteristic in the percentage differential plane:

$$\frac{I'_d}{I_r} = k_{1\_\min} = \sqrt{2}\sqrt{1-\cos\varphi} \tag{3}$$

If in addition capacitance charging current of the line, usually of 1A per kilometer for 400kV overhead lines is concerned, then the operating characteristic is biased by off-set $I_{d\_\min}$.

$$I_{d\_\min} = I_C * l \tag{4}$$

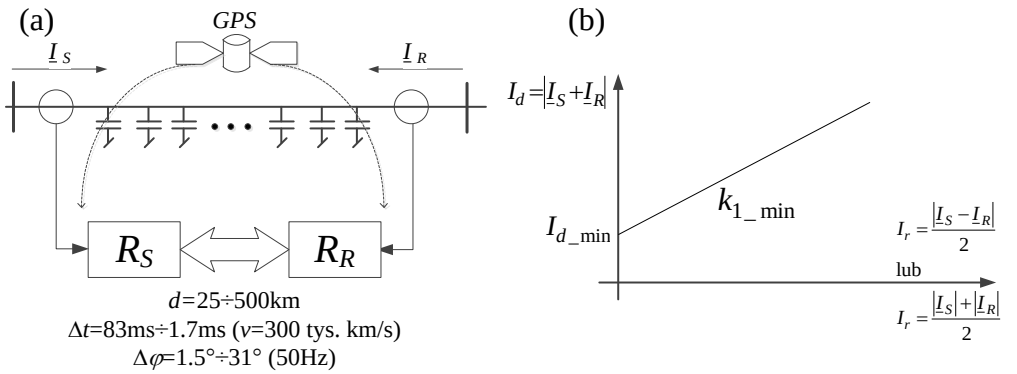

Fig. 1. Operational scheme of differential-current protection of feeder (a) and percentage differential characteristic (b).

For the worse conditions of line differential protection operation as far as uncompensated data transmission delay and capacitance charging currents are concerned the operational characteristic set according to eqs. (3) and (4) is depicted in Fig. 1(b). The differential element trips CBs when the magnitude of the differential current is greater than the sum of pre-set pick-up current $I_{d\_\min}$ and $k_{1\_\min}$ percentage of restraint current.

1.3. TRANSMISSION CHANNEL DELAY - REMEDIES

So far a few approaches to the current data aligning have been proposed. The simplest one is to assume a constant delay evaluated before commencement of protection

system. Such approach despite simplicity is effective, yet only for dedicated communications channels.

When the transmission path can change due to e.g. failure of the primary transmission system configuration or multiplexed channel are used then more sophisticated methods of data alignment are required. One of the most effective solutions is "ping-pong" algorithm [1]. Transmitted data are stamped locally with time tags which allow for estimation of actual delay in both directions even in case of channel propagation time asymmetry.

The most precise method of delay compensation and sampling synchronization is based on GPS [2, 3]. However, reliance on the system independent of the protection system owner is not optimal solution.

2. CHANNEL TIME-DELAY COMPENSATION METHOD

2.1. APPARENT PHASE SHIFT ESTIMATION

The conception of the method is based on the knowledge of the total positive susceptance of the line B_1. The locally measured current is not delayed whereas the current received from the opposite terminal is lagged by φ with respect to expected remote counterpart of the local current, so that $\underline{\tilde{I}}_R = \underline{I}_R \exp(-j\varphi)$.

Resulting apparent differential current is the vectorial sum of charging current and geometrical difference between expected (remotely sampled current) and locally received one:

$$\underline{\tilde{\Delta}} = \underline{I}_S + \underline{\tilde{I}}_R = \underline{I}_{CS} + \underline{I}_{CR}\exp(-j\varphi) + \underline{I}_{LOAD}(1.0 - \exp(-j\varphi)) \tag{5}$$

where $\underline{I}_{CL(R)}$ are capacitive currents incoming into the line and $\underline{I}_{LOAD}$ is load current theoretically invisible in differential current measured by inversely connected CTs as depicted in Fig. 2.

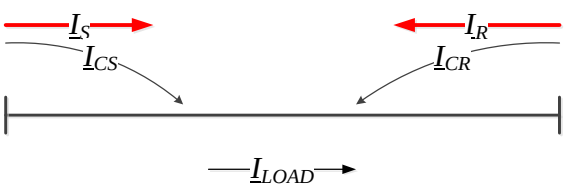

Fig. 2. Currents in analyzed line.

Let us remove from both sides of eq. (5) capacitive current estimated on the basis of locally measured phase voltage related to the geometrical center of the line:

$$\begin{aligned}\tilde{\underline{\Delta}} - j\underline{V}_{1/2L}B_1 \approx \underline{I}_{CS} + \underline{I}_{CR}\exp(-\varphi) + \underline{I}_{LOAD}(1.0 - \exp(-j\varphi)) - \underline{I}_{CS} - \underline{I}_{CR} = \\ = (\underline{I}_{LOAD} - \underline{I}_{CR})(1 - \exp(-j\varphi))\end{aligned} \tag{6}$$

where

$$\underline{V}_{1/2L} = \underline{V}_L - 0.5Z_1\underline{I}_S \tag{7}$$

Moreover we know that

$$\tilde{\underline{I}}_R = (\underline{I}_{CR} - \underline{I}_{LOAD})\exp(-j\varphi). \tag{8}$$

Substitution of (8) into (6) yields

$$\tilde{\underline{\Delta}} - j\underline{V}_{1/2L}B_1 = (\exp(-j\varphi) - 1)\frac{\tilde{\underline{I}}_R}{\exp(-j\varphi)} \tag{9}$$

One can estimate the lagging angle of the received current from (9) as:

$$\varphi = -angle\left(-\frac{\tilde{\underline{I}}_R}{\tilde{\underline{\Delta}} - j\underline{V}_{1/2L}B_1 - \tilde{\underline{I}}_R}\right). \tag{10}$$

Substituting $\tilde{\underline{\Delta}} = \underline{I}_S + \tilde{\underline{I}}_R$ into (10) one gets the final formula of the lagging phase of the received current resulting from the channel time delay as

$$\varphi = -angle\left(\frac{\tilde{\underline{I}}_R}{j\underline{V}_{1/2L}B_1 - \underline{I}_S}\right) = angle\left(\frac{j\underline{V}_{1/2L}B_1 - \underline{I}_S}{\tilde{\underline{I}}_R}\right) \tag{11}$$

2.2. LAGGING PHASE COMPENSATION

At least two approaches to the compensation for the lagging phase of received current phasor are possible. The correction can be carried out in an angular and time domains. The former method can be related to received phasor which should be advanced by angle resulting from eq. (11).The corrected differential current would be as follows:

$$\hat{\underline{\Delta}}_1 = \underline{I}_S + \hat{\underline{I}}_R = \underline{I}_S + \tilde{\underline{I}}_R \exp(j\varphi) \tag{12}$$

The angular correction can be related to locally measured current as well. In this case the local current phase must be delayed by angle (11) resulting in compensated differential current as follows:

$$\hat{\underline{\Delta}}_2 = \hat{\underline{I}}_S + \tilde{\underline{I}}_R = \underline{I}_S \exp(-j\varphi) + \tilde{\underline{I}}_R . \tag{13}$$

In the third method the compensation is made in time domain, i.e. samples of local current are saved in the FIFO register and utilized with time delay resulting from the estimated channel delay and assumed sampling frequency according to following formula:

$$\hat{\Delta}_3(n) = \hat{I}_S(n) + \tilde{I}_R(n) = I_S(n-k) + \tilde{I}_R(n) \quad \text{where} \quad k = round\left(\frac{\varphi}{2\pi}\frac{f_s}{50}\right). \tag{14}$$

The two former methods compensate for the apparent phase shift, yet they do not align samples of signal. As result, compared phasors may temporally relates to pre- and fault conditions. The impact of this effect has to be examined for concerned protective algorithm. The latter method is free of data misaligning problem, yet delay of ALARM or tripping signal issue will be inevitable.

2.3. SYSTEM MODELED

The investigations of the algorithm have been carried out on the basis of relaying signals obtained from computer simulations of the power system with double circuit 400kV overhead transmission line. The system was supplied from high (left hand side)

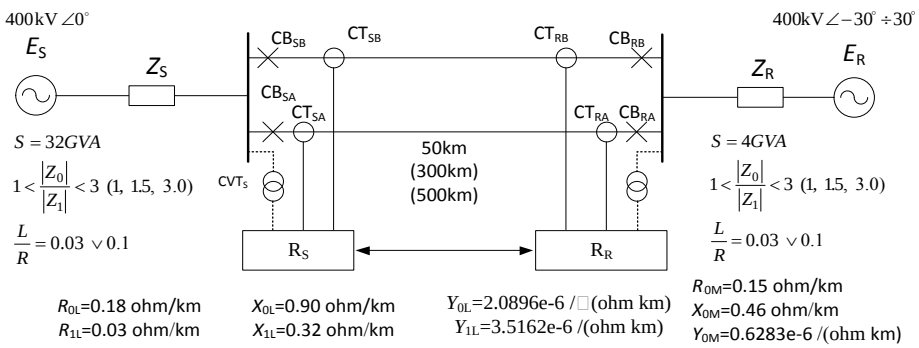

Fig. 3. The basic diagram of the test system

and low (right hand side) power capacity equivalent power systems as depicted in Fig. 3. The loads were variable and ranged from 0MW to the nominal value of the line.

Relaying signals have been synchronously sampled with 6.4 kHz rate and transmitted with apparent lagging phase shift in the ranges 2°÷12°, 30°÷40°, 40°÷50° for 50 km, 300 km and 500 km line lengths respectively. The shifts chosen for every load case remained constant, i.e. no variability of communications channel time delay was modelled.

3. THE ALGORITHM PERFORMANCE

3.1. PERFORMANCE OF THE ALGORITHM FOR CORRECT CHOICE OF B_1

First of all, the investigations covered relation of compensation errors for given line length to the restraint current resulting from the load of the line. The restraint current was computed as difference between phasors of sending and receiving (delayed) terminal phase currents. Figs. 4(a), 5(a) and 6(a) show location of the operating quantity on the percentage differential plane in pre-fault conditions for no channel delay correction. One can notice the increase of slope of the edge of restraining region as well as the increase of pick up differential current to be set in potential differential relay as the line length increases. The figures allow for estimation of theoretical maximal sensitivity of the differential algorithm. Making assumption of constant voltage along the line the simple computations for maximal loads give resistances of 385 Ω, 210 Ω, 220 Ω possible to be detected for lines of 50 km, 300 km and 500 km lengths, respectively.

Figs. 4(b), 5(b) and 6(b) depict efficiency of the proposed correction method. As can be seen the load of the line has essential impact on accuracy of compensation. In

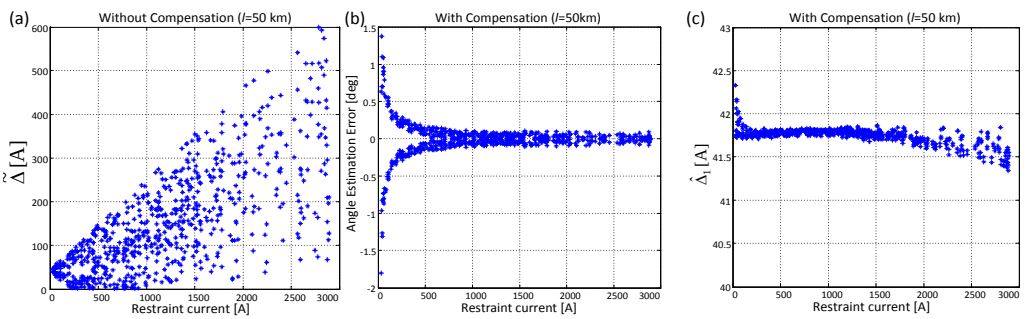

Fig. 4. Differential current in pre-fault conditions on the line of 50 km length with delay transmission angle from the range of 2°÷12° before (a) and after compensation (c). Errors of delay angle estimation (b).

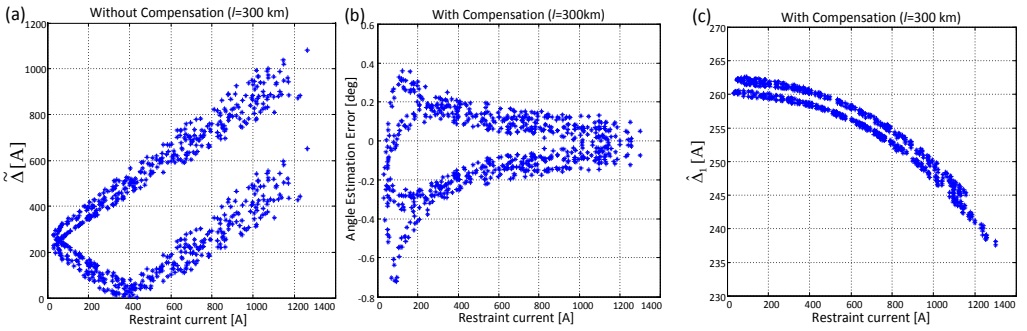

Fig. 5. Differential current seen in pre-fault conditions on the line of 300 km length with delay transmission angle from the range of 30°÷40° before (a) and after compensation (c).
Errors of delay angle estimation versus the load (b).

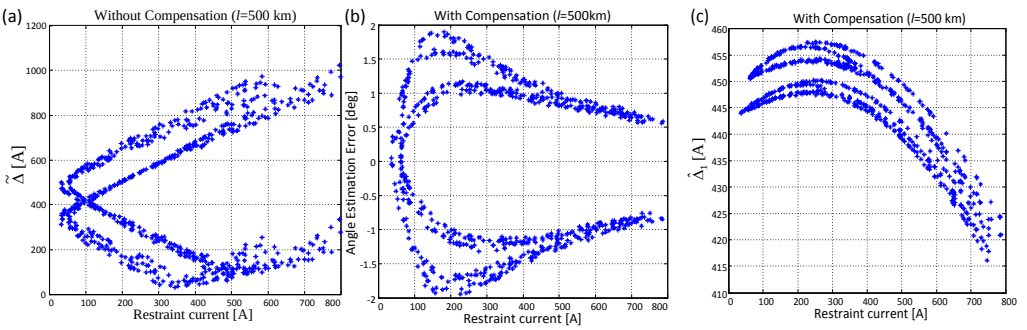

Fig. 6. Differential current seen in pre-fault conditions on the line of 500 km length with delay transmission angle from the range of 40°÷50° before (a) and after compensation (c).
Errors of delay angle estimation versus the load (b).

fact the effect is not cause by the load as such, yet relatively high CT errors for currents much less than the nominal current and an inaccuracy of the mean line voltage computation with use of eq. (7). However, the absolute errors of compensation are less than 2°. It gives maximal relative errors of 16% (50 km) , 2% (300 km) and 4% (500 km). One can notice that accuracy improvement appears with increasing restraint current (increasing load) what is very valuable feature of the method. Therefore, the magnitude of the vectorial sum of the line charging current and apparent differential current after compensation is almost constant and takes values of 43 A, 260 A, 460 A for line lengths of 50 km, 300 km, 500 km, respectively. These in turn results in improved sensitivity for faults via resistances of up to 5 kΩ, 890 Ω and 500 Ω.

Figs. 4(c), 5(c), 6(c) show the differential current seen in pre fault conditions after compensation of the transmission delay. It is readily noted that apparent differential current decreases with the increase of the load current.

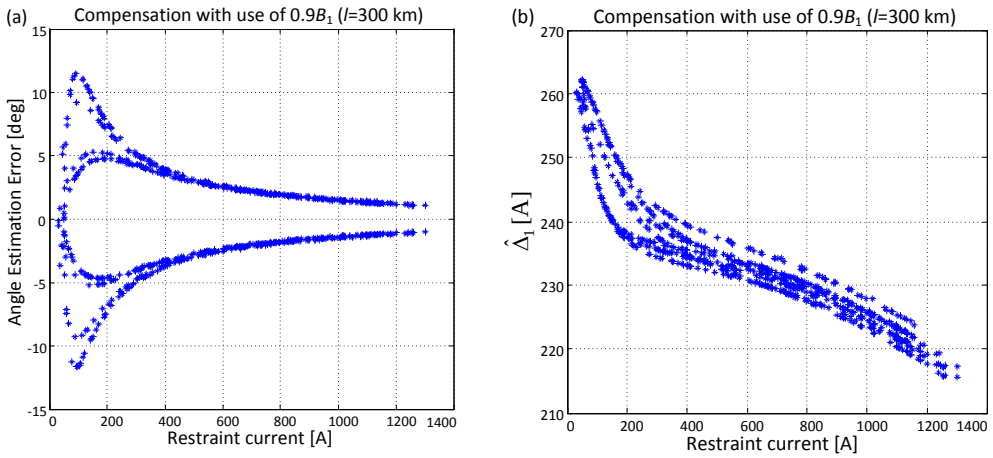

Fig. 7. Delay angle estimation errors versus the load (a) and differential current in pre-fault conditions (b) on the line of 300 km length with delay transmission angle from the range of 30°÷40° for 0.9B_1 used in computations

3.2. PERFORMANCE OF THE ALGORITHM FOR INCORRECT CHOICE OF B_1

As line parameters can be known imprecisely the question arises as to method robustness to some discrepancy between the actual line positive sequence susceptance and value of B_1 used in the algorithm. Therefore, additional investigations have been carried out for under- and overestimated susceptance of 300 km length line.

Fig. 7 depicts outcomes for susceptance underestimated by 10% with respect to the actual value. It is well visible that despite essentially worsened angle estimation the differential current is still below 270 A and decreases for higher through currents. For overestimated susceptance used in the algorithm the maximum of differential current in pre-fault conditions is below 290 A (Fig. 8).

4. CHANGE OF PATH DELAY OR FAULT IN THE SYSTEM

The estimated angle shift is to be saved and used for correction of the incoming remote phase current phasors. However, the question arises as to the necessary action to be undertaken after actuation of the relay. The reason for such a case may be either actual internal fault or essential change of the path delay. The proposal of flow chart for action to be undertaken after relay actuation is shown in Fig. 9.

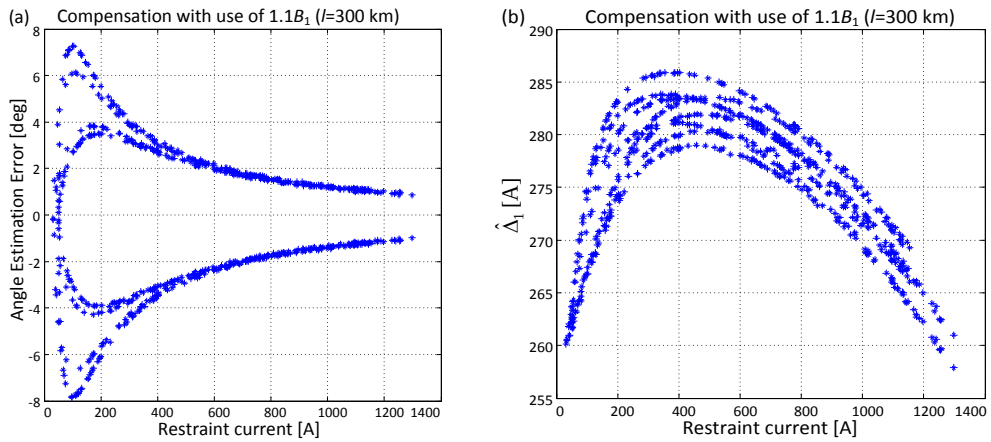

Fig. 8. Delay angle estimation errors versus the load (a) and differential current in pre-fault conditions (b) on the line of 300 km length with delay transmission angle from the range of 30°÷40° for 1.1B_1 used in computations

4.1. REAL CHANGE OF PATH DELAY

It is assumed that the saved estimate will be updated cyclically. In case of relatively slow and slight changes of the path delay the differential element should not become actuated. However, in case of essential change of actual delay the differential relay will be probably actuated. In such scenario tripping may be restrained by verification of magnitudes of currents from both line terminals. The negligible change of magnitudes should indicate the failure to operate. In aforementioned cases the corrective angle should be updated.

4.2. FAULTS

In case of external fault and valid pre-estimate of corrective angle the differential element will not be actuated. In case of internal fault the relay is expected to be actuated and the short circuit in the line will be additionally confirmed by essential change of current magnitudes at both terminals.

4.3. SIMULTANEOUS PATH DELAY CHANGE AND FAULT CONDITIONS

Simultaneous internal or external fault conditions and change of the path delay is unlikely scenario. However, for such situations there is no solution and it probably

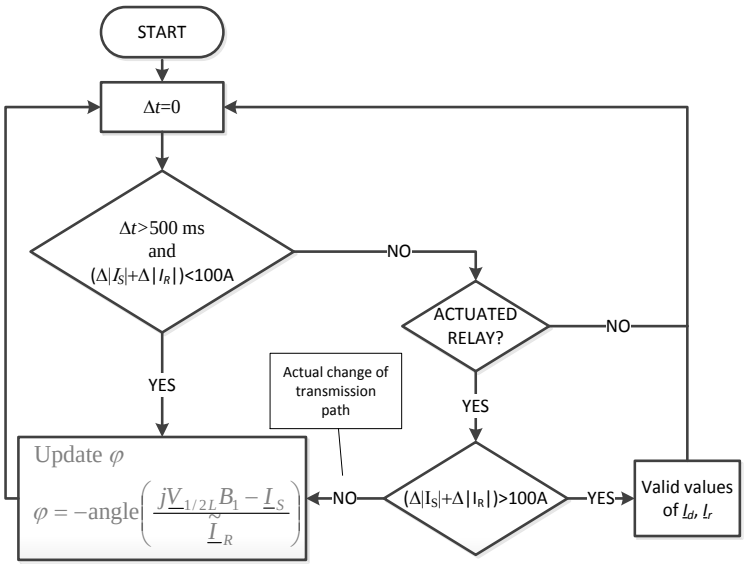

Fig. 9. The flowchart of the corrective angle updating algorithm

will result in issue of ALARM. The less discrepancy between the corrective angle estimates for all free phases may be the additional criterion for the acceptance of updating.

5. CONCLUSIONS

The presented algorithm allows for essential increase of feeder differential protection sensitivity. It has been shown that compensation of communications channel time delay under no charging line current compensation provides detection of faults via resistances up to 5 kΩ, 890 Ω and 500 Ω on lines of 50 km, 300 km, 500 km lengths, respectively. Moreover, 10% error in setting of line susceptance results in 30% error of communications path time delay estimation. However, actual performance of the compensating algorithm should be tested with the prospective protection algorithm, i.e. percentage differential algorithm, α-plane method etc.

REFERENCES

[1] Mills D. L., *Internet Time Synchronization: The Network Time Protocol*, IEEE Transactions on Communications, Vol. 39, No. 10, October 1991.

[2] IAN HALL, PHIL G. BEAUMONT, GARETH P. BABER, ITSUO SHUTO,MASAMICHI SAGA, KOICHI OKUNO, HACHIDAI ITO, *New Line Current Differential Relay using GPS Synchronization*, IEEE Bologna PowerTech Conference, June 23-26, Bologna, Italy 2003.

[3] LI, H.Y. ;SOUTHERN, E.P. ; CROSSLEY, P.A. ; POTTS, S. ; PICKERING, S.D.A. ; CAUNCE, B.R.J. ; WELLER, G.C.; *A new type of differential feeder protection relay using the Global Positioning System for data synchronization*, IEEE Transactions on Power Delivery, Vol. 12 , Issue 3, July 1997.

NOWA METODA KOMPENSACJI EFEKTU OPÓŹNIENIA TRANSMISJI DANYCH DLA POTRZEB PRĄDOWO-RÓŻNICOWYCH ZABEZPIECZEŃ LINII PRZESYŁOWYCH

W artykule zaprezentowano nowa metodę synchronizacji danych przesyłanych kanałem teleinformatycznym dla potrzeb przekaźników różnicowoprądowych napowietrznych linii elektroenergetycznych. Szacowanie opóźnienia przesyłu danych dokonywane jest na podstawie znajomości susceptancji linii oraz lokalnego pomiaru napięcia, lokalnego prądu fazowego i przesłanego prądu z przeciwległego końca linii w warunkach przedzwarciowych. Dokładność metody została sprawdzona dla różnych stanów pracy dwutorowej napowietrznej linii 400 kV. Wyniki badań potwierdzają dużą dokładność szacowania i tym samym korekcji kątowej między prądami z obu końców linii. Opracowana metoda kompensacji pozwala na zasadniczą poprawę czułości zabezpieczenia różnicowego linii przesyłowych.

Słowa kluczowe: elektroenergetyczna automatyka zabezpieczeniowa, systemy zabezpieczeń w elektrowniach, bezpieczeństwo funkcjonalne systemów programowalnych, zastosowanie normy PN/EN/IEC 61508 i norm pochodnych

Zdzisław ŻURAKOWSKI*

BEZPIECZEŃSTWO FUNKCJONALNE UKŁADÓW ELEKTROENERGETYCZNEJ AUTOMATYKI ZABEZPIECZENIOWEJ OPARTYCH NA URZĄDZENIACH PROGRAMOWALNYCH

W związku z rosnącą liczbą urządzeń programowalnych stosowanych w układach elektroenergetycznej automatyki zabezpieczeniowej (EAZ), rosnącą złożonością systemów technicznych stosowanych w przemyśle, w tym systemów związanych z bezpieczeństwem, oraz rosnącymi wymaganiami odnośnie bezpieczeństwa, do oceny którego włączana jest również ocena niezawodności zasilania, po opublikowaniu międzynarodowej normy IEC 61508, dotyczącej bezpieczeństwa funkcjonalnego systemów programowalnych, w krajach rozwiniętych podjęte zostały prace zmierzające do zastosowania tej normy również w sektorze elektroenergetyki, w tym do układów EAZ. W referacie po krótkim rysie historycznym oraz przedstawieniu podstawowych koncepcji na których oparta jest norma IEC 61508, przedstawiono na podstawie dostępnych publikacji aktualny stan prac zmierzających do wdrożenia tej normy do układów EAZ. W zakończeniu podane są także niektóre prace związane z zastosowaniem tej normy do układów zabezpieczeń w elektrowniach konwencjonalnych.

1. WSTĘP

W literaturze wyróżnia się kilka aspektów bezpieczeństwa systemów komputerowych. Pierwsze z nich, zwane podstawowym (ang. *primary safety*), to bezpieczeństwo samego systemu komputerowego, które obejmuje możliwość porażenia prądem, spalenia się komputera lub wywołania pożaru przez sprzęt komputerowy, itp. Drugi aspekt, to bezpieczeństwo funkcjonalne (ang. *functional safety*), a trzeci wyróżniany w

* Niezależny konsultant; e-mail: zz@pvd.pl

literaturze, to bezpieczeństwo pośrednie (ang. *indirect safety*) z jakim mamy do czynienia np. w związanych z bezpieczeństwem systemach informatycznych (ang. *safety-related information systems*), odnoszące się do pośrednich konsekwencji uszkodzenia komputera lub wytworzenia błędnej informacji. Odnosi się to do szerokiego zakresu systemów, takich jak medyczne systemy zobrazowania lub systemy rejestru danych pacjenta [16].

Bezpieczeństwo funkcjonalne systemu komputerowego, lub ogólnie biorąc systemu programowalnego, polega na wykryciu potencjalnie niebezpiecznych warunków, w wyniku którego następuje uruchomienie urządzeń lub mechanizmów korygujących lub zabezpieczających, mających na celu zapobieżenie zdarzeniu zagrażającemu lub zmniejszenia skutków tego zdarzenia. Przykładem bezpieczeństwa funkcjonalnego może być włączenie systemu gaszenia po wykryciu dymu przez czujniki.

Terminem system związany z bezpieczeństwem (ang. *safety-related system*), określany jest system, który zapewnia bezpieczeństwo danego urządzenia lub obiektu przez implementację w nim funkcji bezpieczeństwa, tzn. funkcji koniecznych do osiągnięcia lub utrzymania stanu bezpiecznego. W przypadku systemów sterowania, system związany z bezpieczeństwem może być częścią systemu sterowania danym obiektem lub być oddzielnym systemem, sprzężonym z danym obiektem przez czujniki i elementy wykonawcze.

Termin system krytyczny dla bezpieczeństwa (ang. *safety-critical system*) jest zwykle używany jako synonim terminu system związany z bezpieczeństwem, chociaż w niektórych przypadkach może sugerować, że chodzi o system o wysokim stopniu krytyczności dla bezpieczeństwa.

W elektroenergetyce, w przypadku elektrowni, funkcje systemów programowalnych związane z bezpieczeństwem obejmują zarówno funkcje związane z regulacją procesów technologicznych jak i z uzupełniającymi ją zabezpieczeniami technologicznymi, stanowiącymi dodatkowe zabezpieczenie pracy zarówno danego urządzenia jak i całego procesu technologicznego. Przykładem mogą być zabezpieczenia kotłów.

Zgodnie z podanymi wyżej definicjami w EAZ przykładami systemów związanych z bezpieczeństwem funkcjonalnym mogą być wszystkie układy zabezpieczeń, których celem jest wykrycie uszkodzenia, na przykład zwarcia, a następnie wyłączenie zabezpieczanego obiektu w celu ochrony go przed zniszczeniem i ewentualnie także innymi stratami, jakie mogłyby powstać w przypadku niewyłączenia uszkodzenia. Takie podejście, od dawna stosowane na przykład w przemyśle procesowym, w EAZ dotychczas nie było stosowane. W związku z rosnącą liczbą urządzeń programowalnych stosowanych w układach EAZ, rosnącą złożonością systemów technicznych stosowanych w przemyśle, w tym systemów związanych z bezpieczeństwem, oraz rosnącymi wymaganiami odnośnie bezpieczeństwa, do oceny którego włączana jest również ocena niezawodności zasilania, po opublikowaniu międzynarodowej normy IEC 61508, dotyczącej bezpieczeństwa funkcjonalnego systemów programowalnych, w krajach rozwiniętych podjęte zostały prace zmierzające do zastosowania tej normy również w

sektorze elektroenergetyki, w tym do układów EAZ. W dalszej części, po krótkim rysie historycznym oraz przedstawieniu podstawowych koncepcji na których oparta jest norma IEC 61508, przedstawiony zostanie na podstawie dostępnych publikacji aktualny stan prac zmierzających do wdrożenia tej normy do układów EAZ. W zakończeniu podane zostaną także niektóre prace związane z zastosowaniem tej normy do układów zabezpieczeń w elektrowniach konwencjonalnych.

2. RYS HISTORYCZNY

Z informacji zawartych w publikacjach można wywnioskować, że kształtowanie się świadomości w przemyśle, świadomości społecznej, uregulowań prawnych i koncepcji na których oparta jest międzynarodowa norma IEC 61508 zaczęło się w latach 1970.

We wstępie do poradnika stosowania normy IEC 61508 autorzy piszą, że na początku lat 1970. w przemyśle procesowym zaczęto uświadamiać sobie, że w przypadku większych zakładów, posiadających duże ilości materiałów niebezpiecznych praktyka uczenia się na błędach (jeśli rzeczywiście ma miejsce) nie jest dłużej do zaakceptowania. Z własnej inicjatywy opracowano metody identyfikacji zagrożeń i ilościowego określania konsekwencji awarii w przeważającym stopniu jako pomoc w procesie podejmowania decyzji, związanych z rozbudową lub zmianami wprowadzanymi do zakładów. Zewnętrzne naciski przyszły później [15].

W sobotę 1 czerwca 1974 roku zakłady chemiczne we Flixborough w Wielkiej Brytanii zostały całkowicie zniszczone w wyniku eksplozji. 28 osób pracujących w tym czasie w zakładach zostało zabitych, a 36 innych odniosło rany. Na zewnętrz zakładów miały miejsce rozległe szkody i zniszczenia. Odnotowano 53 rannych, setki innych, którzy odnieśli relatywnie mniejsze zranienia nie zostało odnotowanych. 1821 domów i 167 sklepów i fabryk doznało większych lub mniejszych zniszczeń. Katastrofa we Flixborough 1974 roku skoncentrowała w Wielkiej Brytanii uwagę społeczeństwa i mediów na tych dziedzinach przemysłu, które mogły stwarzać takie zagrożenie. Istnieje w publikacjach zgodna opinia, że ta katastrofa oraz powtarzająca się po niej cała seria następujących prawie rok po roku kolejnych katastrof [7], miały w jakimś stopniu przełomowe znaczenie dla postrzegania tego typu zagrożeń jakie stwarza przemysł.

W następstwie katastrofy we Flixborough podjęto szereg działań, które w roku 1984 doprowadziły do regulacji CIMACH (Control of Industrial Major Accident Hazards), a w roku 1990 do jej poprawionej wersji w postaci COMACH (Control of Major Accident Hazards).

Ocena zagrożeń w przemyśle procesowym i w innych sektorach stała się powszechna w latach 80-tych dwudziestego wieku, ale formalne wytyczne i normy były

rzadkie i fragmentaryczne i nie dotyczyły całości zagadnień. Prowadzono wówczas prace nad opracowaniem norm w dziedzinie tworzenia oprogramowania dla systemów związanych z bezpieczeństwem i opublikowano pierwsze normy krajowe w tej dziedzinie, miedzy innymi przez TUV w Niemczech i Health and Safety Executive w Wielkiej Brytanii. W wyniku tych prac oraz presji przemysłu na opracowanie wspólnej normy międzynarodowej w tej dziedzinie, w roku 1995 opublikowany został projekt normy IEC 1508, a w latach 1998 – 2000 projekt ten opublikowany został jako międzynarodowa norma IEC 61508 [11].

Norma ta bardzo szybko znalazła powszechne uznanie jako podstawowa norma międzynarodowa w dziedzinie bezpieczeństwa funkcjonalnego systemów programowalnych, umożliwiająca coraz powszechniejsze stosowanie tych systemów w zastosowaniach związanych z bezpieczeństwem. Przed powstaniem tej normy używanie systemów programowalnych do zastosowań związanych z bezpieczeństwem natrafiało na opory, wynikające z braku zaufania do tych systemów, spowodowanego trudnościami ich oceny. W oparciu o tę normę publikowana jest coraz większa liczba norm dotyczących bezpieczeństwa funkcjonalnego w takich zastosowaniach, jak przemysł chemiczny, aparatura medyczna czy transport [1]. Opublikowana została również jako norma europejska EN i polska PN [11].

Z literatury wynika, że jej szybkie i powszechne wdrażanie wiąże się także z coraz bardziej rygorystycznymi wymaganiami rynkowymi dla systemów związanych z bezpieczeństwem. Obejmują one wykazanie z wykorzystaniem międzynarodowych norm, że wymagane bezpieczeństwo funkcjonalne zostało osiągnięte oraz spełnione zostały istniejące uregulowania prawne.

3. PODSTAWOWE KONCEPCJE NA KTÓRYCH OPARTA JEST NORMA IEC 61508

Maszyny, instalacje procesowe i inne urządzenia mogą w przypadku wadliwego działania stwarzać ryzyko dla ludzi i środowiska, związane z takimi zdarzeniami, jak pożary, eksplozje, nadmierne dawki promieniowania, niespodziewane powtórzenie suwu maszyny, itp. Wymienione wadliwe działania mogą powstać z powodu:

- defektów fizycznych w urządzeniu, spowodowanych na przykład przypadkowymi uszkodzeniami sprzętu;
- defektów w oprogramowaniu spowodowanych błędami ludzkimi popełnionymi w specyfikacji i projekcie systemu, które w przypadku określonych kombinacji sygnałów wejściowych mogą ujawnić się w postaci błędu w działaniu;
- warunków środowiskowych, takich jak zakłócenia elektromagnetyczne, temperatura, zjawiska mechaniczne;

- zakłóceń w napięciu zasilającym (zanik lub obniżenie napięcia, powrót napięcia po zaniku), itp.

Omawiana norma została opracowana w celu zapewnienia możliwości bezpiecznego zautomatyzowania instalacji przemysłowych i urządzeń z użyciem systemów programowalnych, które mają wiele korzystnych cech. Norma zawiera szczegółowe wytyczne umożliwiające realizację i ocenę systemu związanego z bezpieczeństwem, który ma zredukować ryzyko uszkodzeń do minimalnego akceptowalnego poziomu, zgodnie z zasadą ALARP, wymagającą żeby każde ryzyko zostało zmniejszone w takim stopniu, w jakim to jest racjonalnie uzasadnione (ang. *As Low As Reasonably Practicable*) [2].

Zgodnie z definicją podaną we wstępie, w normie IEC 61508 termin urządzenia programowalne jest ogólnym określeniem wszystkich urządzeń elektronicznych opartych na oprogramowaniu, takich jak układy komputerowe, sterowniki programowalne, mikrosterowniki, programowalne układy logiczne (PLC). Przez systemy związane z bezpieczeństwem funkcjonalnym podstawowo przyjęto w tej normie układy, których błąd w działaniu spowodować może zranienie lub śmierć osób, ale rozszerza się je również na układy, które w przypadku błędu w działaniu mogą spowodować duże szkody dla środowiska lub duże straty materialne.

Norma IEC 61508 oparta jest na analizie zagrożeń i ryzyka wykonywanej we wstępnej fazie projektu danego systemu. Analiza obejmuje projektowany system wraz obiektem dla którego ma realizować funkcję związana z bezpieczeństwem oraz całym otoczeniem systemu i obiektu, z którym dany obiekt i projektowany system będą wchodzić w interakcję. Ryzyko określa się zwykle jako iloczyn straty powstałej w przypadku zaistnienia danego zagrożenia i przewidywanej częstotliwości występowania tego zagrożenia.

Głównymi narzędziami, służącymi do zrealizowania celu normy są:

- całkowity cykl życia bezpieczeństwa (ang. *overall safety lifecycle*) systemu związanego z bezpieczeństwem;
- nienaruszalność bezpieczeństwa danej funkcji związanej z bezpieczeństwem określana skrótem SIL, od nazwy w języku angielskim *Safety Integrity Level*, podzielona na cztery kategorie, przy czym SIL 1 oznacza najniższy poziom nienaruszalności, a SIL 4 – najwyższy.

Przyjęty całkowity cykl życia bezpieczeństwa definiuje wymagania dla wszystkich etapów życia danego systemu, od etapu tworzenia koncepcji systemu poprzez analizę zagrożeń i ryzyka, określenie wymagań związanych z zapewnieniem bezpieczeństwa, realizację systemu, walidację bezpieczeństwa, przekazanie do eksploatacji oraz eksploatację, konserwację i naprawy aż do wyłączenia z ruchu lub likwidacji. Cykl ten narzuca podział etapu realizacji systemu na poszczególne fazy, organizuje te fazy w proces oraz włącza w proces wytwarzania czynności oceny jakości realizacji systemu w dogodnych punktach tego procesu. Dokumenty z czynności oceny są podstawą do

oceny jakości całego procesu oraz służą jako dowód w procesie oceny uzyskanego poziomu bezpieczeństwa systemu, dokonywanej w procesie certyfikacji.

Celem analizy zagrożeń i ryzyka jest przeanalizowanie wszystkich możliwych do wystąpienia sytuacji zagrażających, jakie mogłyby wystąpić w przypadku błędu w funkcjonowaniu systemu lub w przypadku innych możliwych do przewidzenia okoliczności związanych z danym obiektem lub z otoczeniem systemu i obiektu. Jeśli z analizy wynika, że sytuacje zagrażające nie mogą wystąpić, lub że prawdopodobieństwo ich wystąpienia lub skutki w przypadku wystąpienia są do zaakceptowania, to system taki uważa się za system nie związany z bezpieczeństwem funkcjonalnym i norma IEC 61508 nie ma w tym przypadku zastosowania.

Jeśli analiza wykaże, że zagrożenia o potencjalnych skutkach nie do zaakceptowania mogą wystąpić, to dalszy projekt systemu powinien być wykonywany jak dla systemów związanych z bezpieczeństwem na podstawie normy IEC 61508 lub norm sektorowych opartych na tej normie. W tym przypadku w trakcie analizy zagrożeń i ryzyka tworzona jest specyfikacja wymagań bezpieczeństwa funkcjonalnego definiująca:

- czynności, jakie poszczególne funkcje związane z bezpieczeństwem, tzw. funkcje bezpieczeństwa, mają wykonać w przypadku wystąpienia zagrożenia.
- wymagany poziom nienaruszalności bezpieczeństwa SIL dla każdej funkcji bezpieczeństwa.

Przypisanie danej funkcji bezpieczeństwa jednego z czterech poziomów bezpieczeństwa, określa wymaganą niezawodność z jaką dana funkcja powinna być realizowana, aby zidentyfikowane ryzyko zostało zmniejszone do poziomu akceptowalnego zgodnie z zasadą ALARP. Wysoki poziom SIL oznacza mniejsze prawdopodobieństwo wystąpienia uszkodzeń (niezadziałania) funkcji bezpieczeństwa, przy czym SIL określa tylko prawdopodobieństwo uszkodzeń niebezpiecznych, wymaganych do realizacji funkcji bezpieczeństwa. Odróżnia to SIL od niezawodności, która dotyczy wszystkich uszkodzeń, bezpiecznych i niebezpiecznych.

Na wymaganą wartość prawdopodobieństwa uszkodzeń niebezpiecznych danej funkcji bezpieczeństwa składają się dwa rodzaje uszkodzeń: uszkodzenia przypadkowe sprzętu (ang. *random hardware failure*) i uszkodzenia systematyczne (ang. *systematic failure*). Dlatego zapewnienie wymaganej docelowej miary uszkodzeń funkcji bezpieczeństwa wymaga dwóch rodzajów podejść w procesie tworzenia systemu, uwzględniających dwa różne rodzaje uszkodzeń.

Uszkodzenia przypadkowe spowodowane są degradacją sprzętu i liczbowa wartość prawdopodobieństwa ich wystąpienia może być ustalona przez porównanie wartości liczbowej prognozowanej częstotliwość uszkodzeń sprzętu z wartością docelowej miary uszkodzeń, odpowiadającą przyjętemu poziomowi SIL. Jeśli częstotliwość ta jest niewystarczająca, to dokonujemy zmian, polegających na przykład na przyjęciu innego sprzętu lub zastosowaniu redundancji.

Uszkodzenia systematyczne spowodowane są błędami w projektowaniu, nie mają charakteru przypadkowego i tym samym nie podlegają analizie statystycznej i nie jest możliwe określenie ilościowe prawdopodobieństwa ich wystąpienia. Przyczynami niebezpiecznych uszkodzeń systematycznych funkcji bezpieczeństwa mogą być:

- nieprawidłowa specyfikacją sprzętu lub oprogramowania;
- przeoczenia lub pominięcia w specyfikacji wymagań bezpieczeństwa (na przykład pominiecie niezbędnych funkcji bezpieczeństwa);
- systematyczne mechanizmy błędów w sprzęcie;
- błędy w oprogramowaniu;
- błędy ludzkie;
- zakłócenia elektromagnetyczne;
- konserwacja lub modyfikacja.

Określenie obu powyższych rodzajów nieprawidłowości w działaniu urządzeń programowalnych jako „uszkodzenia", użyte zostało za polską wersją normy IEC 61508, w której użyte one zostały jako odpowiedniki angielskich terminów *random failure* i *systematic failure*, mimo że nieprawidłowe działanie spowodowane na przykład błędem w oprogramowaniu nie ujawnia się zwykle jako uszkodzenie systemu programowalnego, a jako jego błędne działanie.

Zapewnienie wymaganej częstotliwości występowania uszkodzeń systematycznych odpowiadającej przyjętemu poziomowi SIL, uzyskuje się przez zastosowanie zalecanych w normie metod i środków dla danego SIL, uznanych na podstawie aktualnej wiedzy i doświadczenia za odpowiednie do osiągnięcia danego poziomu częstotliwości występowania uszkodzeń systematycznych. Poziom SIL spełnia w normie rolę parametru, określającego jakie środki i z jakim rygorem należy zastosować w procesie tworzenia systemu, aby uzyskać wymaganą częstotliwości występowania uszkodzeń systematycznych. Jest to główna rola SIL w omawianej normie.

Podawana w części pierwszej normy wymagana liczbowa wartość prawdopodobieństwa uszkodzeń niebezpiecznych funkcji bezpieczeństwa dla danego poziomu SIL odnosi się tylko do uszkodzeń przypadkowych sprzętu. Wymagana niezawodność uszkodzeń systematycznych ustalana jest jakościowo, przez zastosowanie technik i środków narzucanych przez przyjęty poziom SIL.

Przyjęcie poziomu SIL jako parametru do uzyskania wymaganego poziomu występowania uszkodzeń systematycznych jest procedurą uproszczoną, wynikająca z aktualnych możliwości techniki w tym zakresie. Szereg czynników wpływa na nienaruszalność bezpieczeństwa oprogramowania i nie jest możliwe podanie dokładnego algorytmu doboru technik i innych środków. W każdym konkretnym przypadku techniki oprogramowania powinny być rozważnie dobrane z uwzględnieniem takich czynników, jak [5]:

- kompetencje i doświadczenie wykonawcy oprogramowania w stosowaniu technik;

- zaznajomienie wykonawcy oprogramowania z aplikacją i przewidywane trudności;
- rozmiar i złożoność aplikacji;
- rekomendacje i rozwiązania dobrej praktyki istniejące w danym sektorze przemysłu;
- opublikowane krajowe i międzynarodowe normy.

4. ZASTOSOWANIE NORMY IEC 61508 DO UKŁADÓW ELEKTROENERGETYCZNEJ AUTOMATYKI ZABEZPIECZENIOWEJ

Jako przykład pojawiającego się w literaturze podejścia do układów EAZ, jak do systemów związanych z bezpieczeństwem funkcjonalnym zgodnie z normą IEC 61508, może być opis przekaźnika przeznaczonego do zabezpieczeń linii średnich napięć, opracowanego w firmie Schneider Electric [9]. W podsumowaniu referatu autorzy piszą, że jak każdy system związany z bezpieczeństwem, przekaźniki do zabezpieczeń linii średnich napięć muszą spełniać wymagania SIL zdefiniowane w normie IEC 61508. Funkcją bezpieczeństwa części programowej przekaźnika jest wykrycie powstałego uszkodzenia w sieci, a następnie wysłanie do wyłączników sygnału wyłączenia, w celu izolowania dotkniętej uszkodzeniem części sieci. Wykrycie i izolacja uszkodzeń musi nastąpić w czasie podanym w normie IEC 60255. Jako typowe stany towarzyszące uszkodzeniom autorzy wymieniają przeciążenia, zwarcia, uszkodzenia izolacji, itp. Referat opisuje opracowane w Schneider Electric podejście do konstrukcji oprogramowania, umożliwiające zbudowanie przekaźnika o deterministycznej stałej zwłoce czasowej. W przeprowadzonych testach uzyskano formalne potwierdzenie, że czas zwłoki od powstania uszkodzenia do wykrycia go przez algorytmy zabezpieczeniowe przekaźnika ma stałą wartości $t_{\text{detection}}$ = 26,664 ms. Autorzy podają, że zagwarantowanie stałego czasu działania umożliwia poprawienie selektywności zabezpieczeń i wymagane jest także do zagwarantowania przekaźnikowi poziomu nienaruszalności bezpieczeństwa SIL 2.

W publikacjach takie podejście, jak opisywane w referacie [9], spotyka się jednak rzadko. Norma IEC 61508 i normy pochodne, jak norma IEC 61511, przeznaczona dla przemysłu procesowego [12], w pierwszej kolejności wdrażane były do systemów programowalnych związanych z bezpieczeństwem w takich sektorach, jak przemysł procesowy, petrochemiczny, aparatura medyczna, systemy bezpieczeństwa maszyn, gdzie w grę wchodziło bezpieczeństwo pracowników i innych osób oraz gdzie w związku z tym obowiązują wymagania prawne krajowe i Unii Europejskiej. W elektroenergetyce w odniesieniu do EAZ takich wymagań prawnych nie ma i normy te nie były stosowane w tym sektorze i nawet nie były znane, poza elektrowniami jądrowymi, gdzie normy na układy zabezpieczeń oparte na systemach programowalnych sto-

sowane są od dawna, a w ostatnich latach wydana została oparta na IEC 61508 norma IEC 61513 [8].

4.1 ZASTOSOWANIE NORMY IEC 61508 I NORM POCHODNYCH DO EAZ W SYSTEMACH ZASILANIA I SIECIACH WEWENĘTRZNYCH ZAKŁADÓW PRZEMYSLOWYCH

Układy realizujące funkcje związane z bezpieczeństwem składają się z takich elementów jak czujniki, urządzenia programowalne, systemy komunikacyjne, elementy wykonawcze oraz zasilanie. Dla zapewnienia danej funkcji bezpieczeństwa wymaganego poziomu SIL, wszystkie urządzenie i podsystemy, tworzące układ realizujący tę funkcję, muszą posiadać zdolność wypełniania swojej funkcji do poziomu SIL, który w odniesieniu do takich elementów jak czujniki i urządzenia programowalne, podawany jest w danych katalogowych tych elementów. Podobne wymagania odnośnie wymaganego poziomu SIL odnoszą się do zasilania. Zarówno do układów UPS, zasilających urządzenia i podsystemy realizujące daną funkcję bezpieczeństwa, jak i do całego systemu zasilania danego zakładu czy procesu technologicznego w energię elektryczną, od którego zależeć może funkcjonowanie układów i urządzeń, na przykład napędów elektrycznych, dla których układy UPS są niewystarczające. Zapewnienie systemom zasilania odpowiedniego poziomu SIL wymaga aby odpowiedni poziom SIL posiadały również przekaźniki do zabezpieczeń, stosowanych w tych systemach zasilania. Z publikacji wynika, że rozwiązania takie zaczynają być stosowane w takich sektorach, jak petrochemia, przemysł procesowy czy transport miejski, co jak się wydaje spowodowane jest coraz bardziej rygorystycznym egzekwowaniem uregulowań prawnych dotyczących bezpieczeństwa w tych sektorach, które powoduje objęcie wymaganiami tych uregulowań także systemów zasilania zakładów w tych sektorach. Przykładem może być przekaźnik zabezpieczeniowy SEPCOS-PRO firmy Sécheron, posiadający certyfikat SIL 2, przeznaczony do stosowania w stacjach zasilających transportu publicznego, jak metro, linie trolejbusowe i pociągi podmiejskie [14] oraz wytyczne projektowania układów EAZ dla systemów zasilania zakładów petrochemicznych z uwzględnieniem wymaganego poziomu SIL [6].

We wstępie do opublikowanych przez Instytut Energetyki w Londynie wytycznych [6] podano, że powodem opracowania zawartej w tej publikacji metodologii opartej na ryzyku i normach IEC 61508/IEC 61511 jest rosnące zastosowanie mikroprocesorów i urządzeń programowalnych w EAZ oraz wymagana w Wielkiej Brytanii ocena ryzyka w tym sektorze przez uregulowania prawne takie jak Control of Major Hazard Regulations (COMAH), która powinna zawierać ocenę nienaruszalności zasilania i scenariusze wyłączania instalacji.

Publikacja dostarcza wytycznych i danych liczbowych do stosowania opartej na normach IEC 61508/IEC 16511 metodologii oceny wymaganego poziomu nienaruszalności bezpieczeństwa SIL oraz alokacji SIL do urządzeń i układów zabezpieczeń zasilania elektrycznego, łącznie z silnikami i innymi urządzeniami mechanicznymi,

związanymi z daną instalacją. W oparciu o te wytyczne, projektujący układy EAZ powinni sprawdzać przyjmowane schematy, szczególnie różniące się od stosowanych poprzednio, między innymi także w celu upewnienia się czy przyjmowany poziom SIL nie jest wyższy od wymaganego dla danego zastosowania. Wytyczne podają, że w zastosowaniach objętych wytycznymi, wymagany poziom SIL nie jest zwykle wyższy niz SIL1. Podają także, że postępując zgodnie ze stosowanymi poprzednio dobrymi praktykami w projektowaniu urządzeń i układów zabezpieczeń, łącznie z odpowiednim testowaniem, procedurami kontroli i obsługi w celu zapewnienia niskiego poziomu uszkodzeń, w większości przypadków powinno się osiągnąć taki poziom SIL [6], [4].

4.2 ZASTOSOWANIE NORMY IEC 61508 DO UKŁADÓW EAZ W SIECIACH PRZESYŁOWYCH I ROZDZIELCZYCH ELEKTROENERGETYKI

Z dostępnych publikacji wynika, że wdrożenie normy IEC 61508 w sektorze elektroenergetyki jest na etapie początkowym szczególnie, jeśli idzie o układy EAZ w sieciach przesyłowych i rozdzielczych. Z publikacji wywnioskować można, że najbardziej zaawansowana w tym zakresie jest elektroenergetyka brytyjska, co wiązać należy zapewne z dużą rolą, jaką w Wielkiej Brytanii w zapewnieniu bezpieczeństwa w przemyśle odgrywa organizacja Health and Safety Executive (HSE), będąca niezależną rządową organizacją sprawującą w interesie publicznym nadzór nad ochroną przed zagrożeniami dla życia i zdrowia w obiektach przemysłowych, w tym w instalacjach nuklearnych, kopalniach, w systemach dostawy gazu i elektryczności, oraz w sąsiedztwie tych obiektów. HSE sprawowała również jedną z wiodących ról w opracowaniu normy IEC 61508 i posiada duże doświadczenie w zagadnieniach związanych z zastosowaniem tej normy w różnych sektorach przemysłu.

Publikacja [13] jest podsumowaniem wyników przeglądu dokonanego w sektorze przesyłu i rozdziału w Wielkiej Brytanii przez HSE wspólnie z tymi sektorami. Przegląd ten miał na celu ocenę zakresu zastosowania elektroniki programowalnej w układach EAZ związanych z bezpieczeństwem funkcjonalnym oraz ocenę czy odpowiednie techniki i środki były użyte w projektowaniu, weryfikacji i eksploatacji tych układów. Zastosowane podejście polegało na dokonaniu oceny pewnej liczby układów czy są one związane z bezpieczeństwem, a następnie na ustaleniu jaka praktyka stosowana była w projektowaniu, weryfikacji i eksploatacji tych układów. Punktem odniesienia przy ocenie stosowanej praktyki była norma IEC 61508, która jest także normą Europejską EN i Brytyjską BS.

Analizowane układy obejmowały:

- układy zabezpieczeń;
- urządzenia łączeniowe z programowalnym interfejsem;
- zdalne układy sterowania i monitorowania;

− układy automatycznej restytucji zasilania.

Ustalono, że układy zabezpieczeń, układy automatycznej restytucji zasilania oraz programowalny interfejs urządzeń łączeniowych są związane z bezpieczeństwem z różnym poziomem ryzyka. Ponadto ustalono, że systemy SCADA, zależnie od realizowanych funkcji, mogą być związane z bezpieczeństwem. Ustalenia te były punktem wyjścia do dalszych prac.

Autorzy stwierdzają, że mimo coraz powszechniejszego stosowania urządzeń programowalnych w EAZ aktualnie stosowana praktyka przy projektowaniu, badaniu i eksploatacji tych urządzeń jest wciąż oparta na doświadczeniu, wynikającym z wieloletniego stosowania urządzeń elektromechanicznych. O ile schematy funkcjonalne stosowane przy zastosowaniu urządzeń elektromechanicznych są dalej ważne, o tyle zastosowanie w tych układach urządzeń programowalnych wymaga innego podejścia do weryfikacji działania tych układów. Wynika to z różnic między układami wykorzystującymi urządzenia elektromechaniczne, a odpowiadającymi im układami opartymi na urządzeniach programowalnych.

Urządzenia elektromechaniczne mają bardzo ograniczoną funkcjonalność. Ich zachowanie jest stosunkowo proste, łatwo zrozumiale i łatwe do sprawdzenia. Nienaruszalność bezpieczeństwa zapewniana przez te urządzenia, określana jest przez ich niezawodność i może być stosunkowo łatwo i pewnie oceniona przez testowanie typu. Uszkodzenia sprzętu mają charakter przypadkowy, wynikający między innymi ze zużycia sprzętu, dlatego przez zastosowanie redundancji takim samym lub podobny urządzeniem można łatwo poprawić niezawodność układu. Redundancja i prostota, umożliwiająca łatwe sprawdzenie wszystkich funkcji, daje de facto poczucie rozwiązania deterministycznego. Dlatego tradycyjne układy nie wymagają podejścia opartego na ocenie ryzyka i taka ocena nie jest stosowana.

Prawdopodobnie między innymi z tego względu autorzy stwierdzają, że norma IEC 61508 jest słabo rozumiana w sektorze przesyłu i rozdziału oraz wciąż jest trochę dyskusji na temat jej przydatności w tym sektorze. Z dyskusji, jakie miały miejsce w początkowym okresie wdrażania normy także w innych sektorach, można wywnioskować, że pewną trudność w zrozumieniu normy i pewną nieprzystawalność tej normy do tradycyjnie stosowanych metod oceny urządzeń może sprawiać także fakt, że jest to norma na proces, a nie na produkt.

Urządzenia programowalne realizują wiele funkcji w jednym urządzeniu. Mają inną charakterystykę błędów w działaniu, przy czym nad błędami spowodowanymi uszkodzeniami przypadkowymi sprzętu przeważają uszkodzenia systematyczne. Uszkodzenia systematyczne odnoszą się szczególnie do błędów w oprogramowaniu i prawdopodobieństwo tego rodzaju uszkodzeń rośnie, wraz ze wzrostem złożoności i ilości funkcji zaimplementowanych w jednym urządzeniu. Dlatego projektując układ redundancyjny trzeba uwzględnić możliwość wystąpienia niewłaściwego działania, spowodowanego takim samym błędem w oprogramowaniu urządzenia wykorzystanego do redundancji. Oznacza to, że w przypadku projektowania redundancji w oparciu

o urządzenia programowalne większą uwagę należy poświęcić zróżnicowaniu rozwiązania w urządzeniu redundancyjnym.

W przypadku oprogramowania testowanie też jest niezbędne do zapewnienia niezawodności i jest niezawodnym sposobem zapewnienia niezawodności działania w warunkach określonych w testowaniu, ale jest bardzo niewystarczające do oceny, czy dany układ może niewłaściwie zadziałać w innych, pozornie nieszkodliwych warunkach.

Ze względu na złożoność układów opartych na urządzeniach programowalnych, takie aspekty jak istniejące kompetencje i szkolenia wszystkich zaangażowanych w projektowanie, wprowadzanie do eksploatacji i eksploatację tych układów nabierają coraz większego znaczenia.

W wyniku przeglądu dokonanego przez HSE wspólnie z firmami sektora przesyłu i rozdziału firmy tych sektorów zaakceptowały, że wprowadzenie urządzeń i systemów programowalnych do sektora przesyłu i rozdziału wymaga uwzględnienia normy IEC 61508 i podjęły się opracowania poprzez Energy Networks Association (ENA) zwartych wytycznych do stosowania IEC 61508 tych sektorach. Odbiorcami tych wytycznych mają być przedsiębiorstwa energetyczne, a poprzez ich związki kontraktowe stosowanie opracowanych wytycznych zostanie rozszerzone na inne strony. Dokument ten ma promować wspólne podejście do dobrej praktyki w zakresie stosowania normy IEC 61508 i dążyć do przezwyciężenia jej złożoności.

Opracowywane wytyczne podzielono na dwie odrębne części. Pierwsza, która w trakcie pisania omawianej publikacji, była na etapie końcowym, dotyczy zasadniczego pytania czy dany system lub urządzenie wykonuje funkcję związaną z bezpieczeństwem, i jeśli tak, to jaki poziom SIL jest właściwy. Jest to bardzo ważna część wytycznych, ponieważ użytkownik lub jego pośrednik musi być w stanie dokonać opartej na ocenie ryzyka, oceny krytyczności funkcji spełnianej przez dane urządzenie lub system, który użytkownik zamierza zastosować.

Druga część wytycznych dotyczy metod zapewnienia i utrzymania wymaganego poziomu bezpieczeństwa przez cały czas życia danego układu w oparciu o tzw. cykl życia bezpieczeństwa. Odpowiedzialność za cykl życia bezpieczeństwa danego układu podzielona została pomiędzy wytwórców urządzeń i podsystemów, integratorów systemów oraz użytkowników. Zgodnie z wytycznymi:

- Wytwórcy urządzeń i podsystemów odpowiedzialni są za projektowanie i weryfikację zdolności danego urządzenia lub podsystemu do wypełniania swojej funkcji do określonego poziomu SIL (ang. SIL capability).
- Integratorzy systemów odpowiedzialni są za projektowanie i weryfikację systemów, złożonych z urządzeń i podsystemów o określonym SIL, spełniających funkcje bezpieczeństwa zgodnie z wymaganym poziomem SIL.
- Użytkownicy (przedsiębiorstwa przesyłu i rozdziału) odpowiedzialni są za specyfikację właściwego poziomu SIL dla danej funkcji bezpieczeństwa i upewnie-

nie się, że systemy zastosowane w ich sieciach zostały właściwie zaprojektowane i zweryfikowane dla wyspecyfikowanego poziomu SIL oraz za właściwą ich obsługę i konserwację. Ponoszą również odpowiedzialność za zapewnienie ciągłej kontroli nad zarządzaniem tymi systemami, obejmującym takie zagadnienia jak aktualizacja oprogramowania, zmiany nastawień, zabezpieczanie haseł, zmiana konfiguracji, itp. Odpowiedzialni są również za zarządzanie końcem pracy tych systemów, gdy malejąca niezawodność może zmniejszyć początkową wartość SIL.

W publikacji podano, że powyższy zakres odpowiedzialności w swojej podstawowej postaci nie różni się tak bardzo od stanu aktualnie oczekiwanego w przedsiębiorstwach, w których narzędzia i procedury procesu zarządzania są skutecznie stosowane. Jest jednak oczywiste, że w przypadku systemów programowalnych w podanych zakresach odpowiedzialności poszczególnych stron większy nacisk oprócz testowania powinien być położony także na zarządzanie. Efektywne zarządzanie cyklem życia systemów programowalnych wymaga coraz bliższej współpracy między wszystkimi stronami dla zapewnienia, że stosowane u nich procesy zarządzania opracowane zostały pod kątem potrzeb urządzeń programowalnych i są ze sobą spójne.

W końcowej części publikacji ponownie zawarte jest stwierdzenie, że zastosowanie układów programowalnych w EAZ jest obecnie w bardzo dużym stopniu oparte na poprzednio stosowanej, sprawdzonej przez wiele lat praktyce, jaka ukształtowała się przy zastosowaniu układów elektromechanicznych. O ile jednak praktyka ta pozostaje właściwa w odniesieniu do funkcjonalności układów programowalnych o tyle nie jest efektywna, jeśli idzie o zapewnienie odpowiedniego poziomu nienaruszalności bezpieczeństwa. Dlatego zaproponowano żeby dokonać przeglądu istniejących procedur w zakresie EAZ i żeby to poprawione podejście było oparte na obecnych normach dla systemów związanych z bezpieczeństwem, a w szczególności na normie IEC 61508. Uwzględnienie tych norm nieuchronnie wpłynie na sposób, w jaki urządzenia będą projektowane, wytwarzane, weryfikowane, konserwowane i eksploatowane. Jednak zmiany powinny w większości zmierzać raczej do korekt lub ponownego przeanalizowania stosowanych obecnie procesów niż prowadzić do całkowitych zmian.

W podsumowaniu omawianej publikacji zawarte jest stwierdzenie, że elektroenergetyka brytyjska w oparciu o wytyczne HSE opracowuje aktualnie wytyczne zastosowania zasad normy IEC 61508 do zabezpieczeń w sektorze przesyłu i rozdziału. Jednak ze względu na międzynarodowy charakter działalności w tych sektorach oraz międzynarodowy charakter normy IEC 61508 ważne jest żeby zagadnienie to przedyskutowane było na poziomie międzynarodowym w celu osiągnięcia wspólnych uzgodnień. Następnie przeanalizowane muszą być zależności miedzy IEC 61508 a innymi normami IEC/CENELEC i normami innych organizacji na produkt lub system w dziedzinie przesyłu i rozdziału. Ma to na celu uzyskanie wspólnego rozumienia wpływu normy IEC 61508 na sektor przesyłu i rozdziału w najlepszym interesie

wszystkich zainteresowanych stron i intencją zarówno HSE jak i energetyki brytyjskiej jest dążyć do takiego celu.

5. NIEKTÓRE PRACE ZWIĄZANE Z ZASTOSOWANIEM NORMY IEC 61508 DO UKŁADÓW ZABEZPIECZEŃ W ELEKTROWNIACH KONWENCJONALNYCH

Prace związane z wdrożeniem w sektorze elektroenergetyki w Wielkiej Brytanii metody projektowania układów automatyki i zabezpieczeń opartej na ocenie zagrożeń i ryzyka z wykorzystaniem normy IEC 61508 i norm pochodnych prowadzone są również w odniesieniu do elektrowni konwencjonalnych sektora wytwórczego. Prace przedstawione w opublikowanych informacjach obejmowały zastosowanie podejścia opartego na normie IEC 61508 zarówno w nowych układach zabezpieczeń, jak i do oceny poziomu bezpieczeństwa w układach istniejących, powstałych nieraz na długo przed powstaniem normy IEC 61508, w latach 1960., 1970. i w połowie lat 1990., kiedy podejście oparte na ocenie ryzyka, na którym oparta jest norma IEC 61508, nie było stosowane w sektorze elektroenergetyki. Zakres dokonanej oceny obejmował układy zabezpieczeń kotłów, turbin, itp. we wszystkich tradycyjnych elektrowniach sektora wytwórczego: węglowych, olejowych, gazowych i wodnych, łącznie z kogeneracją [18], [17], [10].

Publikacja [18] opisuje pierwsze kroki związane z wprowadzeniem normy IEC 61508, jakie wkrótce po wprowadzeniu tej normy podjął RWE npower w odniesieniu do swoich elektrowni węglowych i olejowych. Zawiera również opis zrealizowanego studium przypadku, które służyło do zademonstrowania sposobu zastosowania opracowanego w RWE npower diagramu sekwencji technik bezpieczeństwa, jako podejścia do tworzenia w elektrowniach systemów związanych z bezpieczeństwem zgodnie z IEC 61508. W podsumowaniu publikacja stwierdza, że RWE npower ocenia ogólne podejście zawarte w normie IEC 61508 jako doskonałe podejście do budowy systemów związanych z bezpieczeństwem.

6. PODSUMOWANIE

Omówione wyżej z braku miejsca bardzo pobieżnie publikacje [6], [13] i [18] oraz prezentacje [4], [17], [10], zawierają opis ważnego doświadczenia z praktycznych prac, związanych z wprowadzaniem nowego podejścia do projektowania i eksploatacji układów EAZ i układów zabezpieczeń w elektrowniach, coraz powszechniej opartych na urządzeniach programowalnych, które powoli wypierają tradycyjne układy elektromechaniczne.

Wytwórca systemu czy urządzenia programowalnego może podać, że przetestował oprogramowanie tak dokładnie jak to jest możliwe. Jest to jednak subiektywna ocena wytwórcy, oparta na kwalifikacjach i możliwościach, jakimi dysponuje. I nie chodzi tylko o to, że może to być za mało dokładne testowanie, ale także o to, że może być zbyt dokładne, z czym wiążą się duże niepotrzebne koszty, jak i o znaczenie prawne takiej deklaracji na wypadek nieszczęśliwego zdarzenia. Potwierdzenie wymaganego poziomu nienaruszalności bezpieczeństwa systemu, w tym oprogramowania, zgodnie z powszechnie zaakceptowaną normą międzynarodową, daje wszystkim, wytwórcom, klientom i organom nadzoru, poczucie należytej staranności w dążeniu do zapewnienia bezpieczeństwa.

Z publikacji wynika, że w przemyśle, gdy rozważane jest zastosowanie normy IEC 61508 w miejsce istniejących metod zapewnienia odpowiedniego poziomu bezpieczeństwa powszechne jest narzekanie, że procedury wymagane przez tę normę są zbyt rozbudowane i znacznie podniosą koszty urządzeń i systemów. W prezentacji [3] podano, że w przemyśle maszynowym zastosowanie podejścia opartego na ocenie ryzyka, na którym oparta jest norma IEC 61508 i normy pochodne, wciąż uważane jest za zbyt wielkie obciążenie i aby być po bezpiecznej stronie wymaga się najwyższego poziomu SIL 4, który w praktyce wymagany jest rzadko. Z publikacji wynika, że nienaruszalność bezpieczeństwa wymagana dla EAZ jest zwykle SIL1, a najwyżej SIL2, natomiast dla systemów zabezpieczeń w elektrowniach SIL2 lub SIL3. Miedzy nienaruszalnością SIL1 i SIL2 a SIL3 i SIL4 jest skokowa zmiana wymagań odnośnie stosowanych procedur i tym samym kosztów.

LITERATURA

[1] ACOS references to IEC 61508 series in other standards, dokument 65A/571/INF, 02-19-2010 (http://www.iec.ch/functionalsafety/pdf/65A_571e_INF.pdf).

[2] *ALARP "at a glance"* http://www.hse.gov.uk/risk/theory/alarpglance.htm.

[3] FALLER R., *Evolution of European Safety Standards*, Exida, 2002 (http://www.exida.com/articles/Rockwell.pdf).

[4] FREEMAN P., *SIL evaluation: Practical Experience of Developing IP Gaidance on Assesssing the Safety Integrity of Electrical Supply Protection*, The IET Seminar on SIL Determination: Principles and Practical Experience, London, 28 March 2007.

[5] *Frequently Asked Questions*, IEC Safety Zone, http://www.iec.ch/functionalsafety.

[6] *Guidance on assessing the safety integrity of electrical supply protection*, The Energy Institute, London, 2006.

[7] *HSE accident reports* http://www.icheme.org/resources/safety_centre/publications/hse_accident_reports.aspx

[8] IEC 61513: *Nuclear power plants – Instrumentation and control for systems important to safety – General requirements for systems*.

[9] JAN M., DAVID V., LALANDE J., PITEL M., *Usage of the safety-oriented real-time OASIS approach to build determiniostic protection relays*, International Symposium on Industrial Embedded Systems, IEEE, 2010.

[10] McCOLLUM D., *Legacy Systems Issues*, The IEE Seminar on SIL Determination: Principles and Practical Experience, 2006.
[11] PN/EN/IEC 61508: *Bezpieczeństwo funkcjonalne elektrycznych/elektronicznych/ programowalnych elektronicznych systemów związanych z bezpieczeństwem*. Część 1: *Wymagania ogólne*, Część 2: *Wymagania dotyczące elektrycznych/elektronicznych /programowalnych elektronicznych systemów związanych z bezpieczeństwem,* Część 3: *Wymagania dotyczące oprogramowania,* Część 4: *Definicje i skrótowce*, Część 5: *Przykłady metod określania poziomów nienaruszalności bezpieczeństwa*, Część 6: *Wytyczne do stosowania IEC 61508-2 i IEC 61508-3*, Część 7: *Przegląd technik i miar*.
[12] PN/EN/IEC 61511: *Bezpieczeństwo funkcjonalne - Systemy Automatyki Zabezpieczeniowej dla Przemysłu Procesowego*, cz. 1-3.
[13] PUREWAL S., WALDRON M.A., *Functional safety in application of programmable devices in power system protection and automation*, Eighth IEE International Conference on Developments in Power System Protection, 2004.
[14] *SEPCOS-PRO*, przekaźnik firmy Secheron, http://www.secheron.com/uk/products-services/gamm24-sepcos-pro-protection-relay.html.
[15] SMITH D.J., SIMPSON K.G.L., *Functional Safety-A Straightforward Guide to Applying IEC 61508 and Related Standards*, 2nd Edition, Elsevier, 2004.
[16] STOREY N., *Safety-Critical Computer Systems*, Addison-Wesley Longman 1996, 2-8.
[17] WYMAN P.,M., *The Approach to legacy systems within the non-nuclear power station sector*, 4th IET Seminar on SIL Determination – Minimising the Risk in Your Systems, 5th December 2008.
[18] WYMAN P.M., *A Case Study of The Application of BS:EN 61508 in Electrical Power Generation*, 2nd Institution of Engineering and Technology International Conference on System Safety, 2007.

FUNCTIONAL SAFETY OF RELAY PROTECTION SYSTEMS BASED ON PROGRAMMABLE DEVICES

In connection with the growing number of programmable devices used in relay protection systems, the growing complexity of technical systems used in industry, including safety-related systems, and increasing demands for safety, that requires also consideration of the reliability of power supply, after publication of the international standard IEC 61508 in developed countries works were undertaken connected with application this standard also in the electric power industry, including to power systems relay protection. The paper presents a brief historical overview, the basic concept on which the IEC 61508 standard is based and the status of current work to implement this standard for power systems relay protection. At the end are given also some works related to the use of this standard for protection systems in conventional power plants.

Słowa kluczowe:
elektroenergetyczne sieci inteligentne,
Smart Power Grid

Andrzej WISZNIEWSKI*

DLACZEGO SIECI ELEKTROENERGETYCZNE POWINNY BYĆ INTELIGENTNE

Wzrost zainteresowania sieciami inteligentnymi, a w szczególności ich spodziewanym potencjałem operacyjnym wymaga podania rzeczowych argumentów za rozwojem tej idei. W artykule przedstawiono większość powodów, dla których należy wspierać rozwój sieci typu *smart*.

1. WSTĘP

Od ponad 100 lat świat z każdym rokiem jest coraz bardziej uzależniony od energii elektrycznej, która jest najbardziej uniwersalną i najbardziej przyjazną dla użytkownika formą energii. Jednak aktualna sytuacja w zakresie elektroenergetyki jest, co najmniej, trudna. Oto najważniejsze problemy, z jakimi mamy do czynienia.

Wzrost zapotrzebowania wynosi ok. 0.7 – 0.8 % na każdy procent przyrostu PKB, co dla Polski oznacza ok. 2.5% - 3% rocznie. (W okresie 10 lat powoduje to wzrost o 30 – 35%, a w ciągu 20 lat o ok. 65 – 80%.). Ta sytuacja będzie narastać ze względu na wzrastające stosowanie samochodów elektrycznych oraz bogacenie się społeczeństwa (np. coraz powszechniejsze klimatyzatory).

Przestarzała i niedostateczna infrastruktura sieciowa, powstała 30 – 50 lat temu, przyrastająca dwukrotnie wolniej niż zapotrzebowanie. Szacuje się, że w ciągu 15 lat potrzeba wybudować lub zmodernizować 50 tys. km linii w państwach Unii Europejskiej. Jeśli idzie o linie napowietrzne, jest to niemożliwe ze względu na trudności z „prawem drogi".

---

* Instytut Energoelektryki, Politechnika Wrocławska, Wybrzeże Wyspiańskiego 27, 50-370 Wrocław, andrzej.wiszniewski@pwr.wroc.pl

Straty przesyłowe wynoszą 6 – 9 % energii, a potrzeby własne zużywają ok. 10% energii wyprodukowanej. Oznacza to, że na pokrycie samych strat powinna bez przerwy pracować obecnie elektrownia o mocy 1400 MW, w roku 2020 elektrownia o mocy 1900 MW, zaś w roku 2030 elektrownia o mocy 2030 MW.

Wymogi Unii Europejskiej nazwane 20/20/20 (do roku 2020 20 procent wzrostu efektywności energetycznej, czyli zmniejszenie o 20% zużycia energii, 20% zmniejszenia emisji gazów cieplarnianych oraz 20% udziału energetyki odnawialnej w produkcji energii).

Liczba rozwijających się awarii prowadzących do blackoutów rośnie i na świecie wynosi kilkanaście w skali roku.

Niebywały rozwój informatyki i telekomunikacji stwarza nowe narzędzia, jakie mogą być wykorzystane w elektroenergetyce.

2. SIECI INTELIGENTNE

Smart Grid jest sposobem na złagodzenie braków infrastrukturalnych, dzięki wykorzystaniu środków teletransmisyjnych. Zapewnia zmniejszenie zużycia energii, wyrównanie obciążeń dobowych, obniżenie strat oraz zwiększenie bezpieczeństwa przesyłu.

Smart power grid to system elektroenergetyczny wykorzystujący narzędzia telekomunikacyjne i informatyczne. Dzięki temu integruje w sposób inteligentny działania wszystkich uczestników generacji, przesyłu, dystrybucji i użytkowania energii elektrycznej w sposób niezawodny, bezpieczny i ekonomiczny, z uwzględnieniem wymogów ochrony środowiska.

Smart Grid realizuje:

- zarządzanie popytem,
- sterowanie operacyjne,
- zabezpieczenia nowej generacji,
- szybką restytucję.

2.1. ZARZĄDZANIE POPYTEM W STANACH NORMALNYCH I AWARYJNYCH

Dzięki otrzymywanym informacjom następuje zmniejszenie zapotrzebowania na energię przez świadomych odbiorców. (szacuje się że w skali 2 – 10%).

Wyrównanie dobowych obciążeń, dzięki czemu uzyskuje się zmniejszenie strat, zmniejszenie obciążeń torów, eliminowanie najmniej wydajnych a jednocześnie najbardziej zanieczyszczających źródeł oraz zmniejszenie zagrożenia rozwijającymi się awariami.

2.1.1. Przyczyny rosnącej liczby blackoutów

40 lat temu odnotowywano niewielką liczbę poważnych blackoutów (1-2 rocznie). Obecnie jest ich więcej – kilkanaście w skali roku. Przy czym mowa tu o blackoutach, które pozbawiły zasilania co najmniej milion odbiorców. Główne przyczyny tego stanu rzeczy to:

- zjawiska klimatyczne i klęski żywiołowe
- wzrost obciążeń sieci, a w szczególności linii przesyłowych
- błędy ludzkie, nieumiejętność prognozy konsekwencji decyzji operatorskich i/lub zjawisk awaryjnych.
- błędne działania zabezpieczeń i układów sterowania systemem.
- terroryzm i wandalizm.
- atak na urządzenia energetyczne i cyber atak: terrorystyczny, szczeniacki i pracowniczy.

Typowy przebieg awarii jest następujący:

1. zdarzenie inicjujące,
2. reakcja łańcuchowa na skutek niestabilności systemu,
3. podział systemu i masowe wyłączenia odbiorców, a niekiedy także generatorów,
4. długotrwała restytucja.

Rodzaje niestabilności systemowej:

- Niestabilność częstotliwościowa, czyli brak równowagi między generacją i poborem mocy.
- Niestabilność kątowa – statyczna i/lub dynamiczna, czyli przekroczenie granicznej wartości kąta między napięciem zasilającym a napięciem na zaciskach odbiorców.
- Niestabilność napięciowa, czyli nadmierne i lawinowo pogłębiające się obniżenie napięcia na zaciskach odbiorców.
- Niestabilność termiczna, czyli lawinowe wyłączanie przeciążonych linii lub transformatorów.
- Najczęściej podczas rozwijających się awarii występuje więcej niż jedna forma niestabilności systemowej.

2.2. STEROWANIE OPERACYJNE

W sieciach inteligentnych wykorzystując otrzymywane informacje można zrealizować następujące działania:

- Dynamiczne sterowanie obciążeniami linii, zależne od istniejących w danym momencie ograniczeń stabilnościowych oraz warunków termicznych.
- Sterowanie kompensacją mocy biernej i urządzeniami typu FACTS.
- Sterowanie przełącznikami zaczepów transformatorów odbiorczych, dla zapewnienia odpowiedniego poziomu napięć u odbiorców przy zachowaniu właściwego marginesu stabilności napięciowej.
- Predykcja skutków decyzji operatorskich i zakłóceń.
- Integracja generacji odnawialnej, a w szczególności farm wiatrowych.
- Interfejs operatora, zapewniający selekcję informacji szczególnie w stanach awaryjnych.

2.3. INTELIGENTNE ZABEZPIECZENIA LOKALNE I OBSZAROWE

Strategia stosowania zabezpieczeń powoli ulega pewnej modyfikacji. Dotychczas na pierwszym miejscu była ochrona zabezpieczanych obiektów. Obecnie priorytetem staje się ochrona systemu przed rozwijającymi się awariami. Wiąże się to z możliwym wyeliminowaniem działań zbędnych. Tym bardziej, że jeśli następuje działanie brakujące zabezpieczenia, to zapewne dane urządzenie zostanie wyłączone przez zabezpieczenia rezerwowe. Natomiast działania zbędne i niepotrzebne wyłączenie urządzenia silnie obciążonego może spowodować konsekwencje lawinowego rozwoju awarii prowadzącego do blackoutu.

Kompromis między niezawodnością a selektywnością można uzyskać dzięki szerokiemu stosowaniu zabezpieczeń adaptacyjnych oraz wykorzystywaniu zabezpieczeń obszarowych synchronizowanych przez GPS.

Inteligentna restytucja poawaryjna może zapewnić:

- Określenie charakteru awarii i lokalizację miejsca uszkodzenia.
- Optymalny podział na podsystemy, możliwie zbilansowane jeśli idzie o generację i zapotrzebowanie na energię.
- Inteligentne wyłączanie awaryjne obciążeń i/lub generatorów.
- Inteligentne scenariusze restytucyjne.

3. SMART GRID – GŁÓWNE TRUDNOŚCI

- Świadomość i wola odbiorcy, który może być niechętny stosowaniu inteligentnych liczników. (sytuacja taka ma miejsce w Holandii, gdzie odbiorcy wypowiedzieli się przeciw inteligentnym pomiarom rozliczeniowym).

- Brak skutecznej i niezawodnej infrastruktury telekomunikacyjnej oraz informatycznej.
- Niedostatki w zakresie opomiarowania linii i stacji oraz wykorzystania nowych możliwości (np. PMU, czyli układów mierzących fazory).
- Niełatwa współpraca operatorów sieci przesyłowych i operatorów sieci dystrybucyjnych.
- Brak inteligentnych (adaptacyjnych) algorytmów sterujących i zabezpieczających, oraz restytucyjnych.
- Brak inteligentnych układów odciążających w stanach awaryjnych.

4. WNIOSKI

Należy zdawać sobie sprawę, że technologia *smart grid* nie zastąpi niezbędnych inwestycji sieciowych, ale na pewno może złagodzić aktualne braki, obniżyć tempo przyrostu zapotrzebowanie na energie elektryczną, zmniejszyć straty tej energii oraz skutecznie zwiększyć bezpieczeństwo generacji, przesyłu i rozdziału energii. Dlatego powszechne na świecie zainteresowanie inteligentnymi sieciami jest w pełni uzasadnione, a Polska powinna wykorzystać swój potencjał ludzki i gospodarczy do włączenia się w rozwój tych technik.

WHY POWER GRID SHOULD BE SMART

Interest in Smart Grid, particularly in its expected operational potential, requires the exposure of matter-of-fact argumentation for development of this approach to power system control. In this paper fundamental reasons justifying support of Smart Grid technology development have been presented.